6-1-2016

Biomimetic Calcium Phosphate/PEM Coatings For Sequential Multifactor Delivery

Emily E. Jacobs
University of Connecticut, emily.e.jacobs@gmail.com

Biomimetic Calcium Phosphate/PEM Coatings For Sequential Multifactor Delivery

Emily Elizabeth Jacobs, PhD
University of Connecticut, 2016

Many of the most promising strategies for tissue engineering and regeneration aim to replicate natural cellular microenvironments including matrix components, growth factors, and cellular proteins as a means to guide the migration, proliferation, and differentiation of progenitor cells. Combinations of growth factors synergistically enhance tissue regeneration, but typically require sequential, rather than co-delivery from biomaterials for maximum efficacy. Polyelectrolyte multilayer (PEM) coatings can deliver multiple factors without loss of activity; however, sequential delivery has been limited due to interlayer diffusion of multiple factors that results in co-delivery.

This dissertation examined the incorporation of a biomimetic calcium phosphate (bCaP) layer into a poly-L-Lysine/poly-L-Glutamic acid PEM film (bCaP-PEM) to provide sequential delivery of two different factors. The bCaP-PEM was uniformly deposited onto two-dimensional (2-D), and three-dimensional (3-D) porous substrates. Measurements of MC3T3-E1 osteoprogenitor cell proliferation and viability over time were used to evaluate kinetics of active biomolecule delivery and demonstrate that bCaP-PEM enables sequential delivery of a proliferative factor (fibroblast growth factor -2 (FGF-2) followed by a cytotoxic factor (antimycin A, AntiA) a few days later. Alterations to the PEM composition via increasing the number of bilayers or using the *D*- enantiomer polyelectrolytes hindered delivery of the proliferative factor. Increasing the bCaP layer thickness resulted in sustained delivery of the embedded factor as compared to burst delivery. Accelerated cell-mediated delivery kinetics from the bCaP-PEM coating was demonstrated *in vitro* using a murine macrophage cell line. Scanning

electron microscopy revealed the bCaP-PEM coating could be uniformly applied to the 3-D, commercially available bone graft substitute Healos®, (DePuy Synthes Spine, Raynham, MA). Effects of sequential delivery of FGF-2, then bone morphogenetic protein 2 (BMP-2), from a bCaP-PEM coated Healos® scaffold was evaluated *in vivo* in a mouse calvarial defect model. This work resulted in the development of a novel, biomimetic coating capable of sequential delivery of two factors. This technology has potential to be applied in multiple research applications where a sequential delivery profile activated by cell degradation of the biomaterial is desired.

Biomimetic Calcium Phosphate/PEM Coatings For Sequential Multifactor Delivery

Emily Elizabeth Jacobs

B.S., University of Connecticut, **2009**

M.S., University of Connecticut, **2011**

A Dissertation

Submitted in Partial Fulfillment of the

Requirements for the Degree of

Doctor of Philosophy

at the

University of Connecticut

2016

APPROVAL PAGE

Doctor of Philosophy Dissertation

Biomimetic Calcium Phosphate/PEM Coatings For Sequential Multifactor Delivery

Presented by

Emily Elizabeth Jacobs, B.S., M.S.

Major Advisor _____
Liisa T. Kuhn

Associate Advisor _____
Gloria Gronowicz

Associate Advisor _____
Marja Hurley

Associate Advisor _____
A. Jon Goldberg

Associate Advisor _____
Caroline Dealy

University of Connecticut

2016

Acknowledgements

I would like to start by thanking my parents. Their love and support has been everything to me and I could not have done this without their encouragement and support. They instilled in me from a young age the drive and desire to excel and do my personal best in all aspects of life, whether it be school, sports, work, or even just a board game. I could not have asked for a better upbringing. I would like to thank my brother for being born first, sparking an instant competitiveness in me that has greatly contributed to my desire to achieve. I could not have imagined growing up without him by my side. I would like to thank my amazing grandparents. I wish my grandfathers could have seen this moment; they left behind two of the most amazing women I know. My grandmothers are both strong, independent women and have served as inspirational role models. I would like thank my entire family including my sister-in-law, my niece and nephew, my aunts, uncles, cousins, godparents, and all those close personal family friends that get lumped in with family. I am truly fortunate to have such an amazing family filled with people who have always loved and supported me through all my life's endeavors.

I would also like to thank my friends. I honestly have such a remarkable group of friends that have always been there for me. They have offered so much support, and have been a much needed source to vent to, de-stress, and then get back on track. There is no way I could have gotten through this PhD journey without them.

Lastly I would like to thank my major advisor, Dr. Liisa Kuhn, and my committee members Dr. Gloria Gronowicz, Dr. Marja Hurley, Dr. Jon Goldberg, and Dr. Caroline Dealy. They have all contributed greatly in helping me develop my skills as a scientist, an engineer, and a writer. I am incredibly grateful for their instruction, patience, and support during my graduate education.

Table of Contents

List of Figures

Figure 2.6 Percent LIVE® stained area of MC3T3-Es cultured for 1 day on sandblasted disks coated with normal AntiA (TCPsb-AntiA), AntiA after "PEM" processing, AntiA after "bCaP" processing, and no AntiA (TCPsb). AntiA = 213 μg/disk. (**** $p \leq 0.0001$).

Figure 2.7 Day 1 percent cell death of MC3T3-E1s cultured on TCPsb coated with AntiA, AntiA embedded under PEM8, and AntiA embedded under CaP-PEM8 relative to their AntiA-free controls **(A)**. Percent LIVE® stained area of MC3T3-E1s cultured on TCPsb coated with CaP-PEM8 (blue) and AntiA embedded under CaP-PEM8 (red) for days 1, 3, and 5 **(B)**. AntiA = 213 μg/disk. (* $p \leq 0.05$, ** $p \leq 0.01$, *** $p \leq 0.001$, **** $p \leq 0.0001$).

Figure 2.8 Percent LIVE® stained area of MC3T3-E1s cultured on TCPsb coated with CaP-PEM30 (blue) and Anti embedded under CaP-PEM30 (red) for days 1, 3, 5, and 7. AntiA = 213 μg/disk. (* $p \leq 0.05$, ** $p \leq 0.01$).

Figure 2.9 Day 1 % LIVE® stained area of MC3T3-E1s cultured on AntiA with no coating compared to its AntiA-free control, AntiA embedded under PEM30 compared to its AntiA-free control, and AntiA embedded under bCaP-PEM30 compared to its AntiA-free control **(A)**, (**** $p\ value \leq 0.0001$). The calculated day 1 % cell deaths of AntiA, AntiA-PEM30, and AntiA-bCaP-PEM30 relative to their AntiA-free controls **(B)**, (* $p\ value \leq 0.05$, *** $p\ value \leq 0.001$, **** $p\ value \leq 0.0001$). Fluorescent images of LIVE® staining of MC3T3-E1s cultured on TCPsb **(C)** vs. TCPsb coated with AntiA **(D)**, PEM30 **(E)** vs. AntiA-PEM30 **(F)**, and bCaP-PEM30 **(G)** vs. AntiA-bCaP-PEM30 **(H)**. Scale bar = 250 μm.

Figure 2.10 MC3T3-E1 FGF-2 dose response day 1 LIVE® staining. (* $p \leq 0.05$, ** $p \leq 0.01$, **** $p \leq 0.0001$). The 150 ng FGF-2 dose was selected to use for all studies.

Figure 2.11 Schematic representation of Factor 1 **(A)** and Factor 2 **(B)** location within the bCaP-PEM30 coating. The theoretical immediate, and delayed delivery profiles of Factor 1 **(C)** and Factor 2 **(D)** respectively.

Figure 2.12 LIVE® stained area of MC3T3-E1s cultured on bCaP-PEM30-FGF2 (blue) and bCaP-PEM30 (green) for up to 5 days **(A)**, (** $p \leq 0.01$, *** $p \leq 0.001$, **** $p \leq 0.0001$) (FGF-2 = 150 ng/disk). Fluorescent images of day 1 LIVE® staining of MC3T3-E1s cultured on TCPsb coated with bCaP-PEM30-FGF2 **(B)** and bCaP-PEM30 **(C)**. Scale bar = 250 μm.

Figure 2.13 Percent LIVE® stained area of MC3T3-E1s cultured on TCPsb coated with bCaP-PEM30 (green, -A/-F) and bCaP-PEM30-FGF2 (blue, -A/+F) at 4h **(A)**, and day 1 **(B)**, (** $p \leq 0.01$). Fluorescent images of LIVE® staining of MC3T3-E1s cultured on TCPsb coated with bCaP-PEM30 and bCaP-PEM30-FGF2 after 4 h **(C, D)** and 1 day **(E, F)**.

Figure 2.14 LIVE® stained area of MC3T3-E1s cultured on bCaP-PEM30 (green) and AntiA-bCaP-PEM30 (red) for up to 5 days **(A)**, (* $p \leq 0.05$, ** $p \leq 0.01$, *** $p \leq 0.001$) (AntiA = 213 μg/disk). Fluorescent images of day 3 LIVE® staining of MC3T3-E1s cultured on TCPsb coated with bCaP-PEM30 **(B)** and AntiA-bCaP-PEM30 **(C)**. Scale bar = 250 μm.

Figure 2.15 Percent LIVE® staining of MC3T3-E1s cultured in day 1- or day 3-release medium collected from bCaP-PEM30-FGF-2 (-A/+F, blue) or AntiA-bCaP-PEM30-FGF-2 (+A/+F, ornage) coated disks incubated at 37°C without cells, (FGF-2 = 150 ng/disk, AntiA = 213 μg/disk).

Figure 2.16 Day 1 LIVE® stained area of MC3T3-E1s cultured on the FGF-2 groups (+F) compared to their FGF-2-free controls (-F) (FGF-2 = 150 ng/disk) **(A)**, (*** $p \leq 0.001$, **** $p \leq 0.0001$). Percent LIVE® stained area of MC3T3-E1 cells cultured on bCaP-PEM30-FGF2 (blue)

and AntiA-bCaP-PEM30-FGF2 (orange) over time **(B)**, *(**** $p \leq 0.0001$). Fluorescent images of LIVE® staining of MC3T3-E1s cultured on bCaP-PEM30-FGF-2 (-A/+F), and AntiA-bCaP-PEM30-FGF-2 (+A/+F), at time points 4 h, days 1-5 **(C)**. Scale bar = 250 μm.

Figure 2.17 Schematic representation of "in and out" diffusion and exponential growth of hydrophilic polyelectrolytes during layer-by-layer build up of the PEM film **(A)**. Resulting interlayer diffusion of multiple factors within the PEM layers **(B)** and theoretical co-delivery of factors **(C)**.

Figure 3.1 Percent LIVE® stained area of MC3T3-E1s cultured on AntiA-bCaP-**PEM102**-FGF2 (orange checker) as compared to cells cultured on bCaP-**PEM102**-FGF2 (blue checker) on days 1, 3, and 5 **(A)**, (* $p \leq 0.05$). Percent LIVE® stained area of MC3T3-E1s cultured on the control bCaP-PEM30-FGF2 as compared to cells on bCaP-**PEM102**-FGF2, **(B)**, (*** $p \leq 0$.001). Percent LIVE® stained area of MC3T3-E1s cultured on the control AntiA-bCaP-PEM30-FGF2 as compared to cells on AntiA-bCaP-**PEM102**-FGF2, **(C)**, (* $p \leq 0.05$, ** $p \leq 0.01$). AntiA = 213 μg/disk, FGF-2 = 150 ng/disk.

Figure 3.2 Percent LIVE® stained area of MC3T3-E1s cultured on AntiA-bCaP-**PEM^{D}30**-FGF2 (orange stripes) as compared to cells cultured on bCaP-**PEM^{D}30**-FGF2 (blue stripes) on days 1, 3, and 5 **(A)**, (**** $p \leq 0.0001$). Percent LIVE® stained area of MC3T3-E1s cultured on the control bCaP-PEM30-FGF2 as compared to cells on bCaP-**PEM^{D}30**-FGF2, **(B)**, (* $p \leq 0.05$, ** $p \leq 0.01$). Percent LIVE® stained area of MC3T3-E1s cultured on the control AntiA-bCaP-PEM30-FGF2 as compared to AntiA-bCaP-**PEM^{D}30**-FGF2, **(C)**, (* $p \leq 0.05$). AntiA = 213 μg/disk, FGF-2 = 150 ng/disk.

Figure 4.8 4-week post-surgery x-rays **(A, B)**, microCT 3-D reconstructions **(C, D)**, and microCT cross-sections **(E, F)** of calvaria implanted with Healos® coated with CaP-PEM8 (top panel) and BMP2-CaP-PEM8 (bottom panel). BMP-2 dose = 0.5 μg. New bone formation is circled in red.

Figure 4.9 Schematic representation of where within the defect FGF-2 effects are being observed and quantified 1-week post-surgery **(A)**. Fluorescent images of DAPI and EdU stained cells showing increase in staining with the addition of 25 and 125 ng FGF-2 as compared to BMP-2 alone **(B)**. Quantified results showing 125 ng FGF-2 dose significantly increases number of EdU+ cells on day 7 as compared to BMP-2 alone and 25 ng FGF-2 dose **(C)**. (* $p \leq 0.05$, ** $p \leq 0.01$). (Healos® was coated with BMP2-CaP-PEM8 $\pm$ FGF2).

Figure 4.10 4-week post-surgery microCT 3-D reconstructions **(A, B)**, and microCT cross-sections **(C, D)**, of calvaria implanted with Healos® coated with BMP2-CaP-PEM8 (top panel) and BMP2-CaP-PEM8-FGF2 (bottom panel). BMP-2 dose = 0.5 μg, FGF-2 dose = 125 ng. New bone formation is circled in red and quantified in **(E)**.

Figure 4.11 4-week post-surgery microCT 3-D reconstructions (top panel) and microCT cross-sections (bottom panel) of calvaria implanted with Healos® coated with BMP2-CaP-PEM8 **(A)**, and BMP2-CaP-PEM8-FGF2 with an FGF-2 dose = 0.25 ng **(B)**, 5 ng **(C)**, and 100 ng **(D)**. BMP-2 dose = 0.5 μg. New bone formation is circled in red and quantified in **(E)**. (* $p \leq 0.05$, ** $p \leq 0.01$).

Figure 4.12 3-week post-surgery microCT 3-D reconstructions (top panel) and microCT cross-sections (bottom panel) of calvaria implanted with Healos® coated with bCaP(7)-PEM30 **(A)**,

BMP2-bCaP(7)-PEM8 **(B)**, and BMP2-bCaP(7)-PEM8-FGF2 **(C)**. BMP-2 dose = 2 μg, FGF-2 dose = 5 ng. New bone formation is circled in red and quantified in **(D)**.

List of Abbreviations

-A/-F	no AntiA, no FGF-2
-A/+F	no AntiA, FGF-2
+A/-F	AntiA, no FGF-2
+A/+F	AntiA and FGF-2
AntiA	antimycin A
bCaP	nanocrystalline calcium phosphate made with 24 h in Solution A
bCaP(24)	nanocrystalline calcium phosphate made with 24 h in Solution A
bCaP(48)	nanocrystalline calcium phosphate made with 48 h in Solution A
bCaP(7)	nanocrystalline calcium phosphate made with 7 h in Solution A
BMP-2	bone morphogenetic protein-2
BMP-5	bone morphogenetic protein-5
BMP-6	bone morphogenetic protein-6
BMP-7	bone morphogenetic protein-7
CaP	amorphous calcium phosphate
DAPI	2-(4-amidinophenyl)-1H -indole-6-carboxamidine
DS	dextran sulfate
ECM	extra cellular matrix
EDS	energy dispersive x-ray spectroscopy
EdU	5-ethynyl-2'-deoxyuridine
ELISA	enzyme-linked immunosorbent assay
Factor 1	PEM adsorbed factor to be delivered first
Factor 2	embedded factor to be delivered second

FBS	fetal bovine serum
FDA	Food and Drug Administration
FGF-2	fibroblast growth factor-2
GCSF	granulocyte colony-stimulating factor
GDF-5	growth/differentiation factor-5
HA	hyluronan
IL6	interleukin 6
LBL	layer-by-layer
MC3T3-E1	mouse osteoprogenitor cells
MCSF	macrophage colony-stimulating factor
MSCs	mesenchymal stem cells
OPG	osteoprotegerin
PAA	poly(acrylic acid)
PAH	poly(allylamine hydrochloride)
PDGF	platelet derived growth factor
PDGlut	poly-D-Glutamic acid
PDLys	poly-D-Lysine
PEG	polyethylene glycol
PEM	polyelectrolyte multilayer
PEM102	polyelectrolyte multilayer with 102 bilayers
PEM30	polyelectrolyte multilayer with 30 bilayers
PEM8	polyelectrolyte multilayer with 8 bilayers

PEM^{D}30 polyelectrolyte multilayer made with 30 bilayers of *D*-enantiomer

PLGlut poly-L-Glutamic acid

PLLys poly-L-Lysine

PSS poly(styrene sulfonate)

RANK receptor activator of nuclear factor kappa-β

RANKL receptor activator of nuclear factor kappa-β ligand

RAW RAW 264.7 mouse monocyte-macrophage cells

SBF simulated body fluid

SBFx5 simulated body fluid with 5x normal ionic concentrations

SDF1 stromal cell-derived factor-1

SEM scanning electron microscopy

TCPsb sandblasted tissue culture plastic disk

TGFβ1 transforming growth factor beta-1

TGFβ2 transforming growth factor beta-2

TGFβ3 transforming growth factor beta-3

TNFα tumor necrosis factor alpha

VEGF vascular endothelial growth factor

XRD x-ray diffraction

Chapter 1

Introduction and Specific Aims

1.1 Introduction

We have entered an era of regenerative medicine resulting in new biomimetic coatings and implantable devices focused on not just repairing the injured or diseased tissue, but on stimulating the body's natural tissue regeneration. As a result, new multi-component biomaterial drug delivery systems are being developed to initiate multiple, critical aspects of the natural biological tissue regeneration process, including: infection control [1], as well as recruitment and migration [2], and proliferation and differentiation [3] of progenitor cells. These processes are generally governed by the timely release and exposure to multiple growth factors [4, 5]. Therefore rather than being limited to the delivery of a single growth factor, biomaterial systems are needed to control the release of multiple therapeutic agents at optimized physiological doses, ideally with specific spatiotemporal patterns [6]. This dissertation is focused on the development of a novel, biomimetic, multifactor, sequential delivery system capable of being applied to two-dimensional or three-dimensional substrates; in addition, the delivery system is used to investigate the potential biological benefit of sequential delivery of growth factors to stimulate *in vivo* osteogenesis.

1.1.1 Growth Factors Used in Clinical Trials and Commercial Products

There are a number of growth factors already being clinically investigated to stimulate natural tissue regeneration. These include vascular endothelial growth factor (VEGF, clinical trials) [7-15], fibroblast growth factor-2 (FGF-2, clinical trials) [15-18], bone morphogenetic protein-2 (BMP-2, INFUSE Bone Graft, Medtronic, FDA approved) [19, 20], bone morphogenetic protein-

7 (BMP-7, OP-1 Putty, Stryker, FDA approved) [21, 22], and platelet-derived growth factor (PDGF-BB, GEM 21S, Osteohealth, FDA approved) [23, 24]. VEGF and FGF-2 have been primarily focused on the treatment of cardiovascular diseases, while BMP-2 and BMP-7 have been focused on bone fracture and defect repair, and PDGF-BB was created to enhance periodontal regeneration. To date, no clinical trials in the USA have been conducted on the use of FGF-2 on bone fracture repair, however clinical trials in Japan have shown that local administration of FGF-2 accelerates healing of tibial shaft fractures [25], and stimulates periodontal regeneration [26].

The successful use of growth factors clinically has been very limited. For example, when administered intravenously, VEGF has a half-life of only 30 min [13], resulting in the need for excessive dosing and injections [14, 15]. Excessive VEGF should be avoided because it can lead to pathological vessel formation at non-target sites [27]. BMP-2 delivered via a collagen sponge (INFUSE Bone Graft, Medtronic, FDA approved) significantly enhances bone formation and successful spinal fusion [28]; however its use has been limited due to complications with the required high dose of BMP-2 necessary for adequate bone formation. It only takes nanogram quantities of BMP-2 per gram bone matrix to trigger the bone repair cascade, however microgram quantities of BMP-2 per gram of the matrix material are required to produce adequate bone formation [4, 29]. These complications include severe inflammation, ectopic bone formation, osteolysis, seroma formation, and possible increase in the risk of malignancy, [19, 30]. These problems stem from the collagen sponge's inability to contain the supraphysiologic dose of BMP-2 in the local tissue environment.

Healos® is a commercially available bone graft substitute made of type I collagen fibers with a hydroxyapatite coating (DePuy Synthes Spine, Raynham, MA). Healos® has been

investigated for the delivery of human growth/differentiation factor-5 (GDF-5) [31, 32], and BMP-2 [33] to aide in bone regeneration. Again the success of these approaches has been limited. Gohil et al. discovered that delivery of BMP-2 from Healos® was not confined to the site of BMP-2 implantation and significant bone formation was observed in the neighboring defect site [33].

It is postulated that the reason the clinical use of growth factors and their combination with commercial scaffolding materials have unwanted side effects is because the delivery approaches employed lack any control over release. These factors were intravenously administered [14-16] or were adsorbed as a bolus dose of growth factor to a scaffolding material [19-22]; because these methods lack controlled release, supraphysiologic, excessive, doses need to be used to obtain the desired therapeutic effect. This is because a significant portion of the administered growth factor will diffuse away from the implantation site and be degraded via denaturation, oxidation or proteolysis [34, 35]. If the growth factor manages to remain active, the diffusion can lead to off-target, unwanted side effects [19, 27, 30, 33]. These unfavorable outcomes emphasize the need to develop a way to not only reduce the concentration of growth factor necessary to obtain a therapeutic effect, but to also develop biomaterials capable of controlling the release and delivery of these growth factors.

1.1.2 Biology of Bone Repair

Bone repair and regeneration involves the combination of cells, bioactive factors and extracellular matrix to stimulate the proliferation, differentiation and migration of osteoprogenitor cells [5, 36, 37]. Fracture healing can occur in two ways, primary (direct) fracture healing, or secondary (indirect) fracture healing. Primary fracture healing requires rigid fixation and leads to the regeneration of bone structure without remodeling steps. The majority

of bones heal through secondary (indirect) fracture healing which consists of both endochondral and intramembranous bone healing [38]. Secondary fracture healing involves the following stages: hematoma formation, inflammation, callus formation, revascularization, mineralization and resorption of the callus, and bone remodeling [39]. After fracture, the hematoma will form within hours and begin the acute inflammatory stage that typically lasts around 3 days. This step is critical to bone healing because the hematoma initiates the signaling cascade that leads to successful bone formation [39, 40]. Inflammatory cells, including monocytes, will migrate into the extra cellular matrix (ECM) of the hematoma from the ruptured blood vessels and bone marrow cavity. Mesenchymal stem cells (MSCs) will be recruited to the fracture site when cells within the hematoma release signaling molecules such as interleukin 6 (IL6), tumor necrosis factor alpha (TNFα), granulocyte colony-stimulating factor (GCSF), stromal cell-derived factor-1 (SDF 1), and macrophage colony-stimulating factor (MCSF) [41]. The source of MSCs is an area of active investigation, however it is believed that they derive from the bone marrow and periosteum, and possibly bone lining cells [42].

During the first few days of fracture healing granulation tissue is formed within the defect where cartilaginous tissue will then form (soft callus) around days 7-10 and serve to aid in fracture stabilization [43] (endochondral ossification); simultaneously, an intramembranous ossification response occurs at the proximal and distal ends of the fracture adjacent to the periosteum, generating a hard callus [38]. During this time chondrocytes will undergo hypertrophy and the cartilaginous callus will calcify. Concurrently, blood vessels will penetrate the chondrogenic tissue, bringing with them mesenchymal progenitors that initiate cartilage replacement with woven bone [38]. During this time, collagen type I and II matrix production increases, and expression of members of the transforming growth factor-β superfamily (TGF-β2,

-β3, GDF-5, BMP-2, -5, and -6) which are involved in cell proliferation and differentiation, will elevate [44, 45]. Vascular endothelial growth factor (VEGF), known to be highly expressed in hypertrophic chondrocytes, is considered a key regulator in the transformation of the cartilaginous matrix into vascularized osseous tissue [46]. The osseous matrix, or hard callus, will then gradually be replaced with woven bone via osteoclast resorption of the hard callus. This stage of fracture repair is associated with expression of collagen type I, osteocalcin, and alkaline phosphatase [47], and relies on key regulators of bone homeostasis such as receptor activator of nuclear factor kappa-β ligand (RANKL), receptor activator of nuclear factor kappa-β (RANK) and osteoprotegerin (OPG) [48, 49]. During the remodeling phase, woven bone will be resorbed by osteoclasts and replaced by lamellar bone via osteoblasts, leading to the mechanical and biological restoration of bone function [38].

In the present studies, a critical-sized calvarial defect mouse model was selected for the *in vivo* experiments, which also heals through secondary (indirect) bone formation. Contrary to callus formation and subsequent endochondral ossification, which is the main mechanism of secondary (in direct) fracture healing described previously, calvarial defects repair and regenerate in a slightly different way with their main mechanism of bone healing being intramembranous ossification. Intramembranous ossification is a more direct method of bone formation that skips the cartilaginous steps associated with endochondral ossification. During intramembranous ossification, inflammatory cells and MSCs will first be recruited to the defect site. The MSCs will replicate and condense into compact nodules committing themselves as osteoprogenitor cells. These cells will differentiate into osteoblasts and secrete a collagen-proteoglycan matrix that is able to bind calcium salts [50], and are associated with the expression of type 1 collagen, bone sialoprotein and osteocalcin [51]. Through this binding, the matrix

becomes calcified with the enzyme alkaline phosphatase playing a key role [52]. As calcification proceeds bony spicules will radiate out from the region where ossification began. During this process some osteoblasts will become trapped within the bony pockets and will then differentiate into osteocytes or mature bone cells [52]. Over time, the defect will be filled with spongy bone that will continually be remodeled through the combined action of osteoblasts and osteoclasts. At this point new bone formation is slowed and the compact MSCs surrounding the area of new bone formation will form the periosteum [50]. The mechanism of intramembranous ossification is primarily controlled through fibroblast growth factors (FGFs), with FGF-2 and FGF-18 being considered most important for calvarial regeneration [51], bone morphogenetic proteins (BMPs), and the transcriptional factor core-binding factor alpha (1) (Cbfa1). Cbfa1 is considered to play a critical role during BMP-induced osteoblastic differentiation [53]. In addition it has been shown that BMPs act in concert with FGFs to control calvarial growth, development, and regeneration [54] and will be further discussed in the following section.

Considering the important roles of osteoprogenitors and osteoblasts on bone regeneration, a mouse osteoprogenitor/pre-osteoblast cell line, MC3T3-E1s, was selected for our *in vitro* assays to screen the effectiveness of the biomaterial to provide sequential, multifactor, cell-mediated delivery. In addition to the osteoprogenitors, monocytes and osteoclasts are two other cell types that play a vital role in bone regeneration and fracture healing. As new bone matrix is deposited by osteoblasts on the outer surface of new bone, subsequent resorption of bone matrix on the inner surface is accomplished via osteoclasts. Osteoclasts are multinucleated cells that are derived from the same precursors as monocytes. These monocytes enter the healing defect site through the blood vessels and will differentiate into osteoclasts in the presence of RANKL, which is secreted by the osteoprogenitor cells already present in the defect [55]. The osteoclasts

are capable of dissolving both the inorganic and the protein portions of the bone matrix. They accomplish this by extending their cellular processes into the matrix and pumping out hydrogen ions into the surrounding material, thereby producing an acidic environment that can dissociate the mineralized matrix [50]. The combined action of osteoblasts and osteoclasts must be tightly regulated for bone fracture healing and normal bone maintenance, therefore the cells and their precursors can act on each other. In addition to secreting RANKL and colony-stimulating factor both promoting osteoclast differentiation [56], osteoprogenitors can also secrete osteoprotegerin, deterring the differentiation of osteoclasts [55]. FGF-2 (provided from macrophages, MSCs and osteoblasts [36]) can increase the formation of osteoclast-like cells [57] and activate mature osteoclasts [58]. The actions and effects of all of these cell types are important to consider when developing a biomaterial to enhance bone regeneration, therefore a mouse monocyte cell line, RAW 264.7s, was selected to also screen the effectiveness of the biomaterial to provide sequential, multifactor, cell-mediated delivery *in vitro*.

1.1.3 Growth Factors Involved in Bone Repair and Regeneration

One focus of the research conducted in this dissertation was to use a biomaterial to deliver multiple growth factors to stimulate the production of osteoblasts to produce new mineralized bone tissue. This involves first the recruitment to, and commitment of mesenchymal stem cells to the osteoblast lineage making them osteoprogenitors, followed by the proliferation of the osteoprogenitors, and then differentiation of the osteoprogenitors into functioning osteoblasts [59]. There are a number of growth factors involved in bone regeneration, but the major factor families involved with proliferation and differentiation of osteoprogenitors are fibroblast growth factors, transforming growth factor-βs, and bone morphogenetic proteins [36].

Bone morphogenetic proteins (BMPs) are the main growth factors responsible for the differentiation of osteoprogenitor cells into functioning osteoblasts [36]. BMP-2, -4, and -7 have all been investigated for bone regeneration, however, it has been suggested that BMP-2 may be more osteoinductive compared to other BMPs [60]. BMP-2's use clinically was the result of its extensive investigation *in vivo* in a variety of animal models; BMP-2 has been shown to stimulate bone regeneration in rats [61-63], rabbits [64, 65], dogs [66, 67], sheep [68, 69], and monkeys [65]. Because of its proven effectiveness at regenerating bone *in vivo*, and it use clinically, BMP-2 was selected as one of the growth factors to be delivered in the present studies.

There are twenty-two members to the fibroblast growth factor family [36], however fibroblast growth factor-2 (FGF-2) has been studied most for use in bone fracture healing. This is because FGF-2 is known stimulator of osteoprogenitor proliferation [70] and plays an important role in maintaining bone mass [71]. FGF-2 has been shown to accelerate fracture healing via increasing callus size, mineral content, and mechanical strength of the healing defect site [72-75]. The Fgf2 gene is expressed during all stages of the fracture repair process [76], and its receptor (Fgfr2) is specifically expressed at sites of intramembranous ossification in differentiating osteoblasts [77]. Besides its clear involvement in bone fracture healing, FGF-2 was selected for use in the present studies because of its synergistic effects when used with BMP-2. FGF-2 has been demonstrated to increase the BMP-2 sensitivity of osteoprogenitor cells [78, 79] via up-regulating BMP-2 levels and BMP-2 receptor expression [80, 81]. Recently, low concentrations of BMP-2 were shown to enhance calvarial defect repair in mice overexpressing FGF-2 in osteoprogenitor cells [82], suggesting FGF-2 can augment BMP-2-induced bone repair [83]. These findings lead to the hypothesis that the combined use of FGF-2 and BMP-2 could

decrease the supraphysiologic dose of BMP-2 necessary to stimulate bone formation, thereby decreasing the unwanted, off-target side effects that are associated with BMP-2's clinical use.

1.1.4 Optimizing FGF-2 and BMP-2 for Bone Healing

There have been several studies investigating the combined use of FGF-2 and BMP-2 on *in vitro* and *in vivo* osteogenesis [84-101]. At first glance, the results of these studies have been somewhat contradictory. For the most part, the combined use of FGF-2 and BMP-2 has been reported as stimulatory and synergistic. However there are many examples where their combined use has been reported as inhibitory on osteogenesis [84, 86, 93, 95, 96, 100, 102]. There are many factors to consider when combining growth factors. For example, Charles et al. observed that the co-delivery of FGF-2 and BMP-2 in a mouse calvarial defect model was not stimulatory on *in vivo* osteogenesis over BMP-2 alone in young adult mice; however, the co-delivery of both factors did in fact aid in new bone formation when tested in old mice [84]. There have also been examples where the combined use of FGF-2 and BMP-2 resulted in both stimulatory and inhibitory results [86, 93, 96]. In these studies it was found when combining high doses of FGF-2 (μg quantities) with BMP-2 it was inhibitory, where as low doses of FGF-2 (ng quantities) with BMP-2 tended to be stimulatory. The relative dosing of BMP-2 to FGF-2 also seems to be important. Wang et al. reported that ratios 8:1, 4:1, and 2:1 (BMP-2: FGF-2) were all stimulatory for *in vitro* and *in vivo* osteogenesis, however 2:1 produced the best outcomes [103]. For the examples where both stimulatory and inhibitory results were reported, ratios of 5:1 to 500:1 stimulated osteogenesis, where ratios of 1:1 and 1:25 were inhibitory [86, 93, 96], suggesting the FGF-2 dose should be low compared to the BMP-2.

Besides dosing and taking into account the osteogenic potential of the model/cells being used (young vs. old), sequence of delivery is crucial to the success of the combined use of FGF-2

and BMP-2. The best chance of success when using multiple growth factors is to mimic the natural tissue regeneration process. Growth factors have different effects on tissue regeneration depending on the developmental stage of the healing process they are present during. As previously mentioned FGF-2 has proliferative effects on osteoprogenitors (early), and BMP-2 is the key factor involved in osteoprogenitor differentiation (late). All of the inhibitory examples previously mentioned were co-delivery [86, 93, 95, 96, 100, 102]. *In vitro* studies have demonstrated that spiking first FGF-2 in cell culture medium, and then BMP-2 can increase osteogenesis over co-delivery of both factors and/or single factor delivery [85, 88, 90, 91]. BMP-2 delivered too early, or before FGF-2 has been shown to be inhibitory [89, 104]. These results stress the need for new biomaterials to biomimetically deliver multiple growth factors in a sequential manner to maximize their stimulatory effects.

1.1.5 Material Approaches for Growth Factor Delivery for Bone Regeneration

A successful growth factor delivery biomaterial will maintain therapeutic concentrations of growth factor at the application site in a spatiotemporal pattern that mimics natural bone regeneration. There are two main approaches for the delivery of growth factors from biomaterials: 1) physical encapsulation of the growth factors in the delivery system, and 2) chemical immobilization of the growth factors to the matrix/substrate. Physical encapsulation relies on both the diffusion of the growth factor out of the material and degradation rate of the material; chemical immobilization relies on chemical binding or affinity interactions between the growth factor and the substrate [4, 5, 27]. There are pros and cons to each approach.

Chemical immobilization incorporates a variety of techniques to conjugate growth factors directly to a scaffold or biomaterial. The simplest approach to delivering growth factors for bone regeneration involves the adsorption of growth factors directly to a scaffold through non-

covalent binding (surface adsorption, ionic complexation) [5, 105]. As previously mentioned, surface adsorption approaches can result in rapid release of the growth factor and an inability to contain the growth factor to the local tissue environment due to diffusion away from the implant site [19, 30, 33]. On the contrary, when growth factors have a high affinity for the biomaterial, release tends to be limited. For example, BMP-2 has a high affinity for calcium phosphate/hydroxyapatite type materials; *in vitro* release from these types of materials is usually very low (10-30%) [84, 106-108]. However, this is not necessarily undesirable; the high affinity to the scaffold material means the growth factor is readily available for cells to come into contact with the scaffold, providing a highly localized delivery [27, 109, 110]. Covalently immobilizing the growth factor to the scaffold can provide more prolonged release. This is because if the growth factor remains active after covalently tethering it to the biomaterial or scaffold then it will still activate the growth factor receptors on the cells, but it will be more slowly degraded and internalized [27]. A drawback to this approach is that covalently immobilizing the protein to the scaffold can result in conformation changes to the growth factor's functional groups, resulting in its inactivation [111].

Physical encapsulation approaches include use of polymeric vehicles, hydrogels, and particles for delivery of growth factors. Polymers are advantageous for growth factor delivery because depending on the method of growth factor incorporation, release rate can be controlled by processes such as diffusion, charge interactions, erosion and degradation of the polymer, swelling of the polymer, or dissolution [112, 113]. Disadvantages to polymer delivery include denaturing and deactivation of proteins resulting from the encapsulation processes that usually require the use of harsh solvents, cross-linking agents and high temperatures [4].

A way to physically entrap growth factors but to avoid high temperatures and harsh solvents is to utilize hydrogels [114]. Hydrogels are highly hydrated networks of cross-linked polymer chains formed from natural (collagen and hyaluronic acid), synthetic (polyethylene glycol) or semi-synthetic polymer backbones [115]. Growth factor delivery from hydrogels depends on the physiochemical properties of the polymer structure and the bioactive factor, and control over the growth factor delivery is usually dependent on the type and density of cross-linkers [5]. A variety of materials have been used to produce hydrogels for single osteoinductive factor delivery including alginate [116, 117], gelatin [118, 119], fibrin [120], hyaluronic acid [79], and polyethylene glycol (PEG) [121]. Increasing the amount of cross-linking will decrease the degradation of the hydrogel and slow the release rate of the incorporated factor. For example, *in vitro* and *in vivo* BMP-2 release from hydrogels was found to directly correlate to the density of cross-linkers and water content within the scaffold (cross-linkers released BMP-2 through hydrolysis) [120, 122, 123]. A con to the use of hydrogels is that growth factor release is typically dependent on cross-linking; increasing the extent of cross-linking reduces the cyto-compatibility of the hydrogel and can deactivate incorporated proteins [5]. Hydrogels are also limited to only being able to provide one rate of release at a time; therefore their use for multifactor delivery is limited to co-delivery. Simmons et al. showed they could vary the degradation rate of their alginate hydrogel, therefore they could vary the release of rate of their incorporated factors either individually, or in combination, but they could not sequentially deliver the growth factors in combination [124].

A way to vary the release rates of multiple growth factors from a hydrogel is to make a composite material via the addition of particles to the hydrogel and/or scaffold with each component containing a different factor. Encapsulation of growth factor via a micro- or

nanoparticle [125-129], or liposome [130] is a strategy commonly employed to provide sustained release and retain growth factor activity. Encapsulating a growth factor into a particle, then incorporating those particles into a hydrogel that also has an entrapped growth factor, is way to achieve two distinct release profiles for a multifactor delivery system [131, 132]. Sequential delivery from a system such as this is still difficult to achieve; this is because release of the particles from the hydrogel and release of the entrapped growth factor from the hydrogel are occurring simultaneously, but at different rates. For true, sequential delivery, delayed release or delivery for at least one growth factor must be achievable through the biomaterial.

1.1.6 Polyelectrolyte Multilayer Films

A popular biomaterial strategy for multifactor delivery is the use of polyelectrolyte multilayer (PEM) films. PEM is a layer-by-layer (LBL) build-up of oppositely charged polyelectrolytes, a polyanion (-) and polycation (+), to form a thin film. PEM films were first introduced 20 years ago by Moehwald, Decher, and Lvov [133, 134] in attempts to produce thin films that could be used in biomedical applications to make surfaces more functionalized and render them more biomimetic. In the first 10 years of their introduction PEM films were only used in proof-of-concept studies producing films containing small charged species such as biological molecules (polypeptides, polysaccharides, DNA, proteins, viruses) and various kinds of nanoparticles [135]. It was not until 2001 when the first study with a PEM film was used to observe the behavior of cells interacting with the coating [136]. In the past ten years, possibilities for the spatiotemporal control over cell growth and the use PEM films *in vivo* has been investigated [137].

As mentioned, PEM films are formed by alternately depositing oppositely charged polyelectrolyte that self-assemble and self-organize on a substrate's surface. For the most part

the LBL build up of PEM films relies on the electrostatic interactions between the polyelectrolytes, however non-electrostatic interactions, including hydrophobicity [138], hydrogen bonds [139], Van der Waals forces, halogen interactions [140], and covalent bonding [141] can influence the architecture of the film. The most common PEM application method is to dip coat the substrate [137], i.e. dip the substrate into the polyanion solution, rinse, dip into the polycation solution, rinse, etc.; however, PEM can also be applied via spray coating [142] or spin coating [143]. Dip coating requires rinse steps between polyelectrolyte application because the excess solution needs to be completely removed before application of the next polyelectrolyte otherwise the PEM will precipitate in solution rather than depositing onto the substrate as the next layer; spray coating removes the need of excess solution, therefore rinse steps can be skipped and accelerate the PEM application process [142].

The growth of PEM films via LBL build up can be linear or exponential depending upon the polyelectrolytes used in the film. The original development of PEM films showed linear growth of film thickness with increasing number of layers deposited, and this growth is typical with use of polyelectrolytes such as poly(styrene sulfonate) (PSS) and poly(allylamine hydrochloride) (PAH) [144]. More recently exponential growth of film thickness with increasing number of layers deposited has been described with use of polyelectrolytes such as poly-L-Lysine (PLLys), alginate, and hyluronan (HA) [145, 146]. PEM films made up of polyamino acids and polysaccharides tend to result in exponential film growth [137], however even some synthetic polyelectrolytes such as polyacrylic acid (PAA) will also grow in this manner [147]. The use of natural polyelectrolytes, such as polyamino acids and polysaccharides, is desirable because these materials are biomimetic and have better biocompatibility *in* vivo. Exponential growth of PEM coatings is a result of “in and out” diffusion of the polyelectrolytes

[146]. As the film is exposed to a polyanion (-) solution, the polycation (+) within the film will diffuse to the surface allowing for more binding sites for the polyanion. Vice versa will occur during the next step when the polycation solution is being applied. This results in thicker and thicker layers of PEM being applied with each subsequent step. In addition to the type of polyelectrolytes used, molecular weights of the polyelectrolytes can influence the "in and out" diffusion occurring within the film, thus influencing the exponential growth of the PEM film. Increasing the molecular weight of both synthetic polyelectrolytes (PAA in PAH/PAA film) [148] and natural polyelectrolytes (PLLys in PLLys/HA film) [149] restrained the ability of these polyelectrolytes to diffuse within the film.

The inter-diffusion of polyelectrolytes is now considered a "dominant" process involved with the use of PEM films, and this phenomenon is critical for understanding loading and release kinetics of bioactive molecules deposited into the films [137]. One of the most attractive features of PEM systems in their ability to retain the bioactivity of molecules incorporated into the films and to act as a reservoir for delivery of small molecules [150]. The layer-by-layer assembly technique allows for easy control over the order of which small molecules are incorporated into the film, and because the molecules are directly integrated in the architecture of the film via electrostatic interactions and do not require covalent bonding [151, 152], their secondary structures remain close to their native form and this retains their biological activity [111]. Because the incorporated molecules rely on electrostatic interactions within the PEM films, they too will diffuse throughout the PEM film during exponential film growth. Vodouhe et al. showed that a fluorescently labeled molecule purposely adsorbed within one location of a PLLys/HA film, ultimately could be observed throughout the entire thickness of the film [153]. For single factor delivery from PEM films, this can be considered a desirable effect of the film

growth because the PEM now serves as a reservoir for the molecule. In the same study, it was shown that increasing the film thickness increased the amount of drug that could be loaded into the PLLys/HA film [153].

Issues with the exponential growth of PEM films become a problem when multiple small molecules are being incorporated into the film and the sequence of their release is trying to be controlled. Multiple factors can be adsorbed into PEM films at specific locations within the films but the "in and out" diffusion that occurs during the build up of the film will result in a blended architecture lacking controlled order, therefore resulting in uncontrolled delivery [154]. To prevent interlayer diffusion of molecules through exponentially growing PEM films, "blocking layers" can be added to act as barriers within the films. These can include cross-linking layers within the film [147], using slowly degradable polymers such as poly(lactic-co-glycolic acid) within the film [155], or introducing a third component into the PEM film that acts as a physical barrier [156, 157]. The only way to achieve multifactor, sequential delivery from PEM films made with exponentially growing, biocompatible, polyelectrolytes is to prevent interlayer diffusion within the film.

The use of PEM films by themselves has been shown to aid in the biocompatibility of titanium implants interacting with osteoblast cells [158, 159]. In addition, individual and combinations of bioactive growth factors have been successfully delivered from PEM systems, including osteogenic factors such as FGF-2, TGFβ1, and BMP-2, and retained their bioactivity [160-167]. It was therefore decided that a PEM system could be developed for delivery of FGF-2 and BMP-2 in hopes to stimulate osteogenesis for enhanced bone regeneration.

1.2 Specific Aims

The goal of the research is to develop a biomaterial capable of sequential delivery of multiple, biologically active factors. The long-term goal is to develop a material that can sequentially deliver low dose FGF-2 and BMP-2 and be applied to a commercially available bone graft substitutes to enhance *in* vivo osteogenesis and potentially overcome clinical complications with high dose BMP-2. The successful biomaterial will deliver FGF-2 during the first few days of fracture healing, then deliver BMP-2; inflammation and osteoprogenitor recruitment/proliferation need to subside before delivering the differentiation agent from the biomaterial. The novelty of this work is the incorporation of a biomimetic calcium phosphate (bCaP) barrier layer into poly-L-lysine/poly-L-glutamic acid PEM design to prevent interlayer diffusion of growth factors resulting in a sequential, multifactor, bioactive delivery system that can be applied to two-dimensional (2-D) and three-dimensional (3-D) substrates. It is hypothesized that: ***If bCaP barrier layer can prevent diffusion of multiple factors within a PEM coating, then sequential delivery of factors can be achieved from a bCaP-PEM coated biomaterial.*** This objective will be completed with the following specific aims:

Aim 1: Develop a biomimetic calcium phosphate-polyelectrolyte (bCaP-PEM) coating for sequential, multifactor delivery *in vitro*. *Hypothesis: If bCaP barrier layer can prevent diffusion of multiple factors within a PEM coating, then sequential delivery of factors can be achieved from bCaP-PEM.* Simulated body fluid (SBF) methods have been developed to form bCaP coatings on tissue culture plastic disks [168] that were utilized to achieve this aim. bCaP coatings are expected to provide a biocompatible barrier layer within the PEM design. Scanning electron microscopy (SEM), energy-dispersive x-ray spectroscopy, and x-ray diffraction were used to assess the morphology, composition, and structure the bCaP layer before and after PEM

application. To demonstrate sequential delivery a combination of a proliferative factor (FGF-2) and a cytotoxic factor (antimycin A) with opposing effects on MC3T3-E1 mouse calvarial osteoprogenitor cells were adsorbed into the coating to clearly demonstrate when cells were accessing the incorporated factors. Proliferative and cytotoxic effects were quantified using LIVE® staining (Invitrogen Life Technologies, Grand Island, NY) and ImageJ analysis. Release studies were conducted to determine if factors were released from the bCaP-PEM coating via diffusion.

Aim 2: Demonstrate *in vitro*, cell-mediated delivery kinetics of multiple factors from the bCaP-PEM coating can be tuned by altering the structure/composition of the coating or changing the cell type used with the coating. *Hypothesis: If delivery of the embedded factor is a function of coating thickness, then delivery kinetics of that factor can be further delayed by thickening the bCaP layer within the coating.* Tunable delivery kinetics were assessed using the same MC3T3-E1 proliferation studies on coatings prepared with alterations made to the bCaP layer by increasing or decreasing time in the SBF solutions resulting in a thinner or thicker layer. Alternations to the PEM portion of the coating were also investigated to tune delivery kinetics of the incorporated factors via increasing the number of PEM bilayers and/or the use of *D*-enantiomers polyelectrolytes. Additionally, delivery kinetics were assessed using RAW 264.7 mouse macrophage cells to determine how cell type can change the cell-mediated degradation/delivery of the coating.

Aim 3: Characterize bCaP-PEM coating applied to 3-D scaffolds, and determine the effects of sequential delivery of FGF-2 and BMP-2 on *in vivo* osteogenesis. *Hypothesis: If sequential delivery of low dose FGF-2 and BMP-2 is a beneficial method of stimulating bone formation, then sequential delivery vs. co- or single factor delivery will result in increased in vivo*

osteogenesis. The Kuhn lab previously demonstrated that sequential delivery of low dose FGF-2, followed by BMP-2 enhanced *in vitro* osteogenesis over co- or single factor delivery [88], therefore it is expected that this delivery sequence from bCaP-PEM would stimulate *in* vivo osteogenesis. SEM was used to access surface morphology and coating application of the bCaP-PEM coating applied to a commercially available bone graft substitute scaffold. Sequential delivery of first FGF-2, then BMP-2 from bCaP-PEM applied to a scaffold was evaluated using an *in vivo* mouse calvarial defect model. New bone formation 3-4 weeks post-surgery was assessed using x-ray and microCT. Sequential delivery was compared to BMP-2 only delivery and the scaffold with no coating.

Chapter 2

Biomimetic Calcium Phosphate/Polyelectrolyte Multilayer Coatings for Sequential Delivery of Multiple Biological Agents

2.1 Introduction

New multi-component biomaterial drug delivery systems are being developed to initiate multiple, critical aspects of the natural biological tissue regeneration process, including: infection control [1], as well as recruitment and migration [2] and proliferation and differentiation [3] of progenitor cells. These processes are governed in the body by the timely release and exposure to multiple growth factors [27, 36]. Therefore rather than being limited to the delivery of a single growth factor, biomaterial systems are needed to control the release of multiple therapeutic agents at optimized physiological doses, ideally with specific spatiotemporal patterns [6].

Several different types of delivery systems for multiple growth factors have been developed as potential therapeutics for wound healing/infection, bone, cartilage, muscle, teeth and cancer, and have shown some efficacy both *in vitro* [1, 88, 131, 169, 170], and *in* vivo [101, 167, 171]; however, their success has been limited. The drawback of these systems, including microspheres [1], nanoparticles [169], and hydrogels [131, 171] is their co-delivery of factors. Growth factors have different effects on natural tissue regeneration depending on the developmental stage of the healing process they are present during; therefore, sequence of delivery is important to optimize growth factor activity and healing.

A popular biomaterial strategy for multifactor delivery of growth factors or other biologically active molecules incorporates the use of polyelectrolyte multilayer (PEM) films. PEM is a layer-by-layer (LBL) build-up of oppositely charged polyelectrolytes, a polyanion (-)

and polycation (+). These PEM films offer a means of temporal regulation of bioactive factors without loss of their biological activity [150]. In addition, the release kinetics of factors from PEM can be adjusted by alternating number of layers within the film, changing the type of polyelectrolytes [154], or introducing a third component/barrier layer [156, 157]. PEM can also be applied to two dimensional or three-dimensional porous, intricate substrates and scaffolds as thin films making PEM applications versatile. The layer-by-layer PEM delivery system is now widely being used for co-delivery of multiple factors; however, controlled, sequential delivery from PEM coatings has been limited due to problems associated with interlayer diffusion of incorporated factors within PEM [146, 154, 167].

The novelty of the present study is the introduction of a biomimetic calcium phosphate (bCaP) barrier layer into a poly-L-Lysine (PLLys) and poly-L-Glutamic acid (PLGlut) PEM design. Calcium phosphate was chosen because of its biocompatibility, low cost, and ease of manufacture. It was hypothesized that if the bCaP layer could prevent interlayer diffusion of biological agents, then controlled, sequential delivery of multiple factors would be achieved. This chapter reports the fabrication and characterization of bCaP-PEM coatings and the *in vitro* assessment of the sequential delivery kinetics and bioactivity of two factors with opposing activity (proliferative vs. cytotoxic) delivered from bCaP-PEM coatings. MC3T3-E1 osteoprogenitor cells were used for the cell culture evaluation assays and biological assays were selected because they provide important information about the potential response of host progenitor cells to implanted materials coated with bCaP-PEM.

2.2 Materials and Methods

2.2.1 Design of the Sequential Delivery System

To prevent the issue of interlayer diffusion of multiple factors associated with a PEM-only coating (Fig. 2.1A), a biomimetic calcium phosphate layer (bCaP) was incorporated into a PLLys-PLGlut PEM system, (Fig. 2.1B). It is hypothesized that because of interlayer diffusion, a PEM only coating would result in co-delivery (Fig. 2.1C), but introducing bCaP into the delivery system would result in sequential delivery of multiple factors (Fig. 2.1D).

2.2.2 Material Fabrication

2.2.2.a Preparation of Biomimetic-CaP Disks

Twenty-two mm diameter plastic disks (NUNC, Rochester, NY) were sandblasted with 240-grit aluminum oxide powder (Ivoclar Vivadent, Amherst, NY) to obtain a roughened surface (TCPsb). Both sides were roughened. The sandblasted disks were cleaned by ultra sonication in water and UV-sterilized prior to coating.

A two-step simulated body fluid (SBF) biomimetic calcium phosphate coating (bCaP) protocol originally developed for metal substrates [118, 172-174] and modified for plastic disks by the Kuhn lab [168], was utilized to form the bCaP layer. The coating procedure involves immersion and incubation in two different solutions (Table 2.1): Solution A results in a thin amorphous layer of CaP, Solution B, with less inhibitors of apatite formation, results in the formation of mature apatite crystals as a second layer above the amorphous layer. Coatings were prepared with either just solution A (CaP) or solutions A and B (bCaP). All reagents (Sigma-Aldrich) were used as received.

To prepare Solution A, the inorganic salts in the following order were weighed and dissolved in 800 ml sterile filtered MIlliQ water maintained at 37 ± 0.1°C with stirring: NaCl (32.0 ± 0.001 g), $MgCl_2$, $6H_2O$ (1.216 ± 0.001 g), $CaCl_2$, $2H_2O$ (1.472 ± 0.001 g). The pH was lowered to 4 by bubbling CO_2 gas through the solution at a steady flow for about 5 min. Then Na_2HPO_4, $2H_2O$ (0.712 ± 0.001 g) and $NaHCO_3$ (1.408 ± 0.001 g) were dissolved and CO_2 gas was continually bubbled through the solution until the pH was below 6.2. At this point the solution was spilt in half between two smaller beakers (heated to 37°C), both capable of submerging three custom-made sample holders, each designed to hold 6 disks vertically, about 1 mm apart. Vertical positioning was used to avoid the unwanted settling and attachment of any large homogeneously nucleated particles on the disks [175]. The beakers were sealed with saran wrap with 20–30 small holes in it to allow for gradual CO_2 release, thus restricting homogeneous nucleation/solution precipitation that occurs without a cover, and promoting the formation of the thin amorphous CaP layer directly on the substrate disks. Each beaker was equipped with a stir bar and was placed in a 37°C oven on a stir plate set to match the mixing during the solution preparation (~130 rpm). After approximately 24 h, the samples were sonicated briefly in the reacted Solution A. Prior to immersion in Solution B, the disks were gradually dehydrated by being passed through a graded series of increasing concentrations of ethyl alcohol.

To prepare Solution B, NaCl (32.0 ± 0.001 g), $MgCl_2$, $6H_2O$ (0.240 ± 0.001 g), $CaCl_2$, $2H_2O$ (1.472 ± 0.001 g) were dissolved in 800 ml MilliQ water maintained at 50 ± 1°C followed by CO_2 gas bubbling to obtain a pH below 4.0. Na_2HPO_4, $2H_2O$ (0.712 ± 0.001 g) and $NaHCO_3$ (0.704 ± 0.001 g) were added and CO_2 gas was bubbled through the solution until supersaturation at a pH of 5.8–6.2 was reached. The solution was then split, the disks were immersed, and the beakers sealed as before to limit homogeneous nucleation, and placed in a

50°C oven. The process was allowed to proceed for at least 24 h with stirring, until the pH was ≥ 7.8 at which time the samples were removed, sonicated briefly in the reacted Solution B, then dehydrated in a series of graded ethanol. The samples were stored in a desiccator until further use.

2.2.2.b Polyelectrolyte multilayer application

The PEM coatings were applied to the sandblasted plastic disks, CaP- and/or the bCaP-coated disks by alternate 10 min dippings into 1 mg/ml poly-L-Glutamic acid (PLGlut-) or poly-L-Lysine (PLLys+) solutions (Sigma, St. Louis, MO), with seven saline rinses between each. This dip-coating process was automated with the use of a histology-staining machine (Varistain 24-4, Thermo Shandon, Loughborough, UK) and custom designed sample holders. Eight or thirty bilayers (PLLys-PLGlut = 1 bilayer) were adsorbed on top of the disks. The coated disks were UV-sterilized on both sides prior to cell culture.

2.2.2.c Factor Application

To demonstrate the ability of bCaP addition to PEM to prevent diffusion and delay access to an embedded factor, a model cytotoxic agent antimycin A (AntiA) (213 μg/disk) (Sigma, St. Louis, MO) was used. Prior to bCaP and/or PEM application, 10 μl of 40mM AntiA in ethanol (213 μg/disk) was adsorbed onto the sandblasted plastic surface, and allowed to dry; since AntiA was allowed to completely dry to maximize binding. The disks were rinsed 3x with saline before coating application. During the coating application the disks were protected from light.

To demonstrate sequential delivery from the bCaP-PEM coatings, a combination of a proliferative factor, recombinant human fibroblast growth factor-2 (FGF-2) (150 ng/disk) (R & D Systems, Minneapolis, MN), and the cytotoxic AntiA was used. The AntiA (213 μg/disk) was

embedded beneath the coating. After AntiA adsorption, bCaP and PEM30 application, 375 ng/ml FGF-2 in saline was allowed to adsorb to the coated disks for 1hr, then rinsed 3x with saline. Enzyme-linked immunosorbent assay (ELISA, R&D Systems, Minneapolis, MN) testing was performed and determined approximately 80% FGF-2 binds, (actual adsorbed dose ~120 ng/disk).

The coating procedure is summarized in Figure 2.2 including factor application, calcium phosphate deposition, and PEM adsorption. Factor 1 represents FGF-2, the factor to be delivered first, and Factor 2 represents AntiA, the embedded factor to be delivered at a later time point.

2.2.3 Characterization

2.2.3.a Scanning Electron Microscopy (SEM)

One CaP, bCaP, bCaP-PEM, and PEM coated disks from 3-6 different batches were examined to characterize surface morphology and consistency. The microscopic morphology was characterized using SEM (JSM - 5900LV, Jeol USA Inc. Peabody, MA). Disks were cut in half, allowing examination of the coating cross-section and measurement of the coating thickness in multiple locations.

2.2.3.b Energy Dispersive X-Ray Spectroscopy (EDS)

The elemental composition and Ca/P ratio of the bCaP coatings before and after PEM application were determined with energy dispersive X-ray spectroscopy (FEI Teneo LVSEM and EDAX SDD EDS). The accelerating voltage was 10 kV and the depth of X-ray interaction was estimated to be 1 μm. At least 3–5 locations on each disk were analyzed at 1kX magnification for an area scan, and 10kX for point analysis. Values were compared to those obtained from a hydroxyapatite powder (Sigma, St. Louis, MO).

2.2.3.c X-Ray Diffraction (XRD)

The crystal structure of the bCaP coating before and after PEM application was determined with an X-ray diffractometer (Bruker D8 Advanced, Bruker AXS) using Cu K_α radiation at 40 kV and 44 mA over a 2θ range of 5–75◦ at a scan rate of 2°/min in steps of 0.02°. Sufficient material was scraped from six representative disks to produce powder samples. The crystal structure was identified by comparison to the hydroxyapatite standard and previously published patterns [168].

2.2.3 Cell Culture Assays

MC3T3-E1 mouse calvarial osteoprogenitor cells (ATCC, Manassas, VA) were cultured in alpha-Minimal Essential Medium (α-MEM, No. 12571, Gibco BRL, Invitrogen), supplemented with 10% fetal bovine serum (FBS), and 100 U/ml penicillin and 100 μg/ml streptomycin sulfate. Medium was refreshed every 2–3 days until 80-90% confluent and split at a ratio of 1:8. Passages 10–30 were routinely used. The cells were detached from tissue culture dishes with 0.25% trypsin and 1 mM EDTA (Invitrogen, Cat. No. 25200-056) at 37°C. Cells were counted using an automated cell counter (Bio-Rad, TC20) with trypan blue staining to assess cell number and viability prior to the cell proliferation assays.

The coated disks were sterilized prior to cell culture by exposure to UV light for 10 min to each side of the disks. They were then placed into 12-well treated tissue culture plates (Corning Inc., Corning, NY) and submerged in α-MEM medium for 30-45 min. MC3T3-E1s were seeded at 1 or 4 x 10^4 cells/cm^2 in culture medium and were incubated at 37°C and 5% CO_2 for up to 7 days with medium changed every 3 days. Proliferative and cytotoxic effects of the coatings on the cells were evaluated with LIVE® staining (Invitrogen Life Technologies, Grand Island, NY) following the manufacturer's protocol. Prior to LIVE® staining the disks were transferred to new wells and washed with phosphate buffered saline solution (PBS) to remove

non-adherent cells; LIVE® staining was prepared as instructed and applied to the disks, and then incubated at room temperature for 30 min. After 30 min disks were flipped over and imaged at 100X magnification using an inverted microscope (TE300, Nikon) equipped with a camera (Diagnostic Instruments), and imaging software (Spot Insight, Nikon). ImageJ was used for 3-5 images/well, analysis of 3-6 wells/group. Proliferation was quantified as average percent fluorescent area via ImageJ analysis. Percent cell death was calculated by comparing the average percent fluorescent area of the AntiA group to its AntiA-free control.

2.2.3.a Antimycin A Dose Response and Stability

The embedded factor ("Factor 2") used to assess diffusion prevention was antimycin A (AntiA) (Sigma, St. Louis, MO), known to be cytotoxic to MC3T3-E1 cells [176, 177]. To determine the appropriate cytotoxic dose when delivered from a biomaterial surface a dose response study was first conducted. The following doses of AntiA were absorbed in 10 µl volumes of ethanol to 12-well treated tissue culture plates (Corning Inc., Corning, NY): 40 mM, 20 mM, 12 mM, 6 mM, 2 mM, 0.07 mM, and 0 mM (100% ethanol), n = 3 wells/dose. AntiA solution was allowed to completely dry on the wells to maximize binding. After drying, wells were rinsed 3x with saline and then placed in α-MEM medium for 30-45 min prior to plating. MC3T3-E1s were plated at 1 x 10^4 cells/cm^2. Cytotoxic effects of the adsorbed doses on the cells were evaluated with LIVE® staining after 24 h of culture. ImageJ analysis was performed.

To determine if the coating process inactivated the AntiA, 10 µl of 40mM AntiA in ethanol (213 µg/disk) was adsorbed onto the sandblasted disks, allowed to dry, and then rinsed 3x with saline. N = 4 disks underwent the "PEM" processing but without PEM, meaning disks were subjected to the automated dip procedure that normally would apply the polyelectrolytes but only saline was used. N = 4 disks underwent conditions similar to the "bCaP" processing,

meaning the disks were submerged in MilliQ water (rather than solution A or B) and left in the oven at 37°C for 24 h, then at 50°C for 24 h. After "processing" disks were placed in 12-well plates. Fresh AntiA adsorbed to sandblasted disks (213 μg/disk with 3x saline rinses, n = 4) was used as a positive control. Sandblasted disks with no AntiA were used as the negative control (n = 4). MC3T3-E1s were plated at 4 x 10^4 cells/cm^2. Cytotoxic effects of the disks on the cells were evaluated with LIVE® staining after 24 h of culture. ImageJ analysis was performed.

2.2.3.b Diffusion Studies

AntiA was used as "Factor 2" to evaluate if prevention of interlayer diffusion of an embedded factor could be achieved by the addition of CaP and/or bCaP to PEM. Coatings were prepared as previously described in section 2.2.2c. The following groups/coatings were used for the diffusion studies and repeated at least 2x: TCPsb, TCPsb-AntiA, and TCPsb coated with CaP-PEM8, AntiA-CaP-PEM8, CaP-PEM30, AntiA-CaP-PEM30, bCaP-PEM30, AntiA-bCaP-PEM30, PEM30, and AntiA-PEM30. MC3T3-E1s were seeded at 1 or 4 x 10^4 cells/cm^2 in culture medium and were incubated at 37°C and 5% CO_2 for up to 5 days. LIVE ® staining with ImageJ analysis was performed.

2.2.3.c FGF-2 Dose Response

FGF-2 was selected as Factor 1 for evaluating the bCaP effects on diffusion. FGF-2 stimulates MC3T3-E1 proliferation [36, 88, 178, 179], and has the opposite effect of Factor 2 (cytotoxic AntiA) on the cells. The following doses of FGF-2 were adsorbed to bCaP-PEM30 coated disks, 0, 1.5, 15, and 150 ng/disk as previously described in section 2.2.2c. MC3T3-E1s were seeded at 4 x 10^4 cells/cm^2 in culture medium and were incubated at 37°C and 5% CO_2 for 1 day. LIVE ® staining with ImageJ analysis was performed on day 1.

2.2.3.d Bioactivity of Single Factor Delivery from bCaP-PEM30

The bioactivity of Factor 1 (150 ng/disk FGF-2) and Factor 2 (213 μg/disk AntiA) delivered from bCaP-PEM30 coated disks were investigated individually. Coatings were prepared as previously mentioned, and MC3T3-E1s were plated at 4 x 10^4 cells/cm^2 in culture medium and were incubated at 37°C and 5% CO_2 for up to 5 days with medium changed on day 3. LIVE ® staining with ImageJ analysis was performed on 4h, day 1, 2, 3, 4, and 5. All groups were repeated twice.

2.2.3.e Sequential Delivery from bCaP-PEM30

The sequential delivery (AntiA-bCaP-PEM30-FGF2) coated disks and their controls (bCaP-PEM30-FGF2) were prepared as previously mentioned. MC3T3-E1s were plated at 4 x 10^4 cells/cm^2 in culture medium and were incubated at 37°C and 5% CO_2 for up to 5 days with medium changed on day 3. LIVE ® staining with ImageJ analysis was performed on 4h, day 1, 2, 3, 4, and 5. All groups were repeated at least twice.

2.2.4 Factor Release from bCaP-PEM30 Coatings

AntiA-bCaP-PEM30-FGF2 and bCaP-PEM30-FGF2 coatings were prepared on TCPsb. Coated disks were incubated in culture medium at 37°C and 5% CO_2 for 1 or 3 days without cells or media changes. Release medium was collected at each time point and immediately frozen at -20°C. MC3T3-E1s were plated in a 96-well tissue culture treated plate (Becton Dickinson and Company, Franklin Lakes, NJ) at 2.5 x 10^3cells/cm^2. After 48 h of culture, 50% of the media in each well was removed and replaced with thawed release medium (in triplicate). After an additional 24 h of culture LIVE® staining and ImageJ were used to determine the effects of the release medium on the culture. Enzyme-linked immunosorbent assay (ELISA, R&D Systems, Minneapolis, MN) testing was also performed on FGF-2 group release samples.

2.2.5 Statistical Analyses

Statistical significances were determined by unpaired t-tests and one-way ANOVA with Tukey post-tests, with a *p-value* $\leq$ 0.05 being considered statistically significant. Standard deviations are shown in all figures.

2.3 Results

2.3.1 Characterization of the Coatings

SEM microscopy with EDS point analysis revealed some embedded aluminum oxide used for sandblasting the disks present on the sandblasted plastic disks (Fig. 2.3A). The CaP coating produced with Solution A only resulted in a uniformly deposited, thin, amorphous layer. The CaP layer was so thin it could not be measured via SEM (Fig. 2.3B). The bCaP coating produced with both solution A and solution B resulted in densely packed, nano-crystals that completely coated the TCPsb. The average layer thickness measured via SEM was 5.8 $\pm$ 1.8 μm (Fig. 2.3C). The bCaP crystals became indistinguishable after PEM30 application with an average bCaP-PEM30 coating thickness of 16.3 $\pm$ 2.2 μm (Fig. 2.3D). PEM30 uniformly adsorbed to the TCPsb, but the coating thickness was not measurable via SEM (Fig. 2.3E).

Energy dispersive x-ray spectroscopy (EDS) revealed Ca/P atomic ratios of 1.95 $\pm$ 0.12 and 1.52 $\pm$ 0.50 for bCaP before (Fig. 2.4A) and after PEM30 adsorption (Fig. 2.4B), neither of which is statistically different than the Ca/P ratio of the hydroxyapatite powder, (1.71 $\pm$ 0.04), nor each other (Fig. 2.4C). EDS analysis of bCaP-PEM30 also confirmed the presence of carbon and nitrogen due to the polyelectrolyte compositions. The crystal structure of the bCaP was identified as poorly crystalline/nanocrystallline hydroxyapatite by XRD (Fig. 2.4D). The term poorly crystalline/nanocrystalline is used due to the observed peak broadening [168]. After PEM

adsorption, the bCaP crystal structure became less crystalline as evident by even further peak broadening (Fig. 2.4E).

2.3.2 Antimycin A Dose Response and Stability

The antimycin A dose response study revealed a 50% inhibitory concentration (IC50) of 3.08 mM (Fig. 2.5). The 40 mM dose (213 μg/disk) resulted in almost complete cell death; therefore, it was selected to be used in all studies that use AntiA because it was necessary to observe significant cell death to ensure there were no question the cells were accessing the AntiA.

To ensure the coating procedure did not inactivate the AntiA, antimycin's stability was tested after being treated with multiple saline rinses ("PEM" processing), or when treated with MilliQ water and heat ("bCaP" processing). All AntiAs tested resulted in significant cell death within 24 h of culture as compared to the negative control, TCPsb with no AntiA (Fig. 2.6, **** $p \leq 0.0001$). Furthermore there were no statistically significant differences between the processed AntiAs compared to the fresh/normal AntiA indicating AntiA retains its cytotoxic activity after coating application.

2.3.3 Diffusion Studies

The first attempt at producing a coating that could prevent the interlayer diffusion of embedded 213 μg/disk AntiA was to use an amorphous CaP layer and 8 bilayers of PEM (CaP-PEM8). Day 1 LIVE® staining of MC3T3-E1s cultured on TCPsb coated with AntiA, AntiA embedded under PEM8, and AntiA embedded under CaP-PEM8 resulted in 91.9 $\pm$ 2.3 %, 79.6 $\pm$ 5.2 %, and 42.4 $\pm$ 2.8 % cell death respectively, relative to their AntiA-free controls (Fig. 2.7A). Though CaP-PEM8 was significantly better than the PEM8 coating at preventing diffusion of AntiA (**** $p \leq 0.0001$), it did not provide enough delayed access to the embedded AntiA as indicated by the

significant difference between AntiA-CaP-PEM8 and CaP-PEM8 at day 1 (Fig. 2.7B, **** $p \leq 0.0001$).

The next attempt to improve delayed access to the embedded 213 μg/disk AntiA was to increase the number of PEM bilayers adsorbed to the CaP layer from 8 to 30. This resulted in no difference between AntiA-CaP-PEM30 and CaP-PEM30 on day 1, however, no drop in LIVE® staining with extended time in culture was observed (Fig. 2.8).

It was then decided to increase the thickness and crystallinity of the CaP layer by using both Solution A and Solution B to make bCaP in attempts to prevent diffusion and completely block access to the AntiA in the first day. MC3T3-E1s cultured for one day on TCPsb coated with 213 μg/disk AntiA resulted in a significant drop in % LIVE® stained area as compared to its AntiA-free control (TCPsb vs. TCPsb+AntiA, Fig. 2.9A, **** $p \leq 0.0001$), and this equated to 96.6 $\pm$ 1.2 % cell death (Fig. 2.9B); this is visualized in Fig. 2.9C vs. D. MC3T3-E1s cultured for one day on TCPsb coated with 213 μg/disk AntiA embedded under 30 bilayers of PEM resulted in a significant drop in % LIVE® stained area as compared to its AntiA-free control (PEM30 vs. PEM30+AntiA, Fig. 2.9A, *** $p \leq 0.001$), and this equated to 79.5 $\pm$ 4.2 % cell death (Fig. 2.9B); this is visualized in Fig. 2.9E vs. F. MC3T3-E1s cultured for one day on TCPsb coated with 213 μg/disk AntiA embedded under bCaP and 30 bilayers of PEM resulted in no difference in % LIVE® stained area as compared to its AntiA-free control (bCaP-PEM30 vs. bCaP-PEM30+AntiA, Fig. 2.9A), and this equated to -6.7 $\pm$ 10.6 % cell death (Fig. 2.9B); this is visualized in Fig. 2.9G vs. H. Percent cell death is negative for this group because the day 1 LIVE® staining on the AntiA-bCaP-PEM30 was slightly higher than on the bCaP-PEM30 control, (Fig. 2.9A).

2.3.4 Bioactivity of Single Factor Delivery from bCaP-PEM30

Figure 2.10 displays the results of day 1 LIVE ® of MC3T3-E1s cultured on bCaP-PEM30 coated disks with various doses of FGF-2. Because the 150 ng/disk dose of FGF-2 had the most significant effect on cell proliferation (**** $p \leq 0.0001$), it was selected as the dose to be used for all future coating studies.

Factor 1 (150 ng/disk FGF-2) and Factor 2 (213 μg/disk AntiA) location within the bCaP-PEM30 coating and the expected cell access profiles are illustrated in Figure 2.11. Bio-active FGF-2 was successfully delivered from bCaP-PEM30 coated disks (bCaP-PEM30-FGF2) as indicated by the significant increase in LIVE® staining of the MC3T3-E1 cultures on day 1 and the remaining time points in the study, as compared to the FGF-free control (bCaP-PEM30) (Fig. 2.12). No differences were observed at 4 h (Fig. 2.13). Active AntiA was successfully delivered from bCaP-PEM30 coated disks (AntiA-bCaP-PEM30) as evident by the significant decrease in MC3T3-E1 proliferation on day 3 as compared to the AntiA-free control (bCaP-PEM30) (Fig. 2.14).

2.3.5 Factor Release from bCaP-PEM30 Coatings

Release medium collected from bCaP-PEM30-FGF-2 coated disks incubated without cells for 1 and 3 days had no significant proliferative effect on MC3T3-E1s as compared to controls cultured in normal medium, indicating no FGF-2 release (Fig. 2.15, D1 and D3 –A/+F). Release medium collected after 1 and 3 days incubation with AntiA-bCaP-PEM30-FGF-2 had no cytotoxic effect on cells as compared to release medium collected after 1 and 3 days incubation with bCaP-PEM30-FGF-2 indicating no AntiA release (Fig. 2.15, D1 and D3 +A/+F).

2.3.6 Sequential Delivery of Multiple Factors from bCaP-PEM30 Coatings

Active FGF-2 (150 ng/disk) was delivered from bCaP-PEM30 coated disks with or without embedded AntiA as evident by the significant increase in day 1 MC3T3-E1 LIVE® staining of the FGF-2 groups as compared to their FGF-2-free controls, (Fig 2.16A). No differences in LIVE® stained area were observed between cells cultured on bCaP-PEM-FGF2 and AntiA-bCaP-PEM30-FGF2 for time points 4h, day 1 and day 2, as both groups were exposed to FGF-2 and AntiA was successfully being blocked (Fig. 2.16B, 3.3C); by day 3 a significant decrease in LIVE® staining between groups was observed indicating AntiA delivery, (Fig. 2.16B, 3.3C). At day 4, the cells that survived the AntiA exposure started to recover and continued to proliferate through the duration of the study (Fig. 2.16C).

2.4 Discussion

There is a need for new biomaterials to deliver bioactive growth factors in a sequential manner to maximize their reparative effects. In this study the development of a novel biomimetic calcium phosphate/polyelectrolyte multilayer coating for the sequential delivery of multiple biological agents was reported. *In vitro* studies were used to demonstrate the ability of the bCaP barrier layer to prevent the interlayer diffusion problem associated with PEM films. Two different factors were delivered without loss of activity, and the delivery of factors from the coating was cell-mediated. Most importantly sequential delivery of multiple factors was demonstrated.

The polyelectrolyte multilayer films formed by PLLys and PLGlut occurs by exponential growth with “in and out” diffusion of the polyelectrolytes that allow interlayer diffusion of incorporated factors [146]. As the film is exposed to a polyanion (-) solution, the polycation (+) within the film will diffuse to the surface allowing for more binding sites for the polyanion. Vice versa will occur during the next step when the polycation solution is being applied; because of

this growth pattern, any incorporated factor within the film will constantly be rearranged during the layer build up resulting in a blended architecture lacking controlled order, therefore uncontrolled delivery [154] (Fig. 2.17). To prevent this diffusion from occurring a biomimetic calcium phosphate layer was incorporated into the poly-L-Lys/poly-L-Glut acid PEM design to act as a barrier and keep the factors in separate locations within the coating so sequential delivery could be possible. The combined use of polyelectrolytes and CaP has previously been investigated for bone tissue engineering, but not as a multifactor delivery system [157, 180, 181].

It was observed that the addition of an amorphous CaP layer could significantly improve interlayer diffusion of embedded antimycin A as compared to a PEM only coating, however, 42% of the cells still accessed at least some of the AntiA within the first 24 h resulting in their death (Fig 2.7A). The CaP-PEM8 coating would be insufficient for sequential delivery because the embedded Factor 2 can still be accessed immediately. Increasing the number of PEM bilayers in attempts to prevent cellular access to the embedded AntiA had little to no effect, again suggesting that a CaP-PEM30 coating would also be insufficient for potential sequential delivery. The data indicates that the MC3T3-E1s can access the embedded AntiA within the first 24 h and implies the CaP and PEM30 coatings were too thin; in fact they were not capable of being measured via SEM (Fig. 2.3B, E).

To completely block access of the cells to the embedded AntiA for at least 1 day, it was hypothesized that increasing the thickness of the CaP layer would not only prevent the diffusion of the AntiA up and into the PEM layers, but delay access to the AntiA. It was shown that 30 bilayers of PEM delays access to embedded AntiA better than no coating at all, but it still results in significant cell death within 24 h (Fig. 2.9B). PEM alone could not inhibit the embedded AntiA from diffusing up and through the bilayers, resulting in immediate access of the cells to

the cytotoxic factor. However, when the AntiA is embedded beneath the bCaP layer and 30 bilayers of PEM, almost no cell death occurs by 24 h (Fig. 2.9B). These results confirm that a PEM30 only coating would be insufficient for sequential delivery because it cannot inhibit interlayer diffusion; but the addition of bCaP to the PEM30 coating successfully inhibits diffusion, and prevents access at day 1, suggesting the potential of this coating design for sequential, multifactor delivery.

The PEM system has the ability to release and maintain the bioactivity of the incorporated factors. Because bioactive proteins are directly integrated in the architecture of the film based on electrostatic interactions and do not require covalent bonding [151, 152], their secondary structures remain close to their native form and this retains their biological activity [111]. Individual and combinations of bio-active growth factors have been successfully delivered from PEM systems [160, 163, 165-167]; more specifically, TGFβ1, BMP-2, VEGF, and BMP-2 antagonist (Noggin) have all been delivered from poly-L-Lysine/poly-L-Glutamic acid PEM coatings and retain their bioactivity [161, 162, 164]. Other delivery systems, such as polyethylene glycol (PEG) hydrogels, can inactivate the protein during the immobilization process (crosslinking) via damaging the growth factor's functional groups [27].

It was shown in the present study that delivery of FGF-2 from the bCaP-PEM coating causes significant increase in MC3T3-E1 proliferation confirming that the biological activity of FGF-2 is retained and being delivered in the therapeutic range (Fig. 2.12). It should be noted that FGF-2 did not aid in initial cell attachment, as evident by the lack of significant differences in LIVE® staining of the MC3T3-E1s after 4 h of culture (Fig. 2.13A). It was only after 24 h that an increase was observed (Fig. 2.13B) indicating that the FGF-2 is stimulating the proliferation of the MC3T3-E1s. Literature suggests that FGF-2 will aid in initial cell attachment [182],

however it is hypothesized that the PEM bilayers act as a reservoir for the FGF-2; even though the FGF-2 is adsorbed as the outermost layer of the coating, it is believed that the FGF-2 will diffuse down into the PEM layers. Because of this, cells may not be immediately in contact with the FGF-2, which could explain why no differences are observed after 4h; however, after 24 h and time for the cells to start to degrade the PEM, they gain access to the FGF-2 that stimulates their proliferation. The cytotoxic activity of AntiA is also retained after it is accessed on day 3 of culture on the AntiA-bCaP-PEM30-FGF2 group (Fig. 2.14).

One of the most attractive features of the bCaP-PEM delivery system is its ability to locally deliver factors directly to cells and thereby restrict therapeutic action to a small domain of tissue. Poly-L-Lysine/poly-L-Glutamic acid PEM allows for local delivery of incorporated factors because release depends upon cell-mediated enzymatic degradation of the PEM layers [150], and not diffusion of the factors out of the coating. In systems where the growth factor is simply mixed with a carrier, or adsorbed on the surface without an additional coating, burst release of the growth factor leads to diffusion away from the target site and it can be enzymatically digested or deactivated [6], or can require supraphysiological doses of growth factor that lead to off-target, unwanted side effects, (INFUSE Bone Graft (Medtronic) [19, 30]. Encapsulating the growth factor within a liposome or particle can extend the release and prevent the deactivation of the growth factor [130, 183]; however, the delivery system is still dependent on diffusion of the particles out of a secondary material therefore local, targeted delivery to only the cells of interest can be difficult to achieve. In the present studies there was no indication of release of neither FGF-2, nor AntiA without cells present. There was a lack of measurable quantities of FGF-2 in the release medium and no proliferative or cytotoxic effects of the release medium collected from disks incubated without cells was observed (Fig. 2.15). Due to the cell-

mediated degradation of the bCaP-PEM coating, lower doses of growth factor can be used because delivery is not dependent on diffusion. AntiA has low solubility in solutions other than ethanol; therefore it was unlikely the AntiA would diffuse into an aqueous release medium, which may be why no indication of release without cells present was observed. However, AntiA has a known 50% inhibitory concentration against MC3T3-E1 cells of 70 μM when in solution [176]; in the present studies a 40 mM dose of AntiA before bCaP-PEM30 coating was used. Even if a fraction of this dose were diffusing out of the coating into the media, it would be expected to have a cytotoxic effect on the cells.

The mechanism of which the MC3T3-E1 cells degrade the bCaP to access the AntiA remains unclear. In the Kuhn's lab previous work, it was shown that after 21 days of MC3T3-E1 cultured on the bCaP coating, the coating remained intact [168]. It is hypothesized that rather than physically degrading the bCaP layer, the MC3T3-E1s are actually using their processes to push through small cracks in the coating and access the AntiA. It is known that osteoblasts cultured in three-dimensions [184] or on the surface of bone will form long processes [185, 186]. From the LIVE® staining in the present studies, it is evident the MC3T3-E1s have processes in two-dimensions along the surface of the coating; it is hypothesized these processes also extend down through the coating and that is how the AntiA is being accessed.

Sequential delivery of multiple bioactive factors with complete blocking of access to the embedded factor for three days was demonstrated by introducing a bCaP barrier layer into a 30-bilayer poly-L-lysine/poly-L-glutamic acid PEM system (Fig. 2.16). As previously mentioned, Min et al. used a similar barrier layer strategy for attempted sequential delivery from a PEM coating and demonstrated successful staggered release of first an antibiotic and then BMP-2. Burst release of BMP-2 was prevented and sustained release was demonstrated for several days,

but measurable released BMP-2 was still present at their earliest time points [156]. In a dual-purpose delivery system such as this, where the factors do not influence each other and serve two separate functions (prevent infection, aid in bone healing), this delivery profile is acceptable. However in a system where the growth factors are being delivered in combination for one function, such as the use of FGF-2 and BMP-2 for enhanced bone regeneration, sequential delivery may be necessary because these growth factors can influence the effect of the other.

2.5 Conclusions

This study showed that a poly-L-Lysine/poly-L-Glutamic acid PEM only coating results in interlayer diffusion and immediate access to an embedded factor, proving that this PEM only system could not provide sequential delivery of multiple factors. The addition of amorphous CaP to PEM prevented some interlayer diffusion of an embedded factor, however significant access to the factor was occurring with 24 h, suggesting it would be incapable of sequential delivery. The addition of nanocrystalline bCaP to PEM (bCaP-PEM30) completely prevented unwanted interlayer diffusion of the embedded factor and enabled cell-mediated sequential delivery of multiple factors. Sequential delivery of a proliferative factor, fibroblast growth factor-2, followed by a cytotoxic factor, antimycin A was demonstrated. Both factors retained their bioactivity *in* vitro. The addition of the bCaP layer to the PEM design resulted in delayed access of the embedded antimycin A out to 3 days when cultured with MC3T3-E1 cells. This delivery system has potential to endow biomaterial scaffolds with the ability to mimic natural biological processes that involve a sequential delivery profile activated by cell degradation of matrix.

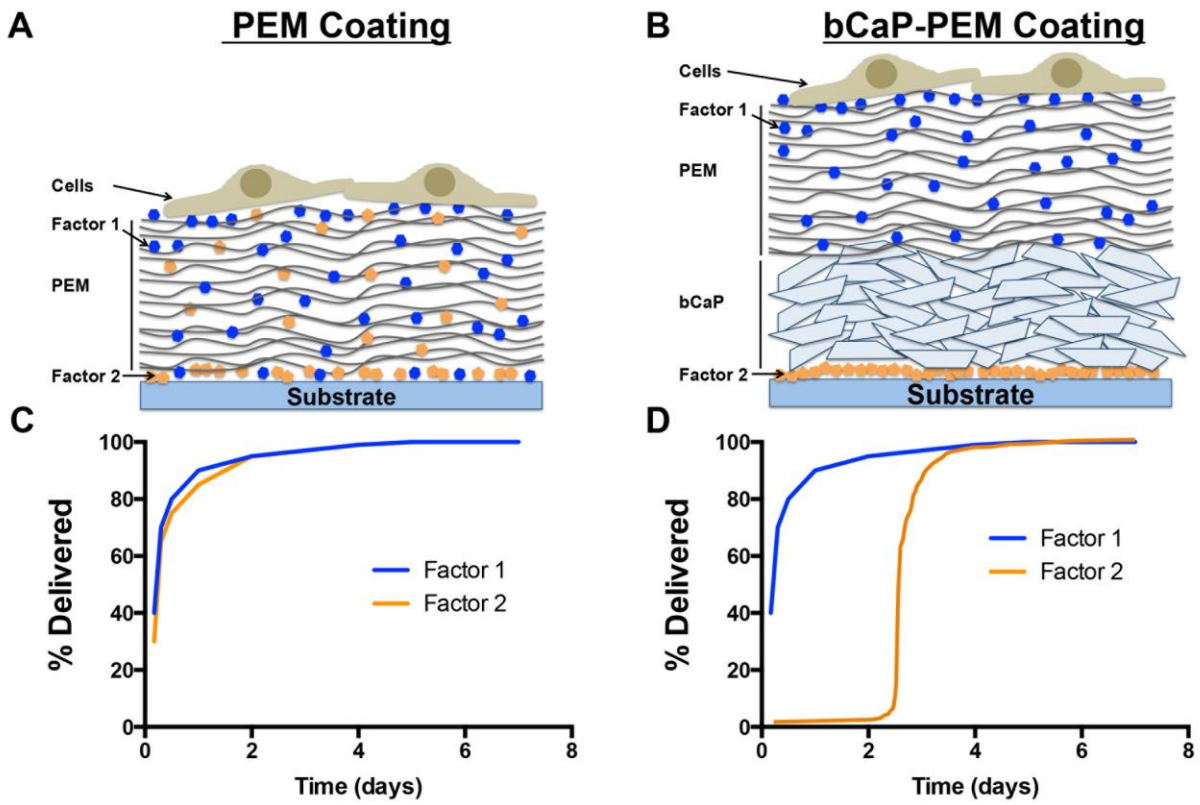

Figure 2.1 Schematic representation of interlayer diffusion of Factors 1 and 2 in a PEM only coating **(A)**, compared to prevention of interlayer diffusion of Factors 1 and 2 with the addition of bCaP to the PEM coating **(B)**. The theoretical co- and sequential delivery profiles from a PEM only coating **(C)** and a bCaP-PEM coating **(D)** respectively.

Table 2.1 Nominal chemical composition of Solutions A and B in mM. Solution B contains less inhibitors of apatite crystal formation (red text).

Inorganic Salt	**Solution A**	**Solution B**	**Reagent Chemical**
Na^+	733.5	733.5	NaCl
Mg^{2+}	7.5	1.5	$MgCl_2 \bullet 6H_2O$
Ca^{2+}	12.5	12.5	$CaCl_2 \bullet 2H_2O$
Cl^-	720	720	
HPO_4^{2-}	5	5	$Na_2HPO_4 \bullet 2H_2O$
HCO_3^-	21	10	$NaHCO_3$

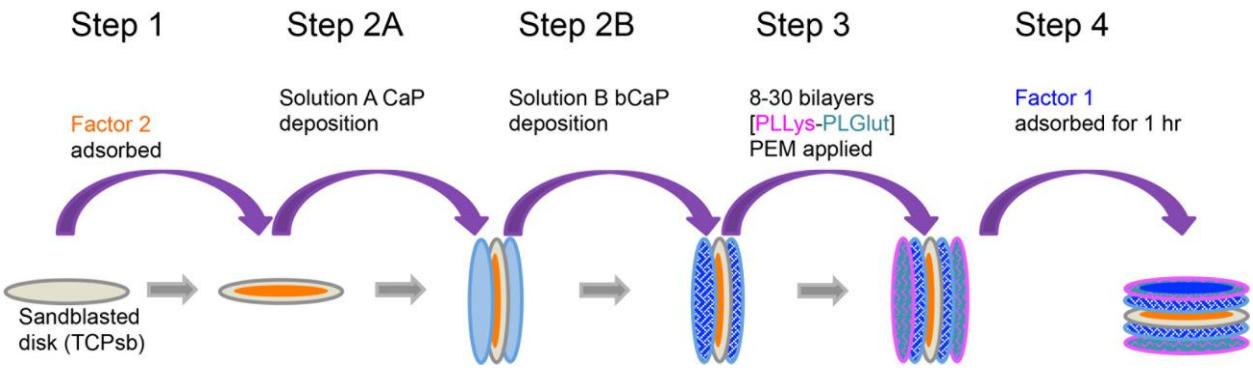

Figure 2.2 Sandblasted disk coating procedure for diffusion studies. Step 1: Factor 2 (AntiA) is adsorbed. Step 2A: disks are submerged in Solution A to deposit a thin layer of amorphous calcium phosphate (CaP). Step 2B: disks are submerged in Solution B to deposit nanocrystalline calcium phosphate, (bCaP). Step 3: 8-30 bilayers of PEM are applied by automated dip procedure. Step 4: Factor 1 (FGF-2) is adsorbed.

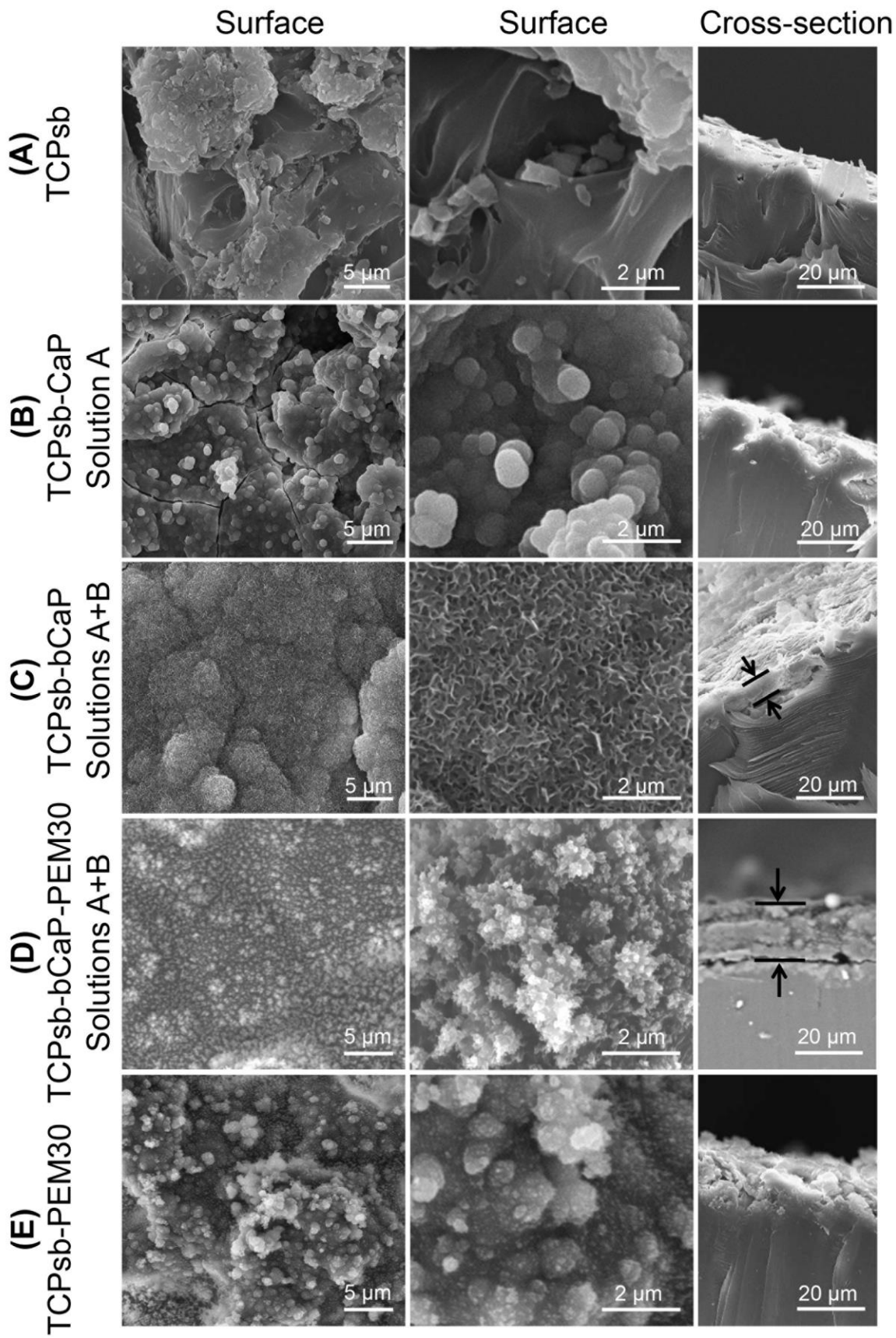
Surface
Surface
Cross-section
(A) TCPsb
(B) TCPsb-CaP Solution A
(C) TCPsb-bCaP Solutions A+B
(D) TCPsb-bCaP-PEM30 Solutions A+B
(E) TCPsb-PEM30
5 µm
2 µm
20 µm

Figure 2.3 Scanning electron microscopy images of the surface morphology and cross-section of a sandblasted disk **(A)**, and the sandblasted disks coated with: amorphous calcium phosphate CaP **(B)**, nanocrystalline calcium phosphate bCaP **(C)**, nanocrystalline calcium phosphate and 30 bilayers of PEM **(D)**, and 30 bilayers of PEM **(E)**. B and E coating thickness was not measurable via SEM. bCaP thickness = 5.8 $\pm$ 1.8 μm **(C)**. bCaP-PEM30 thickness = 16.3 $\pm$ 2.2 μm **(D)**.

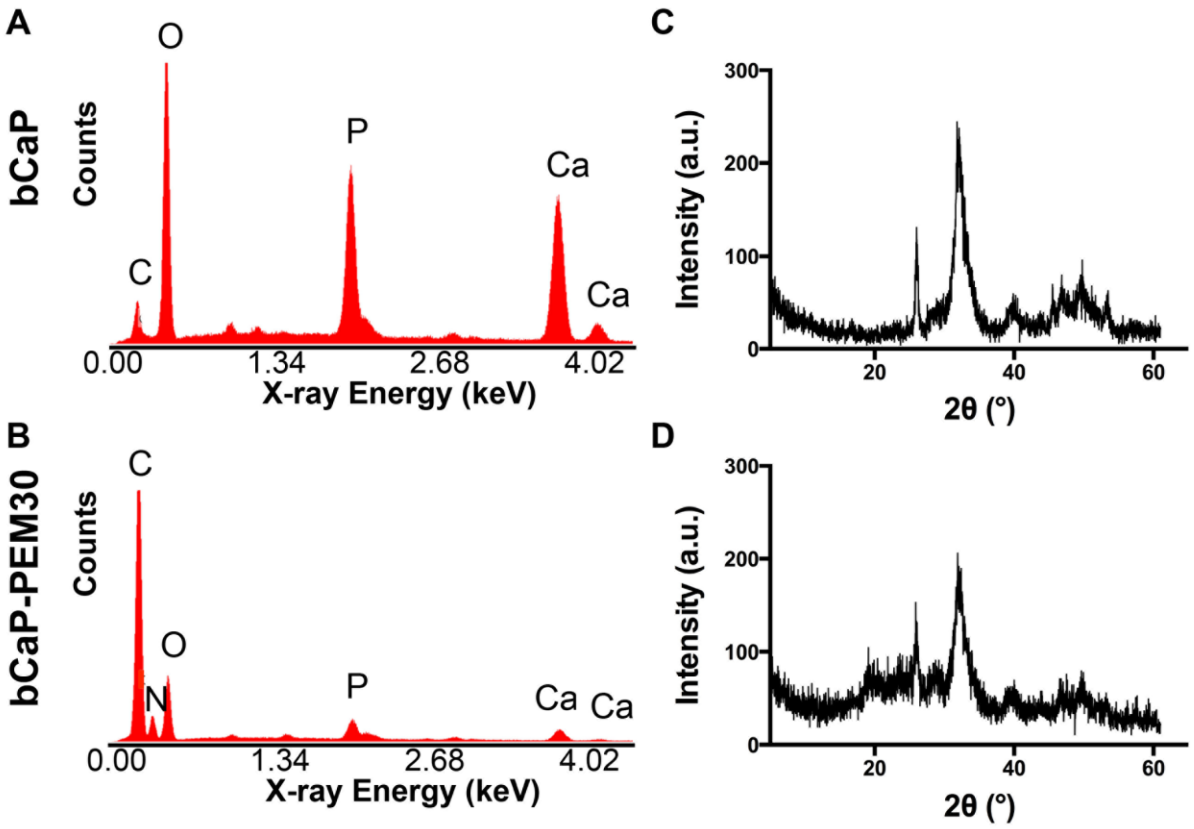

Figure 2.4 EDS analysis of the bCaP deposited on the TCPsb before **(A)** and after PEM30 adsorption **(B)**, revealed Ca/P atomic ratios of 1.95 $\pm$ 0.12 and 1.52 $\pm$ 0.50 respectively, not statistically different from the hydroxyapatite powder (1.71 $\pm$ 0.04) nor each other. The composition of the bCaP coating was identified as poorly crystalline/nanocrystalline hydroxyapatite by XRD **(C)**. After PEM adsorption the bCaP became less crystalline **(D)**.

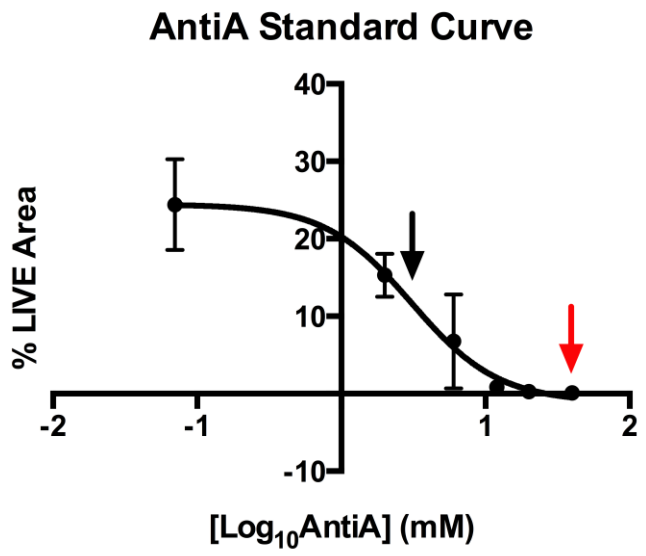

Figure 2.5 AntiA dose response curve. The adsorbed AntiA IC50 was found to be 3.08 mM (black arrow). The dose of AntiA selected to use for all studies was 40 mM (red arrow).

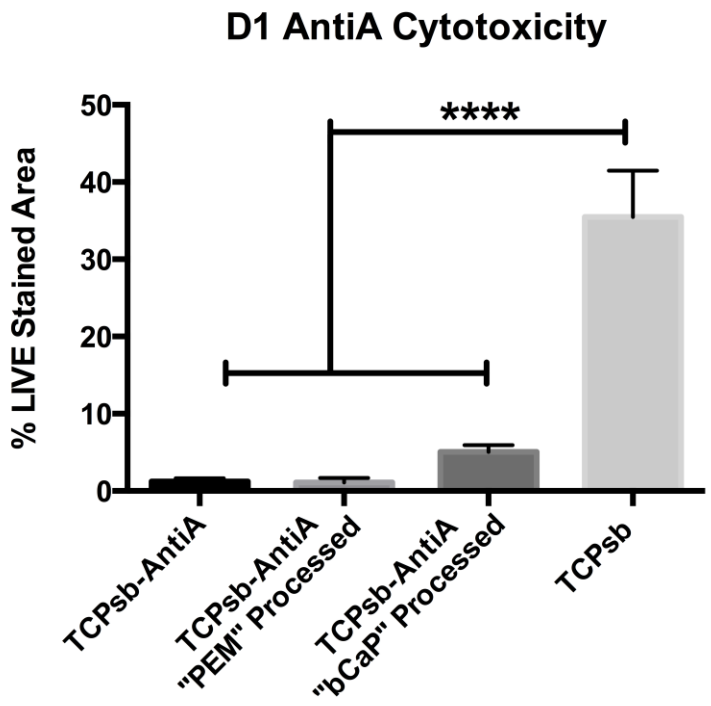

Figure 2.6 Percent LIVE® stained area of MC3T3-Es cultured for 1 day on sandblasted disks coated with normal AntiA (TCPsb-AntiA), AntiA after "PEM" processing, AntiA after "bCaP" processing, and no AntiA (TCPsb). AntiA = 213 μg/disk. (**** $p \leq 0.0001$).

ANOVA P value < 0.0001

Tukey's multiple comparisons test	Mean Diff.	95% CI of diff.	Significant?	Summary
TCPsb vs. TCPsb-AntiA	34.26	28.20 to 40.32	Yes	****
TCPsb vs. TCPsb-AntiA "PEM" Processed	34.35	28.29 to 40.41	Yes	****
TCPsb vs. TCPsb-AntiA "bCaP" Processed	30.43	24.36 to 36.49	Yes	****

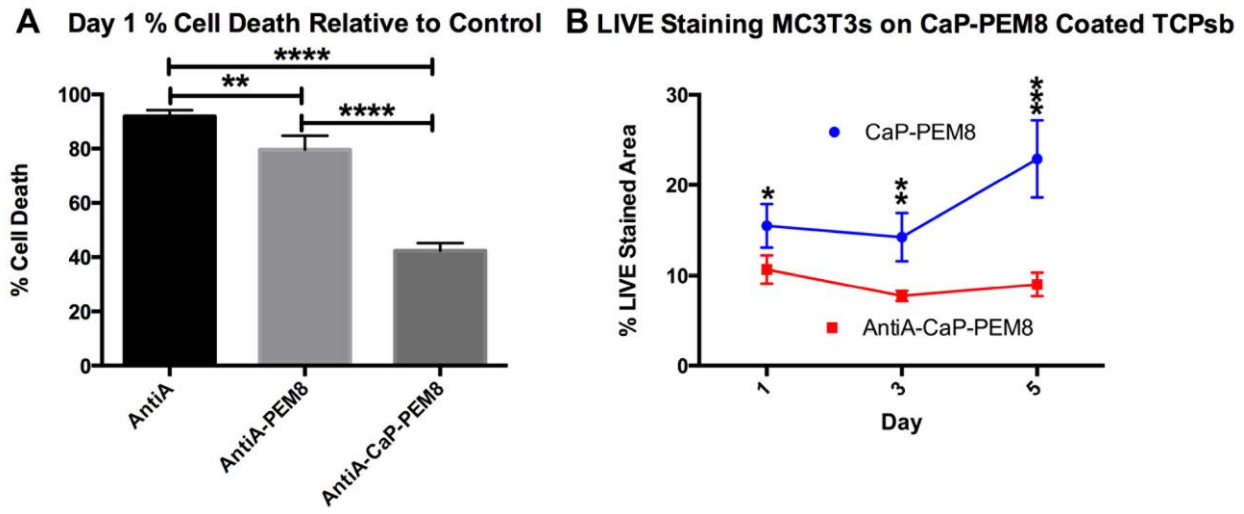

Figure 2.7 Day 1 percent cell death of MC3T3-E1s cultured on TCPsb coated with AntiA, AntiA embedded under PEM8, and AntiA embedded under CaP-PEM8 relative to their AntiA-free controls **(A)**. Percent LIVE® stained area of MC3T3-E1s cultured on TCPsb coated with CaP-PEM8 (blue) and AntiA embedded under CaP-PEM8 (red) for days 1, 3, and 5 **(B)**. AntiA = 213 μg/disk. (* $p \leq 0.05$, ** $p \leq 0.01$, *** $p \leq 0.001$, **** $p \leq 0.0001$).

Figure 2.7A

ANOVA P value < 0.0001

Tukey's multiple comparisons test	Mean Diff.	95% CI of diff.	Significant?	Summary
AntiA vs. AntiA-PEM8	12.30	5.067 to 19.53	Yes	**
AntiA vs. AntiA-CaP-PEM8	49.50	42.27 to 56.73	Yes	****
AntiA-PEM8 vs. AntiA-CaP-PEM8	37.20	29.97 to 44.43	Yes	****

Figure 2.7B

Unpaired t test	
Day 1 P value	0.0152
Day 3 P value	0.0029
Day 5 P value	0.0008

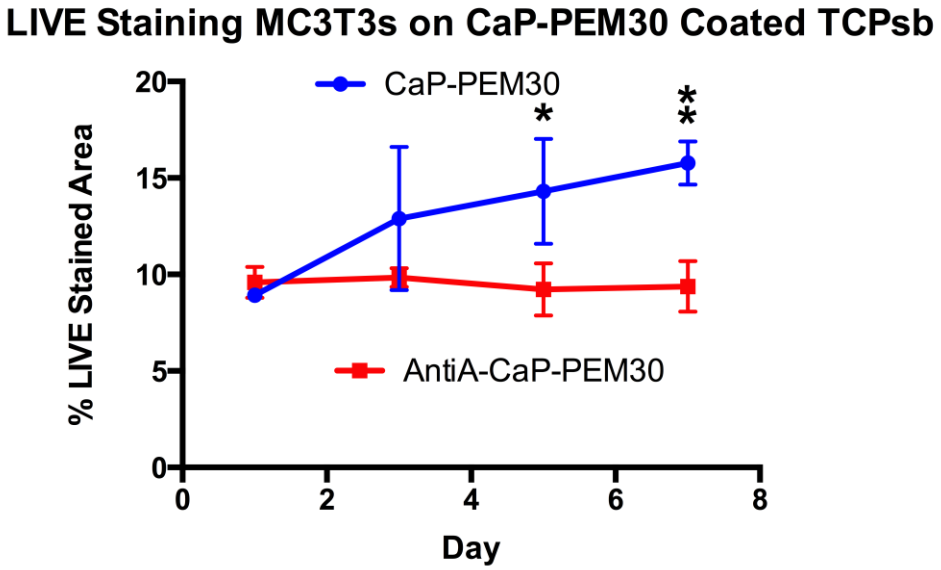

Figure 2.8 Percent LIVE® stained area of MC3T3-E1s cultured on TCPsb coated with CaP-PEM30 (blue) and Anti embedded under CaP-PEM30 (red) for days 1, 3, 5, and 7. AntiA = 213 µg/disk. (* $p \leq 0.05$, ** $p \leq 0.01$).

Unpaired t test	
Day 5 P value	0.0441
Day 7 P value	0.0030

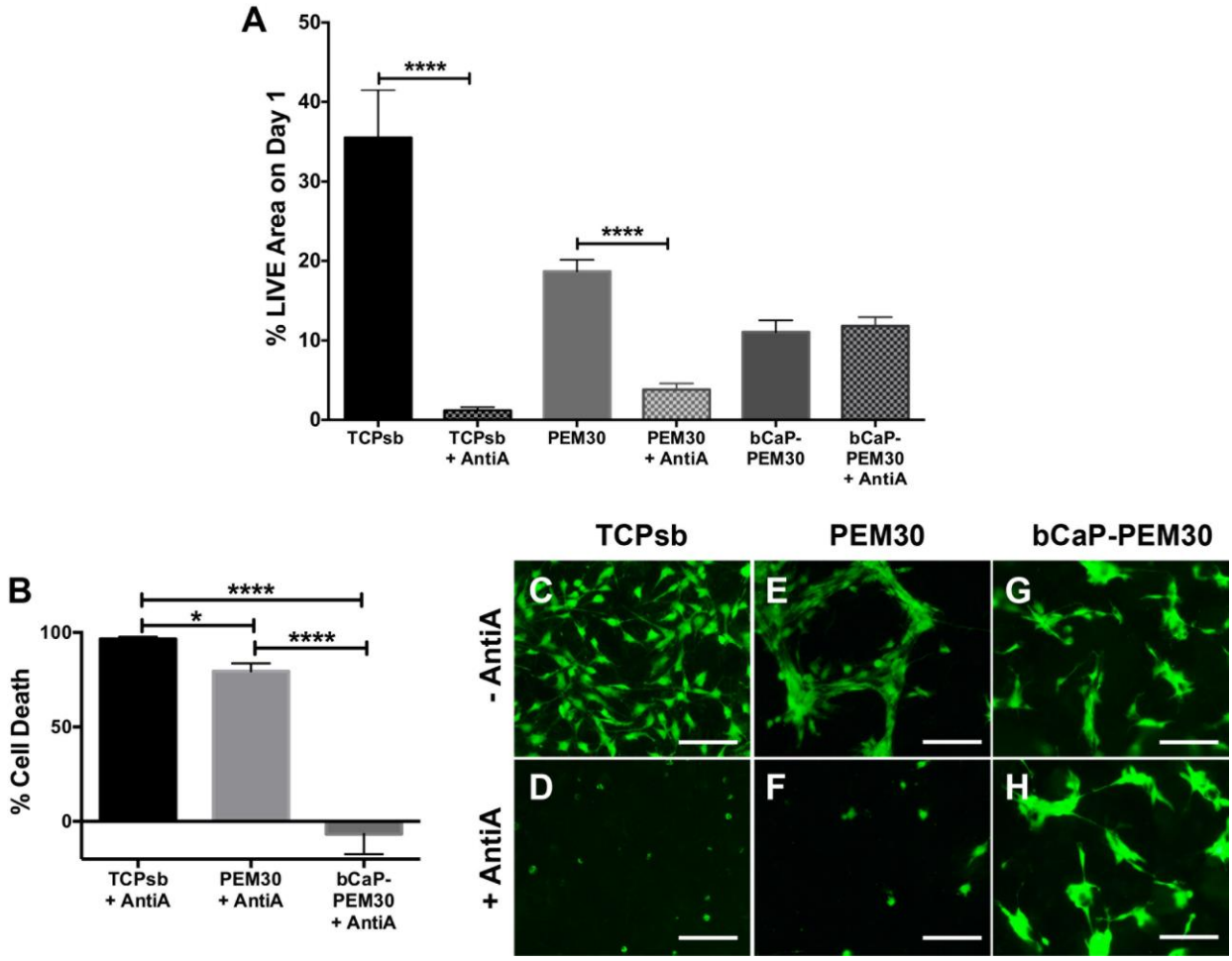

Figure 2.9 Day 1 % LIVE® stained area of MC3T3-E1s cultured on AntiA with no coating compared to its AntiA-free control, AntiA embedded under PEM30 compared to its AntiA-free control, and AntiA embedded under bCaP-PEM30 compared to its AntiA-free control **(A)**, (**** *p value* $\leq$ *0.0001*). The calculated day 1 % cell deaths of AntiA, AntiA-PEM30, and AntiA-bCaP-PEM30 relative to their AntiA-free controls **(B)**, (* *p value* $\leq$ *0.05*, *** *p value* $\leq$ *0.001*, **** *p value* $\leq$ *0.0001*). Fluorescent images of LIVE® staining of MC3T3-E1s cultured on TCPsb **(C)** vs. TCPsb coated with AntiA **(D)**, PEM30 **(E)** vs. AntiA-PEM30 **(F)**, and bCaP-PEM30 **(G)** vs. AntiA-bCaP-PEM30 **(H)**. Scale bar = 250 μm.

Figure 2.9A

ANOVA P value < 0.0001

Tukey's multiple comparisons test	Mean Diff.	95% CI of diff.	Significant?	Summary
TCPsb vs. TCPsb + AntiA	34.26	27.76 to 40.76	Yes	****
PEM30 vs. PEM30 + AntiA	14.84	7.894 to 21.79	Yes	****

Figure 2.9B

ANOVA P value < 0.0001

Tukey's multiple comparisons test	Mean Diff.	95% CI of diff.	Significant?	Summary
TCPsb+ AntiA vs. PEM30 + AntiA	17.11	3.297 to 30.92	Yes	*
TCPsb+ AntiA vs. bCaP-PEM30+ AntiA	103.3	89.50 to 117.1	Yes	****
PEM30+ AntiA vs. bCaP-PEM30+ AntiA	86.20	71.44 to 101.0	Yes	****

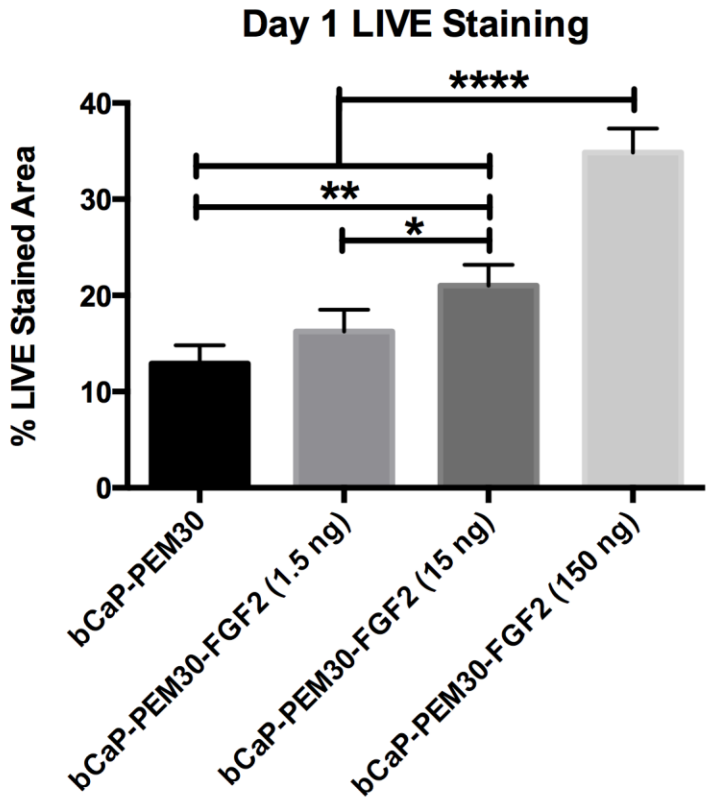

Figure 2.10 MC3T3-E1 FGF-2 dose response day 1 LIVE® staining. (* $p \leq 0.05$, ** $p \leq 0.01$, **** $p \leq 0.0001$). The 150 ng FGF-2 dose was selected to use for all studies.

ANOVA P value < 0.0001

Tukey's multiple comparisons test	Mean Diff.	95% CI of diff.	Significant?	Summary
bCaP-PEM30 vs. bCaP-PEM30-FGF2 (15 ng)	-8.097	-12.74 to -3.452	Yes	**
bCaP-PEM30 vs. bCaP-PEM30-FGF2 (150 ng)	-21.94	-26.58 to -17.30	Yes	****
bCaP-PEM30-FGF2 (1.5 ng) vs. bCaP-PEM30-FGF2 (15 ng)	-4.779	-9.423 to -0.1343	Yes	*
bCaP-PEM30-FGF2 (1.5 ng) vs. bCaP-PEM30-FGF2 (150 ng)	-18.62	-23.27 to -13.98	Yes	****
bCaP-PEM30-FGF2 (15 ng) vs. bCaP-PEM30-FGF2 (150 ng)	-13.84	-18.49 to -9.199	Yes	****

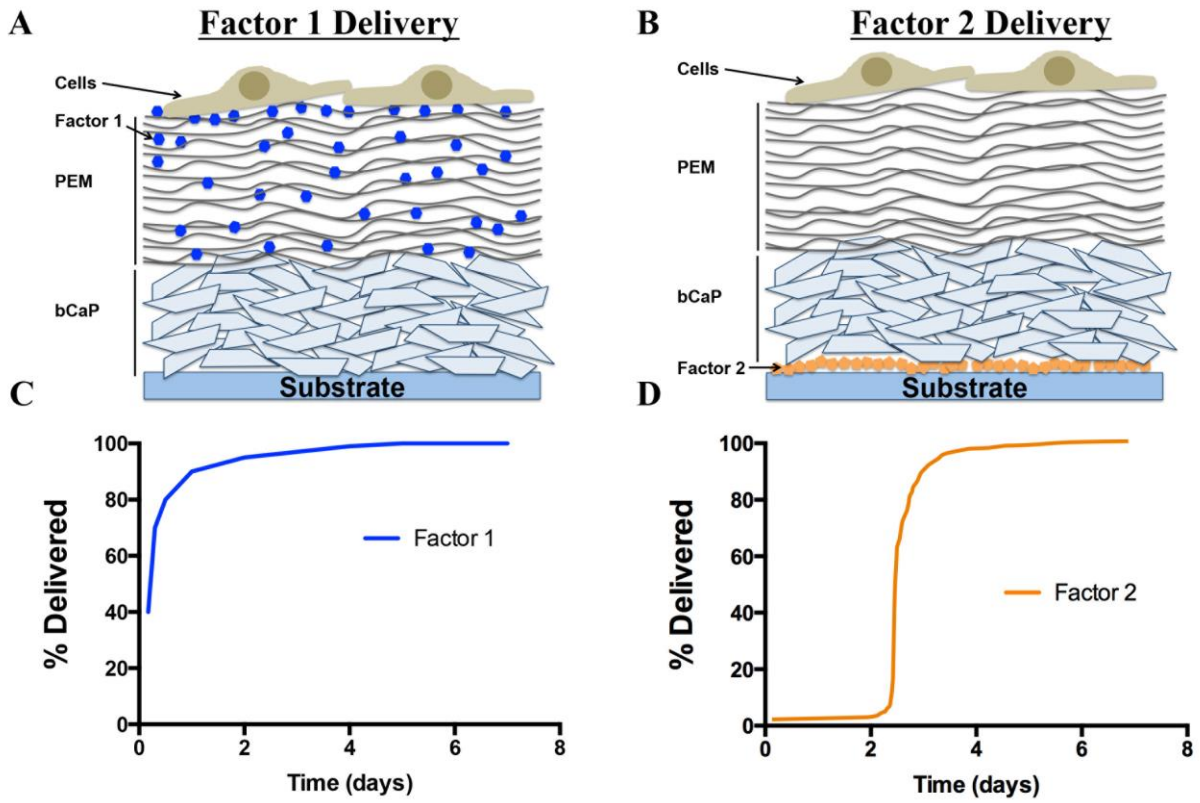

Figure 2.11 Schematic representation of Factor 1 **(A)** and Factor 2 **(B)** location within the bCaP-PEM30 coating. The theoretical immediate, and delayed delivery profiles of Factor 1 **(C)** and Factor 2 **(D)** respectively.

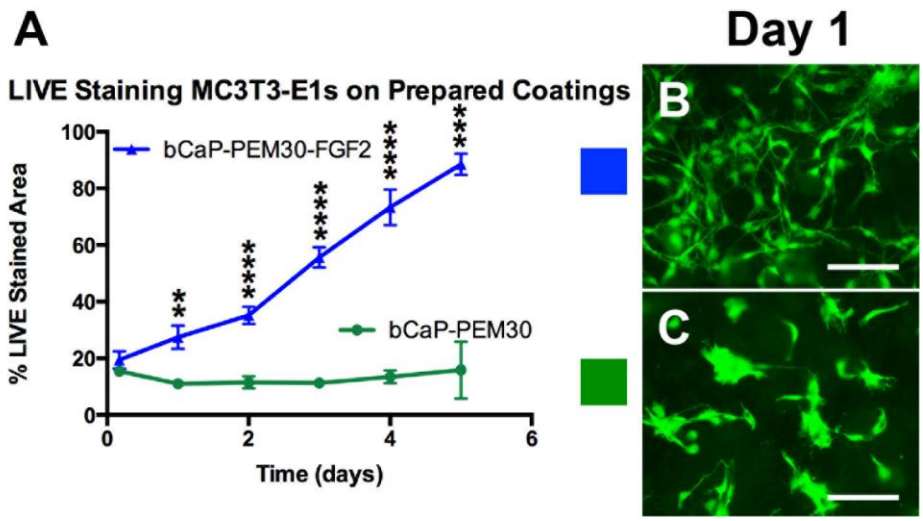

Figure 2.12 LIVE® stained area of MC3T3-E1s cultured on bCaP-PEM30-FGF2 (blue) and bCaP-PEM30 (green) for up to 5 days **(A)**, (** $p \leq 0.01$, *** $p \leq 0.001$, **** $p \leq 0.0001$) (FGF-2 = 150 ng/disk). Fluorescent images of day 1 LIVE® staining of MC3T3-E1s cultured on TCPsb coated with bCaP-PEM30-FGF2 **(B)** and bCaP-PEM30 **(C)**. Scale bar = 250 μm.

Unpaired t test	
Day 1 P value	0.0013
Day 2 P value	< 0.0001
Day 3 P value	< 0.0001
Day 4 P value	< 0.0001
Day 5 P value	0.0003

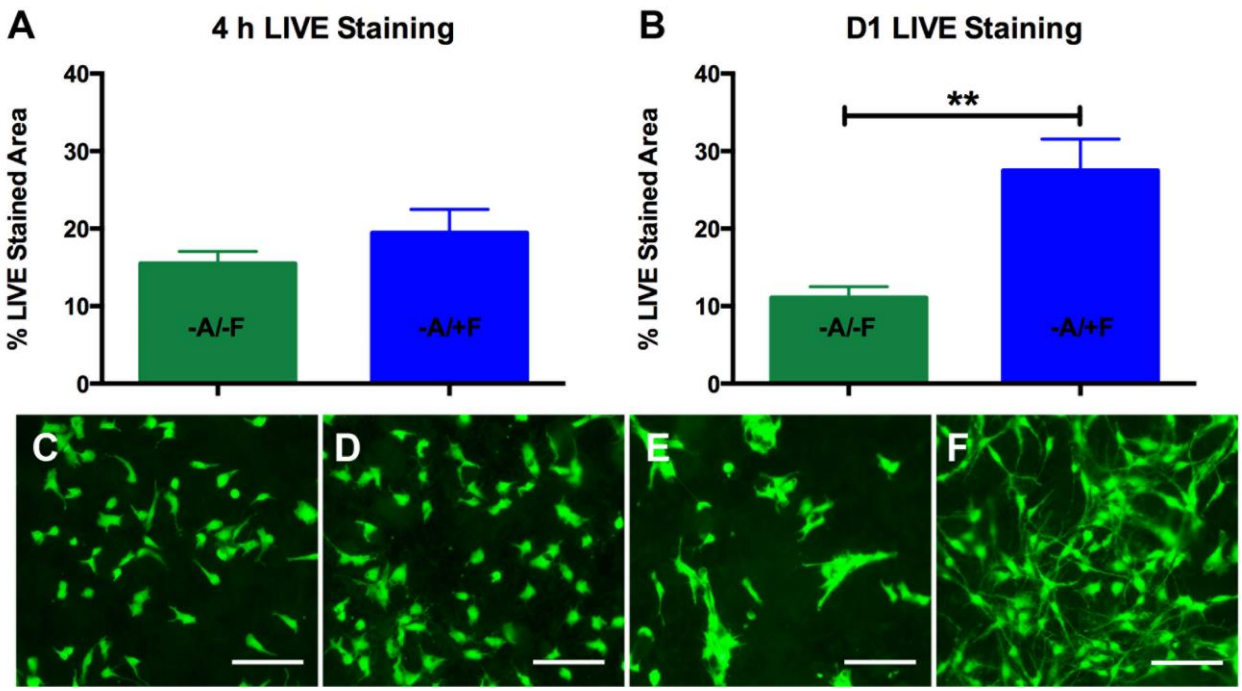

Figure 2.13 Percent LIVE® stained area of MC3T3-E1s cultured on TCPsb coated with bCaP-PEM30 (green, -A/-F) and bCaP-PEM30-FGF2 (blue, -A/+F) at 4h **(A)**, and day 1 **(B)**, (** $p \leq 0.01$). Fluorescent images of LIVE® staining of MC3T3-E1s cultured on TCPsb coated with bCaP-PEM30 and bCaP-PEM30-FGF2 after 4 h **(C, D)** and 1 day **(E, F)**.

Unpaired t test	
Day 1 P value	0.0013

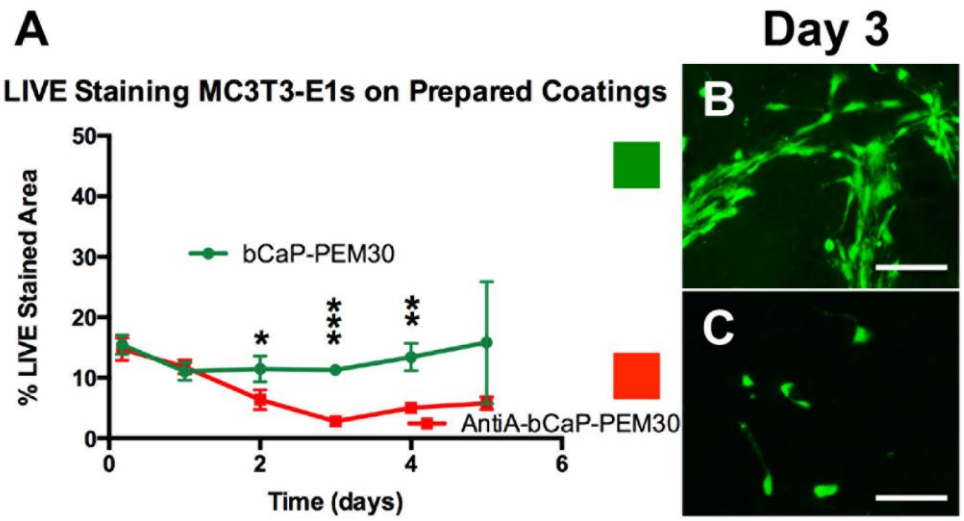

Figure 2.14 LIVE® stained area of MC3T3-E1s cultured on bCaP-PEM30 (green) and AntiA-bCaP-PEM30 (red) for up to 5 days **(A)**, (* $p \leq 0.05$, ** $p \leq 0.01$, *** $p \leq 0.001$) (AntiA = 213 µg/disk). Fluorescent images of day 3 LIVE® staining of MC3T3-E1s cultured on TCPsb coated with bCaP-PEM30 **(B)** and AntiA-bCaP-PEM30 **(C)**. Scale bar = 250 µm.

Unpaired t test	
Day 2 P value	0.0306
Day 3 P value	0.0001
Day 4 P value	0.0031

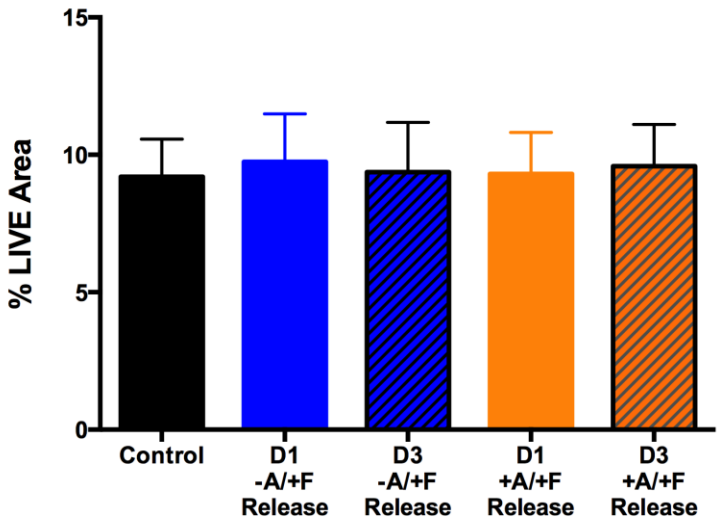

Figure 2.15 Percent LIVE® staining of MC3T3-E1s cultured in day 1- or day 3-release medium collected from bCaP-PEM30-FGF-2 (-A/+F, blue) or AntiA-bCaP-PEM30-FGF-2 (+A/+F, ornage) coated disks incubated at 37°C without cells, (FGF-2 = 150 ng/disk, AntiA = 213 μg/disk).

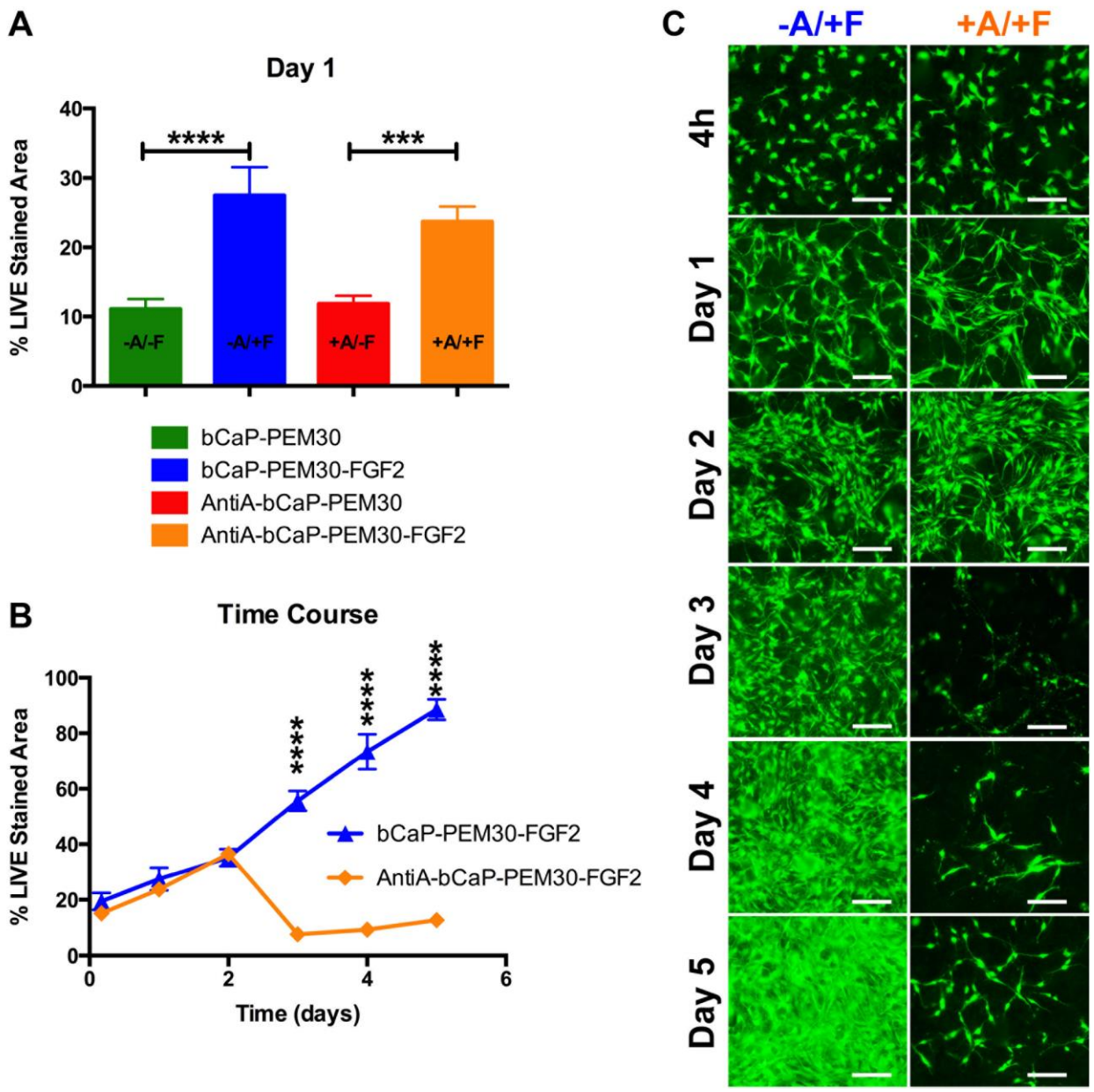

Figure 2.16 Day 1 LIVE® stained area of MC3T3-E1s cultured on the FGF-2 groups (+F) compared to their FGF-2-free controls (-F) (FGF-2 = 150 ng/disk) **(A)**, (*** $p \leq 0.001$, **** $p \leq 0.0001$). Percent LIVE® stained area of MC3T3-E1 cells cultured on bCaP-PEM30-FGF2 (blue) and AntiA-bCaP-PEM30-FGF2 (orange) over time **(B)**, (**** $p \leq 0.0001$). Fluorescent images of LIVE® staining of MC3T3-E1s cultured on bCaP-PEM30-FGF-2 (-A/+F), and AntiA-bCaP-PEM30-FGF-2 (+A/+F), at time points 4 h, days 1-5 **(C)**. Scale bar = 250 μm.

Figure 2.16A

ANOVA P value < 0.0001

Tukey's multiple comparisons test	Mean Diff.	95% CI of diff.	Significant?	Summary
bCaP-PEM30 vs. bCaP-PEM30-FGF2	-16.40	-22.65 to -10.15	Yes	****
AntiA-bCaP-PEM30 vs. AntiA-bCaP-PEM30-FGF2	-11.89	-18.13 to -5.637	Yes	***

Figure 2.16B

Unpaired t test	
Day 3 P value	< 0.0001
Day 4 P value	< 0.0001
Day 5 P value	< 0.0001

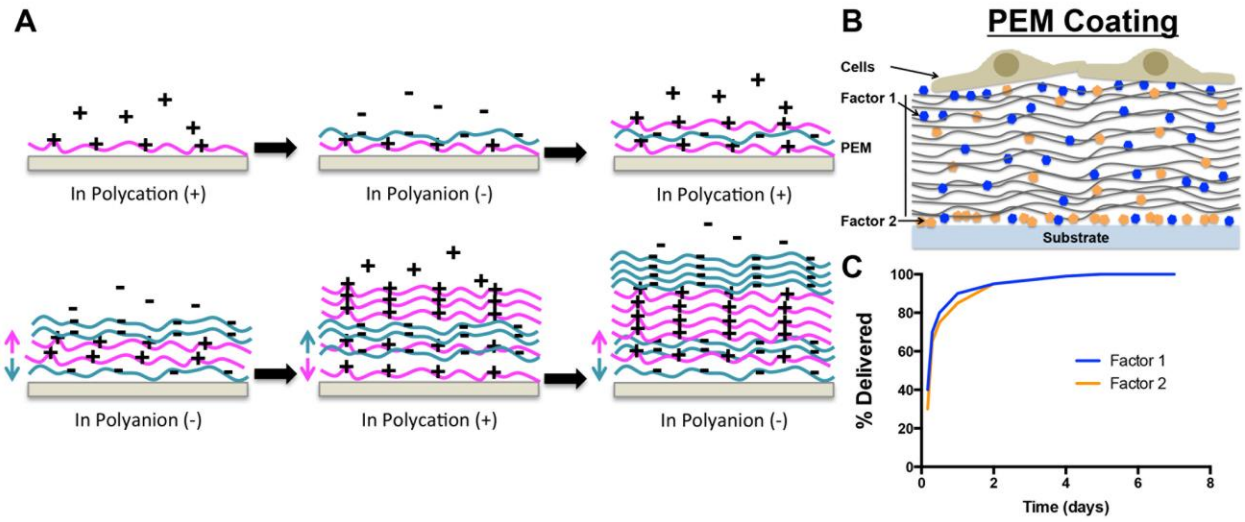

Figure 2.17 Schematic representation of "in and out" diffusion and exponential growth of hydrophilic polyelectrolytes during layer-by-layer build up of the PEM film **(A)**. Resulting interlayer diffusion of multiple factors within the PEM layers **(B)** and theoretical co-delivery of factors **(C)**.

Chapter 3

Tunable Delivery Kinetics of Multiple Factors from Biomimetic Calcium Phosphate/PEM Coatings

3.1 Introduction

The ability to sequentially delivery multiple factors is an important feature of new biomaterials to stimulate successful tissue regeneration. This is because natural healing and regeneration is tightly controlled by a cascade of growth factors and signaling molecules, that all act at specific times during development and repair [4]. Many biological systems need specific growth factor exposure on a time scale of days to weeks, so it is important that new biomaterials offer specific tunability so the delivery of growth factors from the material can best match the natural process, resulting in enhanced tissue regeneration. For example, during bone fracture healing, the first stage of healing, acute inflammation, typically last around three days [38]; during this time monocytes, mesenchymal stem cells (MSCs), and subsequent osteoprogenitor cells are recruited to the defect site. For successful healing to occur, it is important that inflammation subside and these progenitor cells have a chance to proliferate and fill the defect before differentiating. Bone morphogenetic protein-2 (BMP-2) is considered one the key growth factors responsible for osteoprogenitor differentiation [36], and it has been shown that BMP-2 delivered too early can inhibit *in vitro* osteogenesis [104]. Therefore it is critical that this stage of fracture healing completes before delivering the differentiation agent from the biomaterial.

In the previous chapter, it was shown that the biomimetic calcium phosphate/polyelectrolyte multilayer coatings made with 30 bilayers of poly-L-Lysine/poly-L-glutamic acid (bCaP-PEM30), could successfully sequentially delivery two factors *in vitro* to

osteoprogenitor cells, with access to the embedded factor occurring on day 3 of culture. It was also shown that the delivery of the factors was based on the cell-mediated degradation of the coating and not diffusion of the factors out. It is expected that the delivery kinetics *in vivo* would most likely be accelerated due to the presence of other cell-types, such as macrophages, that are known to be capable of rapid resorption of PLLys-PLGlut PEM materials [121]. This motivated the work of this chapter, which is focused on altering the PEM and bCaP portions of the bCaP-PEM30 coating to further delay access to the embedded factor when cultured with osteoprogenitor cells. The PEM component of the coating was altered by increasing the number of bilayers, shown to increase the degradation time of the film *in vitro* [114], and by using the *D*-enantiomers of the polyelectrolytes, poly-D-Lysine and poly-D-Glutamic acid, also shown to slow the cellular degradation of the film [150]. The bCaP layer was altered by increasing time in the simulated body fluid solutions used to produce the layer [168], which is a demonstrated method for increasing the thickness of the bCaP layer [172]. In addition, because delivery of factors from the bCaP-PEM30 coating is cell-mediated, and monocytes/macrophages are one of the first cell-types that would interact with the coating *in vivo* [119], cellular assays were conducted with the mouse macrophage cell line, RAW 264.7, to determine the *in vitro* delivery kinetics of multiple factors from the bCaP-PEM30 coating.

This chapter reports the *in vitro* cell culture assessment of the sequential delivery kinetics of two factors with opposing activity (proliferative vs. cytotoxic) delivered from bCaP-PEM coatings with alternations made to the PEM portion of the coating, or to the bCaP layer of the coating. In addition, changes in factor delivery kinetics resulting from changing the cell type interacting with the coating, were used to investigate the cell-mediated degradation of the coating. MC3T3-E1 mouse osteoprogenitor cells and RAW 264.7 mouse macrophage cells were

used for the cell culture evaluation assays because they provide important information about the potential response of host progenitor cells (MC3T3-E1) and immune response (RAW 264.7) to implanted materials coated with bCaP-PEM.

3.2 Materials and Methods

3.2.1 Factor Application

To demonstrate delivery kinetics from the bCaP-PEM coatings, a combination of a proliferative factor, recombinant human fibroblast growth factor-2 (FGF-2) (150 ng/disk) (R & D Systems, Minneapolis, MN), and a model cytotoxic agent antimycin A (AntiA) (213 μg/disk) (Sigma, St. Louis, MO) was used. It was expected that the FGF-2 would immediately stimulate cellular proliferation, and then at a later time point the cells would access the AntiA and die, indicating successful bio-active delivery of the factors from the coating. Prior to coating application, 10 μl of 40mM antimycin A in ethanol (213 μg/disk) was adsorbed onto the sandblasted plastic surface and was allowed to completely dry to maximize binding. The disks were rinsed 3x with saline before coating application. During the coating application the disks were protected from light because AntiA is light sensitive. After AntiA adsorption, and coating application, 375 ng/ml FGF-2 in saline was allowed to adsorb to the coated disks for 1hr, then rinsed 3x with saline. Enzyme-linked immunosorbent assay (ELISA, R&D Systems, Minneapolis, MN) testing was performed and determined approximately 80% FGF-2 binds, (actual adsorbed dose ~120 ng/disk).

3.2.2 Tuning bCaP-PEM30 Delivery Kinetics

3.2.2.a Increasing Number of PEM Bilayers

AntiA (213 μg/disk) was adsorbed and bCaP was applied as previously described in Ch. 2. 102 bilayers of PEM were applied (PLLys-PLGlut = 1 bilayer). This dip-coating process was automated with the use of a histology-staining machine (Varistain 24-4, Thermo Shandon, Loughborough, UK) and custom designed sample holders. All polyelectrolyte solutions and saline rinses were replaced every 30 bilayers. After PEM102 application, disks were UV-sterilized on both sides. FGF-2 (150 ng/disk) was adsorbed as previously described. The sequential delivery group (AntiA-bCaP-PEM102-FGF2) and its AntiA-free control (bCaP-PEM102-FGF2) were each tested only once to evaluate the feasibility of this approach towards tuning delivery kinetics, and the results should be considered for pilot purposes only.

3.2.2.b Use of "D" Enantiomers

AntiA (213 μg/disk) was adsorbed and bCaP was applied as previously described in Ch. 2. 30 bilayers of PEM were applied by alternate 10 min dippings into 1 mg/ml poly-D-Glutamic acid (PDGlut-) or poly-D-Lysine (PDLys+) solutions (Sigma, St. Louis, MO), with seven saline rinses between each. After $PEM^{D}30$ application, disks were UV-sterilized on both sides. FGF-2 (150 ng/disk) was adsorbed as previously described. The sequential delivery group (AntiA-bCaP-$PEM^{D}30$-FGF2) and its AntiA-free control (bCaP- $PEM^{D}30$-FGF2) were each tested only once to evaluate the feasibility of this approach towards tuning delivery kinetics, and the results should be considered for pilot purposes only.

3.2.2.c Adjusting Time in Solution B to Change bCaP Layer Thickness

AntiA (213 μg/disk) was adsorbed as previously described. During bCaP deposition, Solution A was applied as normal, (~24 h at 37°C); time in Solution B was either increased or decreased from the normal ~24 h at 50°C. Increased times were extended to 48 h (bCaP(48)) in Solution B, decreased times were dropped to 7 h (bCaP(7)) in Solution B. After bCaP(7) or bCaP(48) were deposited, PEM30 and FGF-2 (150 ng/disk) were applied as previously described in Ch. 2. The sequential delivery group using 7 h in Solution B (AntiA-bCaP(7)-PEM30-FGF2) was tested only once to evaluate the feasibility of this approach towards tuning delivery kinetics, and the results should be considered for pilot purposes only. The sequential delivery group (AntiA-bCaP(48)-PEM30-FGF2) and its AntiA-free control (bCaP(48)-PEM30-FGF2) prepared using 48 h in Solution B were each tested at least two times.

bCaP(7) and bCaP(48) coated disks were examined to characterize surface morphology and consistency. The microscopic morphology was characterized using SEM (JSM - 5900LV, Jeol USA Inc. Peabody, MA). Disks were cut in half, allowing examination of the coating cross-section and measurement of the coating thickness with SEM.

3.2.2.d MC3T3-E1 Assays for Assessing Delivery Kinetics

MC3T3-E1 mouse calvarial osteoprogenitor cells (ATCC, Manassas, VA) were cultured in alpha-Minimal Essential Medium (α-MEM, No. 12571, Gibco BRL, Invitrogen), supplemented with 10% fetal bovine serum (FBS), and 100 U/ml penicillin and 100 μg/ml streptomycin sulfate. Cells were maintained and prepared for cell-culture assays as previously described in Ch. 2.

The coated disks were placed into 12-well tissue culture plates and submerged in α-MEM medium for 30-45 min. MC3T3-E1s were seeded at 4 x 10^4 cells/cm^2 in culture medium and were incubated at 37°C and 5% CO_2 for 4h, 1, 2, 3, 4, 5, 6, and 7 days, (medium changed on day

3 and 6). LIVE® staining and ImageJ analyses were performed to determine a measure of cell number as previously described in Ch. 2.

3.2.3 RAW 264.7 Assays for Evaluation of bCaP-PEM30 Delivery Kinetics

3.2.3.a Preparation of bCaP-PEM30 disks

Biomimetic calcium phosphate (bCaP) and poly-l-Lysine/poly-l-Glutamic acid PEM coatings (bCaP-PEM30) were prepared on sandblasted tissue culture plastic disks (TCPsb) as described in Ch. 2. AntiA (213 μg/disk), bCaP-PEM30, and FGF-2 (150 ng/disk) were applied as previously described (AntiA-bCaP-PEM30-FGF2). Control coated disks were also prepared (bCaP-PEM30-FGF2, bCaP-PEM30, AntiA-bCaP-PEM30).

3.2.3.b RAW 264.7 Assays for Assessing Delivery Kinetics

RAW 264.7 mouse monocyte macrophage cells (ATCC, Manassas, VA) were cultured in DMEM high glucose, pyruvate medium, (No. 11995, Gibco BRL, Invitrogen), supplemented with 10% fetal bovine serum (FBS), and 100 U/ml penicillin and 100 μg/ml streptomycin sulfate. Medium was refreshed every 2–3 days until 70-80% confluent and split at a ratio of 1:8. Passages 10–30 were routinely used. The cells were detached from tissue culture dishes by use of a cell-scraper. Cells were counted using an automated cell counter (Bio-Rad, TC20) with trypan blue staining to assess cell number and viability prior to the cell proliferation assays.

The coated disks were sterilized prior to cell culture by exposure to UV light for 10 min to each side of the disks. They were then placed into 12-well treated tissue culture plates (Corning Inc., Corning, NY) and submerged in α-MEM medium for 30-45 min. RAW 264.7s were seeded at 7.9 x 10^3 or 3 x 10^4 cells/cm^2 in culture medium and were incubated at 37°C and

5% CO_2 for up to 3 days. LIVE® staining and ImageJ analyses were performed as previously described in Ch. 2. All groups reported for each cell seeding density were performed twice.

3.2.3 Statistical Analyses

Statistical significances were determined by unpaired t-tests and one-way ANOVA with Tukey post-tests, with a *p-value* ≤ 0.05 being considered statistically significant. Standard deviations are shown in all figures.

3.3 Results

3.3.1 Tuning bCaP-PEM30 Delivery Kinetics

3.3.1.a Increasing Number of PEM Bilayers

MC3T3-E1s cultured on AntiA-bCaP-PEM102-FGF2 resulted in a significant decrease in LIVE® staining on day 3 compared to its AntiA-free control (bCaP-PEM102-FGF2), (Fig. 3.1A), (* $p \leq 0.05$). LIVE® staining of MC3T3-E1s cultured on the control bCaP-PEM30-FGF2 disks were significantly higher on days 3 and 5 as compared to cells on bCaP-PEM102-FGF2 disks, (Fig. 3.1B), (*** $p \leq 0.001$). Significant difference in LIVE® staining were observed between MC3T3-E1s cultured on the control AntiA-bCaP-PEM30-FGF2 disks and AntiA-bCaP-PEM102-FGF2 disks on days 3 and 5, (Fig 3.1C), (* $p \leq 0.05$, ** $p \leq 0.01$).

3.3.1.b Use of "D" Enantiomers

MC3T3-E1s cultured on AntiA-bCaP-PEM^{D}30-FGF2 resulted in a significant decrease in LIVE® staining on day 3 compared to its AntiA-free control (bCaP-PEM^{D}30-FGF2), (Fig. 3.2A), (**** $p \leq 0.0001$). LIVE® staining of MC3T3-E1s cultured on the control bCaP-PEM30-FGF2 disks were significantly higher on days 3 and 5 as compared to cells on bCaP-PEM^{D}30-FGF2 disks, (Fig. 3.2B), (* $p \leq 0.05$, ** $p \leq 0.01$). Significant difference in LIVE® staining

were observed between MC3T3-E1s cultured on the control AntiA-bCaP-PEM30-FGF2 disks and AntiA-bCaP-PEM^{D}30-FGF2 disks on day 5, (Fig. 3.2C), (* $p \leq 0.05$).

3.3.1.c Adjusting Time in Solution B to Change bCaP Layer Thickness

Schematic representations of bCaP-PEM30 made with bCaP after 7 h in Solution B (bCaP(7)), after 24 h in Solution B (the normal bCaP procedure, bCaP(24)), and after 48 h in Solution B (bCaP(48)) are illustrated in Fig. 3.3. Scanning electron microscopy revealed that all bCaPs produced formed densely packed, nano-crystals, (Fig. 3.4). bCaP(7), bCaP(24), and bCaP(48) resulted in coating thicknesses of 1.8 $\pm$ 0.7 μm, 5.8 $\pm$ 1.8 μm, and 24.0 $\pm$ 2.4 μm respectively. Culturing MC3T3-E1s on AntiA-bCaP(7)-PEM30-FGF2 resulted in similar % LIVE® stained area as culturing the cells on AntiA-bCaP(24)-PEM30-FGF2, however culturing the cells on AntiA-bCaP(48)-PEM30-FGF2 resulted in a significant increase in LIVE® staining on day 3 as compared to the other two groups (Fig. 3.5). Culturing MC3T3-E1s on AntiA-bCaP(48)-PEM30-FGF2 resulted in a significant decrease in percent LIVE® stained area on day 3 and throughout the remaining time points in the study as compared to cells cultured on its AntiA-free control (bCaP(48)-PEM30-FGF2) (* $p \leq 0.05$, ** $p \leq 0.01$, *** $p \leq 0.001$, **** $p \leq 0.0001$), (Fig. 3.6), therefore AntiA was still being initially accessed on day 3; however unlike cells cultured on AntiA-bCaP(24)-PEM30-FGF2 where after day 3 the cells start to recover (Fig. 3.6A,B), cells on AntiA-bCaP(48)-PEM30-FGF2 continue to decrease from day 3 through day 7 (Fig. 3.6C,D). It should be noted that the data obtained for days 5-7 came from a separate study than the one that produced data for time points 4h, days 1-4; this is because the number of disks that can be produced at once is limited and can only provide enough replicates for a maximum of 5 time points. Theoretical delivery profiles of FGF-2 and AntiA from bCaP(24)-PEM30 and bCaP(48)-PEM30 are illustrated in Fig. 3.7.

3.3.2 RAW 264.7 Assays for Evaluation of bCaP-PEM30 Delivery Kinetics

Increasing the RAW 264.7 seeding density from 7.9k to 30k cells/cm^2 significantly increased percent LIVE® stained area within 4 hours of culture and throughout all time points of the study when cultured on bCaP-PEM30-FGF2 (Fig.3.8A). Increasing the RAW 264.7 seeding density from 7.9k to 30k cells/cm^2 significantly *decreased* percent LIVE® stained area within 4 hours of culture and throughout all time points of the study when cultured on AntiA-bCaP-PEM30-FGF2 (Fig.3.8B). This indicates that AntiA is being accessed immediately when RAW cells are seeded at 30k cells/cm^2. At the lower seeding density, no differences between cells cultured on bCaP-PEM30-FGF2 and AntiA-bCaP-PEM30-FGF2 were observed at 4 h, day 1, or day 2 (Fig.3.9) indicating the AntiA is not being accessed at these time points. However, at the higher seeding density, a significant decrease in LIVE® staining was observed on the AntiA-bCaP-PEM30-FGF2 group compared to its AntiA-free control at 4 h and throughout the duration of the study (Fig. 3.10); this indicates that sequential delivery is no longer occurring because there is no delayed access to the embedded AntiA. A significant increase in percent LIVE® stained area after 4 h of culture for RAW cells seeded at 30k cells/cm^2 on bCaP-PEM30-FGF2 (blue, -A/+F) was observed as compared to bCaP-PEM30 (green, -A/-F, ** $p \leq 0.01$) and AntiA-bCaP-PEM30-FGF2 (orange, +A/+F, *** $p \leq 0.001$), (Fig. 3.11A); Addition of FGF-2 to bCaP-PEM30 stimulated initial RAW cell attachment and proliferation within 4 h. Addition of FGF-2 to AntiA-bCaP-PEM30 (orange) resulted in significant decreases in RAW cell LIVE® stained area at 4 h, and days 1-3 as compared to the FGF-2-free control (red), (* $p \leq 0.05$, ** $p \leq 0.01$), (Fig. 3.11 B).

3.4 Discussion

The ability to control the timing and rate of delivery of factors from a biomaterial is of critical importance for the success of the biomaterial when its aim is to replicate a natural biological process. In this study the use of a novel biomimetic calcium phosphate/polyelectrolyte multilayer coating was used to demonstrate tunable delivery kinetics of multiple biologically active factors. *In vitro* cell culture studies were used to demonstrate cell-mediated, sequential delivery of a proliferative factor (FGF-2) and a cytotoxic factor (AntiA) from the bCaP-PEM30 coating with alterations made to the bCaP thickness or the PEM composition. Change of delivery kinetics due to change in cell type from pre-osteoblast progenitor to monocyte/macrophage was also demonstrated.

The first attempt at increasing time of access to the embedded factor was to increase the number of PEM bilayers from 30 to 102. Increasing the number of PEM layers has been shown to increase the thickness of the film and time to degrade the film [114]. Increasing the number of PLLys-PLGlut bilayers resulted in AntiA still being accessed on day 3 (Fig. 3.1A), and no significant change in MC3T3-E1 proliferation with time when cultured on bCaP-PEM102-FGF2, (Fig. 3.1B). The inability of the cells to grow on the coating without AntiA could be due to inhibited burst delivery of FGF-2 or the increased concentration of poly-L-Lysine within the coating. PLLys is known to be cytotoxic [116, 117], and it is believed that increasing the number of PEM bilayers exceeded a tolerable level of PLLys for the MC3T3-E1 cells; therefore this is not a viable strategy for improving the sequential delivery profile.

The next attempt to increase the amount of time to access the embedded factor was to use the *D*-enantiomers of the polyelectrolytes, poly-D-Lysine and poly-D-Glutamic acid. Other groups have attempted tuning cellular access of protein in the same 30-bilayer PEM system by

increasing the ratio of *D*- to *L*-enantiomer polyelectrolytes within the film (shown to slow the cellular degradation of the film); this resulted in delayed access to the protein for an additional 6 h [150]. In the present study, AntiA access was still being observed on day 3 (Fig. 3.2A); this is most likely due to the very short-term (hours) tune-ability of the *D*-enantiomer approach. Again, the cells observed slight inhibited growth on bCaP-PEM^{D}30-FGF2 as compared to the bCaP-PEM30-FGF2 control (Fig. 3.2B). Though the *D*-enantiomer approach did not significantly changed access kinetics to the AntiA, it did appear to inhibit the delivery kinetics of the FGF-2.

Not surprisingly, altering the composition or number of PEM bilayers within the coating only seemed to change the delivery kinetics of the FGF-2, which is adsorbed into the PEM layers. Another strategy to delay release of an embedded factor commonly employed with PEM systems is to covalently cross-link the polyelectrolytes. Wood et al. showed a delay up to 25 h of release of an embedded factor with the use of a single thermally cross-linked poly(allylamine hydrochloride)(PAH)/poly(acrylic acid) (PAA) layer; however the cross-linking procedure required the material to be heated to 215°C for 20 min which would denature most biological agents [154]. Hsu et al. showed similar results by cross-linking chitosan/poly(b-l-malic acid) via copper-free click chemistry, and could delay release of an embedded factor up to 24 h [187]. Many biological systems need specific growth factor exposure on a time scale of days to weeks, not hours, therefore these short-term tuning strategies (increasing PEM bilayers, using *D*-enantiomers) are not sufficient for delaying access to the embedded factor nor for *in vivo* purposes.

The final attempt at tuning the delivery kinetics of the embedded factor was to increase the thickness of the bCaP layer by altering the time the samples spent in Solution B of the SBF CaP method during bCaP deposition in the bCaP-PEM30 procedure. As the literature suggested

[118, 172-174], increasing or decreasing this time resulted in an increase or decrease in the bCaP layer thickness (Fig. 3.4). Depositing a thinner bCaP(7) coating resulted in similar delivery kinetics of the embedded AntiA as using the normal bCaP(24) layer (Fig. 3.5). Depositing a thicker bCaP(48) layer resulted in a significant increase in LIVE® staining on day 3 as compared to bCaP(7) and bCaP(24) (Fig. 3.5). Culturing MC3T3-E1s on AntiA-bCaP(48)-PEM30-FGF2 resulted in a significant decrease in percent LIVE® stained area on day 3 and throughout the remaining time points in the study as compared to cells cultured on its AntiA-free control (bCaP(48)-PEM30-FGF2) (Fig. 3.6); therefore AntiA was still being initially accessed on day 3; however unlike cells cultured on AntiA-bCaP(24)-PEM30-FGF2 where after day 3 the cells start to recover (Fig. 3.6A,B), cells on AntiA-bCaP(48)-PEM30-FGF2 continue to decrease from day 3 through day 7 (Fig. 3.6C,D). It is hypothesized that increasing the bCaP layer thickness changed the AntiA delivery from burst (observed with bCaP(24)) to potential sustained delivery (with bCaP(48)), hence why the cells continue to die over the course of multiple days. These theoretical delivery profiles of FGF-2 and AntiA from bCaP(24)-PEM30 and bCaP(48)-PEM30 are illustrated in Fig. 3.7.

It was shown in chapter 2 that the bCaP-PEM30 coating delivery of factors is cell-mediated as indicated by the lack of proliferative or cytotoxic effects observed when cells were cultured with collected release medium (from coated disks incubated without cells) (Fig. 2.15). These results lead to the hypothesis that using a cell-type more capable of degradation or resorption would result in faster delivery kinetics of the embedded factor. Because monocytes are one of the first cells recruited to the area when tissue is damaged or infected [119], these cells may be some of the first to interact with the bCaP-PEM30 coating *in vivo*. RAW 264.7 mouse monocyte macrophage cells (RAW) were therefore chosen for evaluating sequential delivery

kinetics of the bCaP-PEM coatings as a comparison to the pre-osteoblast MC3T3-E1 cells that are present at slightly later stages in the bone repair process. Two different RAW cell densities were tested on the bCaP-PEM30 coatings, 7.9k and 30k cells/cm^2. As expected, the increased cell seeding density resulted in increased LIVE® staining within 4 h on the control coatings (bCaP-PEM30-FGF2, no AntiA, Fig. 3.8A). Surprisingly, the increased cell seeding density did not increase 4 h LIVE® staining of RAW cells cultured on AntiA-bCaP-PEM30-FGF2 coatings (Fig. 3.8B); in fact it resulted in a significant decrease in LIVE® staining, suggesting the RAW cells may be accessing the AntiA within the first 4 h of culture. When the RAW cells are seeded at lower density (7.9k cells/cm^2), no differences in LIVE® staining are observed between the AntiA group and the AntiA-free control at the 4 h, day 1 and day 2 time points (Fig. 3.9); indicating AntiA is being blocked until access on day 3, similar to the osteoprogenitor cells. However, when the seeding density is increased to 30k cells/cm^2, a significant decrease in LIVE® staining is observed at the 4 h time point when comparing the AntiA group to its AntiA-free control (Fig. 3.10). This is much faster AntiA access than the day 3 access observed for the MC3T3-E1s cultured on the same coating, and as a result suggests that the bCaP-PEM30 coating can only provide co-delivery to macrophages at this density, as compared to the desired sequential delivery observed with the osteoprogenitors (Fig. 3.12). These results demonstrate that not only is the type of cells interacting with the coating important, but the number of cells as well; increasing the cell number resulted in faster degradation of the coating.

The two seeding densities selected to be used in the present studies were chosen to possibly mimic a normal, acute inflammation response (lower seeding density), as compared to a more severe, chronic inflammation response that could lead to a foreign body reaction (higher seeding density). The progression of events in inflammation and the foreign body response to an

implanted biomaterial requires the migration of monocytes/macrophages to the implant site (acute inflammation) and then the further propagation of chemoattractive signals such as PDGF, TNF-α, IL-6, granulocyte colony-stimulating factor (GCSF), and macrophage colony stimulating factor (MCSF) to call more macrophages to the wound site leading to chronic inflammation [188, 189]. At the lower seeding density, a 3 day delay to the embedded AntiA was occurring suggesting that a normal acute inflammatory response during the bone fracture healing process would offer some delay to the embedded factor *in vivo*. The higher seeding density that may associate to more severe, chronic inflammation response to the implanted biomaterial, offered no delay to the embedded AntiA meaning a severe reaction to the bCaP-PEM30 coating *in vivo*, would not be able to provide sequential delivery. Though our goals *in vivo* are to influence the osteoprogenitor cells with growth factor delivery, it is important to consider the effects of inflammation, therefore monocyte/macrophage cells, on the coating degradation and ultimate timing of growth factor delivery. A better understanding of cell type and number delivery kinetics of the bCaP-PEM coating would help better predict *in vivo* delivery kinetics.

Macrophages are capable of degrading non-cross-linked polyelectrolyte multilayer films [122]; more specifically, RAW 264.7 cells have previously been shown to digest PLLys-PLGlut multilayer particles [121], therefore it was expected that the RAW cells could degrade the PEM portion of the bCaP-PEM coating. Similar to the MC3T3-E1 osteoprogenitor cells, the RAW cells cannot dissolve or resorb the bCaP layer when in their undifferentiated state, as used in the present studies, (not differentiated into osteoclasts) [190]. It is therefore speculated that the rapid access to the embedded AntiA when the macrophages are seeded at the higher density is the result of their ability to degrade the PEM layers faster than the osteoprogenitors. Similar to the MC3T3-E1s, it is predicted that the RAW cells access the AntiA by being able to migrate

through micro-cracks in the bCaP layer to access the AntiA. FGF-2 has been shown to stimulate macrophage recruitment [191]; Fig. 3.11A shows that addition of FGF-2 to bCaP-PEM30 without AntiA causes a significant increase in initial cell attachment (4h, blue vs. green); however, when AntiA is present in the coating, addition of FGF-2 causes a significant decrease in LIVE® staining at the 4 h time point (Fig. 3.11B). These results indicate that FGF-2 is increasing initial cell attachment and that the increase in cells increases coating degradation as compared to the FGF-2-free control (Fig. 3.11B).

3.5 Conclusions

The bCaP-PEM coating is capable of local, cell-mediated delivery to both osteoprogenitor cells and macrophages. This means that the bCaP-PEM coating has the potential provide controlled, local delivery of growth factors *in vivo*, at the early stages of bone fracture healing. Increasing the number of PEM bilayers (30 to 102) within the coating could not further delay osteoprogenitor access to the embedded AntiA, but potentially inhibited the delivery kinetics of the FGF-2. Changing the chemical composition of the polyelectrolytes (*L*- to *D*- enantiomers) also could not further delay osteoprogenitor access to the embedded AntiA, but did hinder the delivery kinetics of the FGF-2. Increasing the thickness of the bCaP coating (~24 μm) from the normal ~6 μm did not change the initial timing of access to the embedded AntiA, but did change the delivery of AntiA from burst to sustained delivery over the course of 4 days to the osteoprogenitor cells. Changing the cell type used to evaluate delivery kinetics from the coating from osteoprogenitors to macrophages significantly increased access time to the embedded factor. When the macrophages were seeded at a low density (7.9k cells/cm^2) the bCaP-PEM30 coating provided 3 days delayed access to the embedded factor, similar to the osteoprogenitors. When the macrophages were seeded at a high density (30k cells/cm^2) the bCaP-PEM30 coating

failed to provide any delayed access to the embedded factor. These results highlight the importance of cell type and number when evaluating delivery kinetics from a cell-mediated delivery system. Understanding the macrophage response prior to the osteoprogenitor interaction with bCaP-PEM30 will better predict the *in vivo* response to the implanted bCaP-PEM30 coated scaffold.

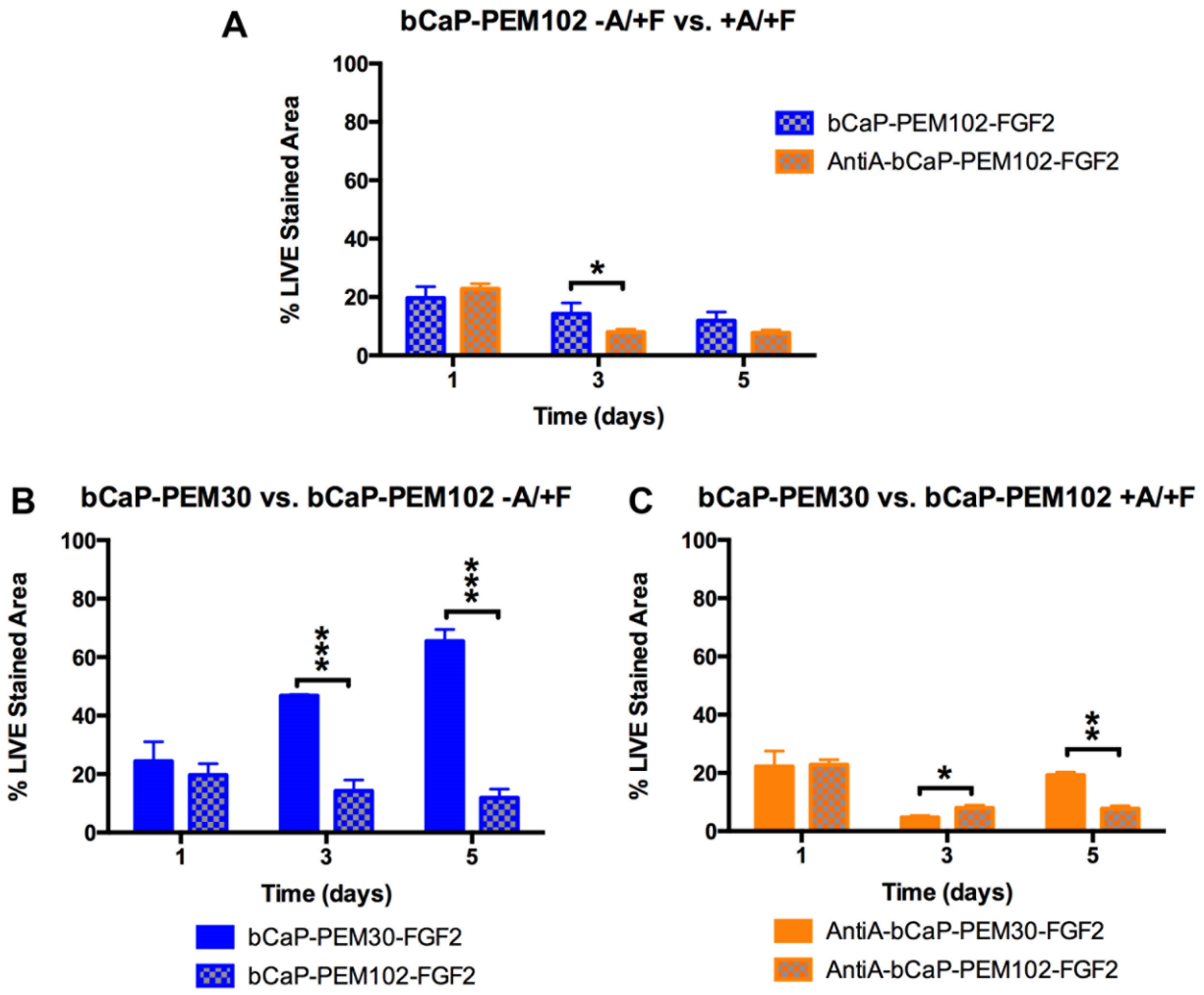

Figure 3.1 Percent LIVE® stained area of MC3T3-E1s cultured on AntiA-bCaP-**PEM102**-FGF2 (orange checker) as compared to cells cultured on bCaP-**PEM102**-FGF2 (blue checker) on days 1, 3, and 5 **(A)**, (* $p \leq 0.05$). Percent LIVE® stained area of MC3T3-E1s cultured on the control bCaP-PEM30-FGF2 as compared to cells on bCaP-**PEM102**-FGF2, **(B)**, (*** $p \leq 0.001$). Percent LIVE® stained area of MC3T3-E1s cultured on the control AntiA-bCaP-PEM30-FGF2 as compared to cells on AntiA-bCaP-**PEM102**-FGF2, **(C)**, (* $p \leq 0.05$, ** $p \leq 0.01$). AntiA = 213 μg/disk, FGF-2 = 150 ng/disk.

Figure 3.1A

Unpaired t test	
Day 3 P value	0.0202

Figure 3.1B

Unpaired t test	
Day 3 P value	0.0003
Day 5 P value	0.0004

Figure 3.1C

Unpaired t test	
Day 3 P value	0.0003
Day 5 P value	0.0004

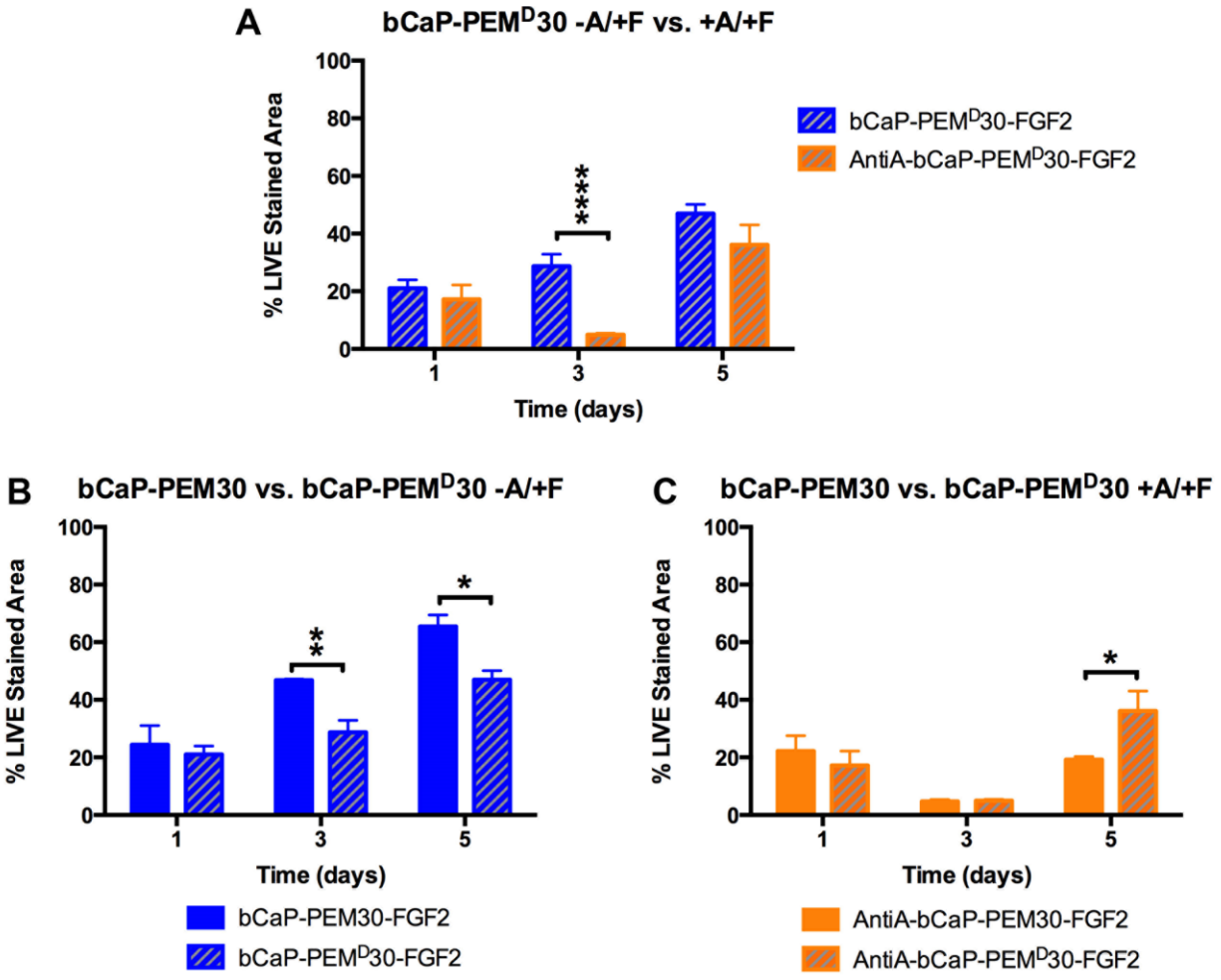

Figure 3.2 Percent LIVE® stained area of MC3T3-E1s cultured on AntiA-bCaP-**PEM^{D}30**-FGF2 (orange stripes) as compared to cells cultured on bCaP-**PEM^{D}30**-FGF2 (blue stripes) on days 1, 3, and 5 **(A)**, (**** $p \leq 0.0001$). Percent LIVE® stained area of MC3T3-E1s cultured on the control bCaP-PEM30-FGF2 as compared to cells on bCaP-**PEM^{D}30**-FGF2, **(B)**, (* $p \leq 0.05$, ** $p \leq 0.01$). Percent LIVE® stained area of MC3T3-E1s cultured on the control AntiA-bCaP-PEM30-FGF2 as compared to AntiA-bCaP-**PEM^{D}30**-FGF2, **(C)**, (* $p \leq 0.05$). AntiA = 213 µg/disk, FGF-2 = 150 ng/disk.

Figure 3.2A

Unpaired t test	
Day 3 P value	< 0.0001

Figure 3.2B

Unpaired t test	
Day 3 P value	0.0100
Day 5 P value	0.0360

Figure 3.2C

Unpaired t test	
Day 5 P value	0.0319

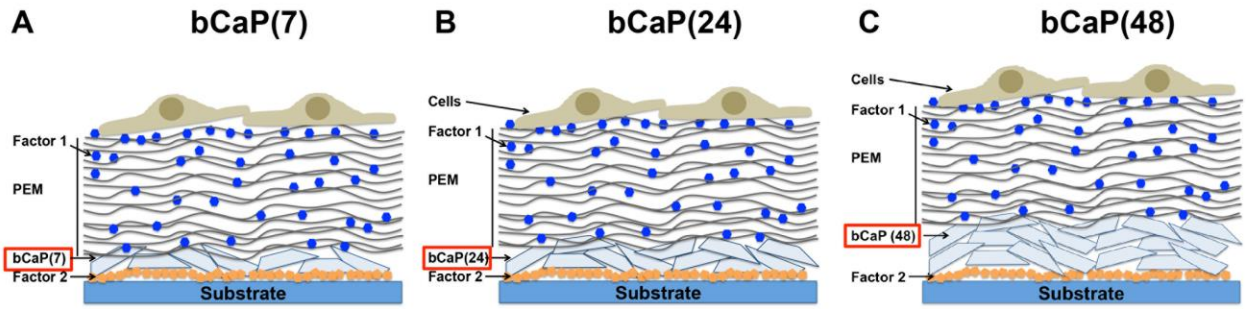

Figure 3.3 Schematic representations of bCaP-PEM30 coatings made with bCaP prepared by 7 h in Solution B **(A)**, normal or 24 h in Solution B **(B)**, and 48 h in Solution B **(C)**.

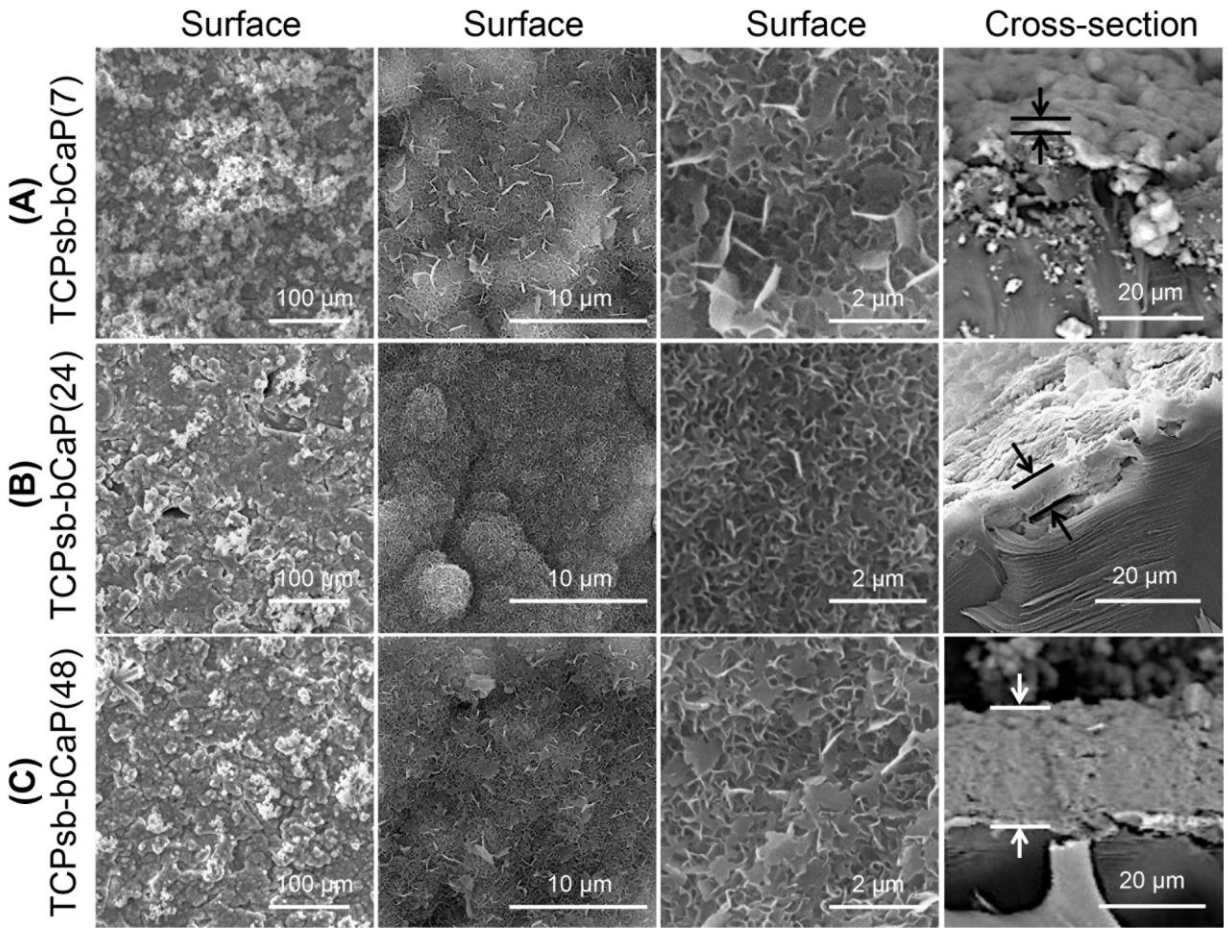

Figure 3.4 Scanning electron microscopy images of the surface morphology and cross-section of bCaP prepared by 7 h in Solution B **(A)**, normal or 24 h in Solution B **(B)**, and 48 h in Solution B **(C)**. bCaP(7) thickness = 1.8 $\pm$ 0.7 µm, bCaP(24) thickness = 5.8 $\pm$ 1.8 µm, and bCaP(48) thickness = 24.0 $\pm$ 2.4 µm.

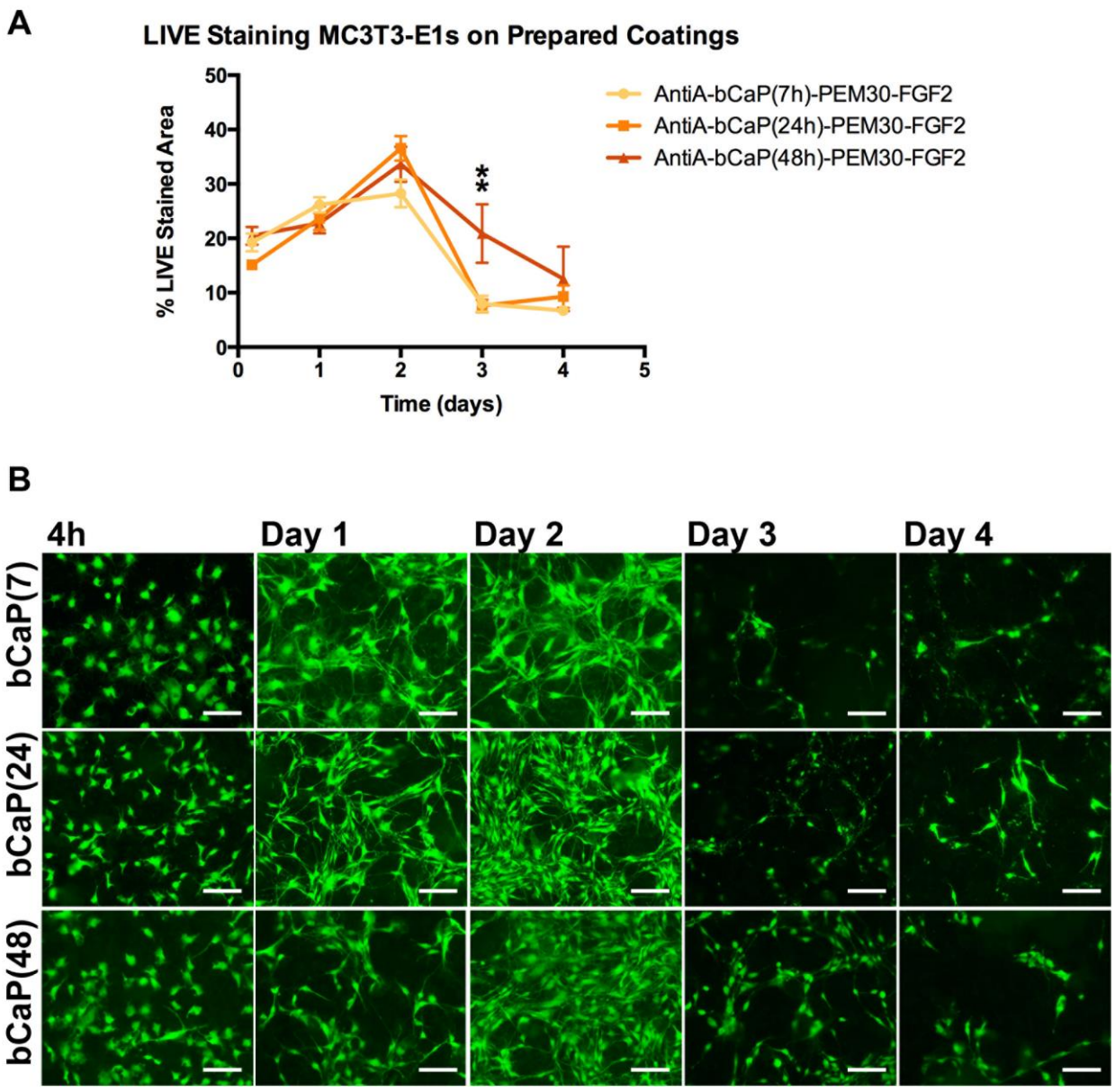

Figure 3.5 Percent LIVE® stained area of MC3T3-E1s cultured on AntiA-bCaP(7)-PEM30-FGF2, AntiA-bCaP(24)-PEM30-FGF2, and AntiA-bCaP(48)-PEM30-FGF2 on time points 4 h, days 1-4 **(A)**, (** $p \leq 0.01$). Fluorescent images of MC3T3-E1s cultured on AntiA-bCaP(7)-PEM30-FGF2, AntiA-bCaP(24)-PEM30-FGF2, and AntiA-bCaP(48)-PEM30-FGF2 **(B)**. AntiA = 213 μg/disk, FGF-2 = 150 ng/disk.

ANOVA P value = 0.0014

Tukey's multiple comparisons test	Mean Diff.	95% CI of diff.	Significant?	Summary
AntiA-bCaP(7h)-PEM30-FGF2 vs. AntiA-bCaP(48h)-PEM30-FGF2	-12.92	-20.32 to -5.528	Yes	**
AntiA-bCaP(24h)-PEM30-FGF2 vs. AntiA-bCaP(48h)-PEM30-FGF2	-13.31	-20.22 to -6.390	Yes	**

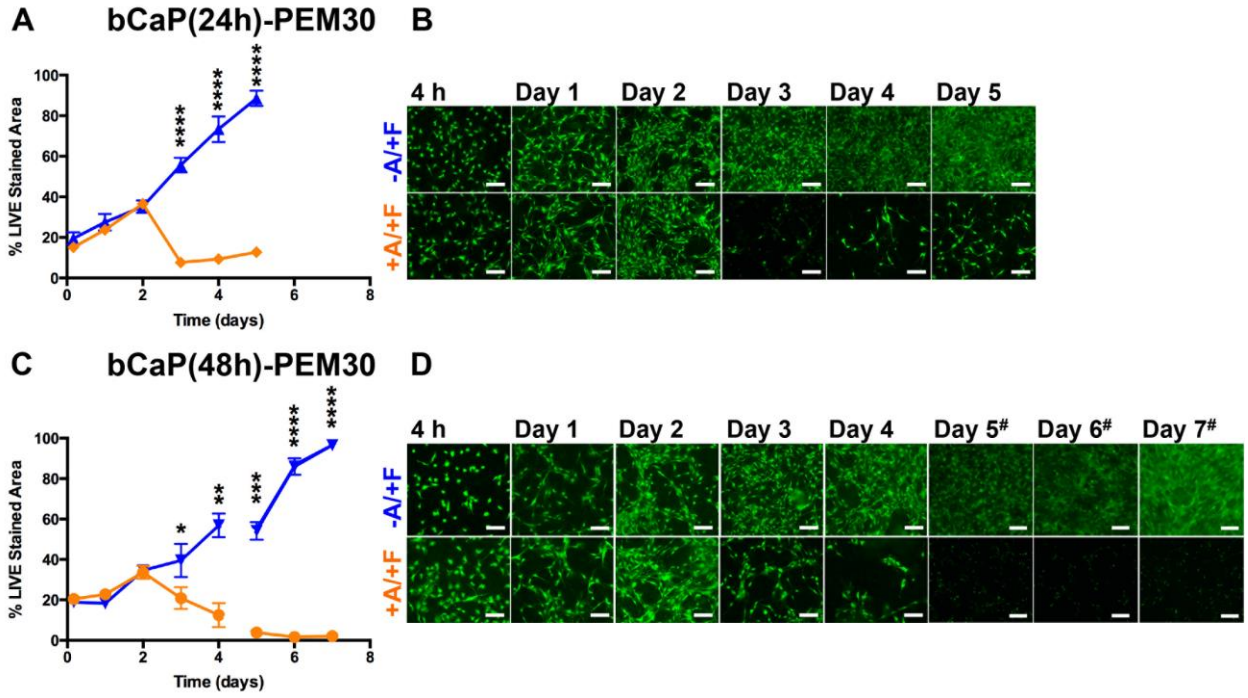

Figure 3.6 Percent LIVE® stained area of MC3T3-E1s cultured on bCaP(24)-PEM30-FGF2 (-A/+F) and AntiA-bCaP(24)-PEM30-FGF2 (+A/+F) **(A)** with corresponding fluorescent images of cells **(B)**, (**** $p \leq 0.0001$). (Note, this data is from Fig. 3.3 and is being shown for reference). Percent LIVE® stained area of MC3T3-E1s cultured on bCaP(48)-PEM30-FGF2 (-A/+F) and AntiA-bCaP(48)-PEM30-FGF2 (+A/+F) **(C)** with corresponding fluorescent images of cells **(D)**, (* $p \leq 0.05$, ** $p \leq 0.01$*** $p \leq 0.001$, **** $p \leq 0.0001$). (Note, data obtain for Days 5, 6 and 7 were obtained from a separate experiment). Scale bar = 250 μm. AntiA = 213 μg/disk, FGF-2 = 150 ng/disk.

Figure 3.6 A, see Figure 2.16B statistics

Figure 3.6B

Unpaired t test	
Day 3 P value	0.0304
Day 4 P value	0.0037

Day 5 P value	< 0.0001
Day 6 P value	< 0.0001
Day 7 P value	< 0.0001

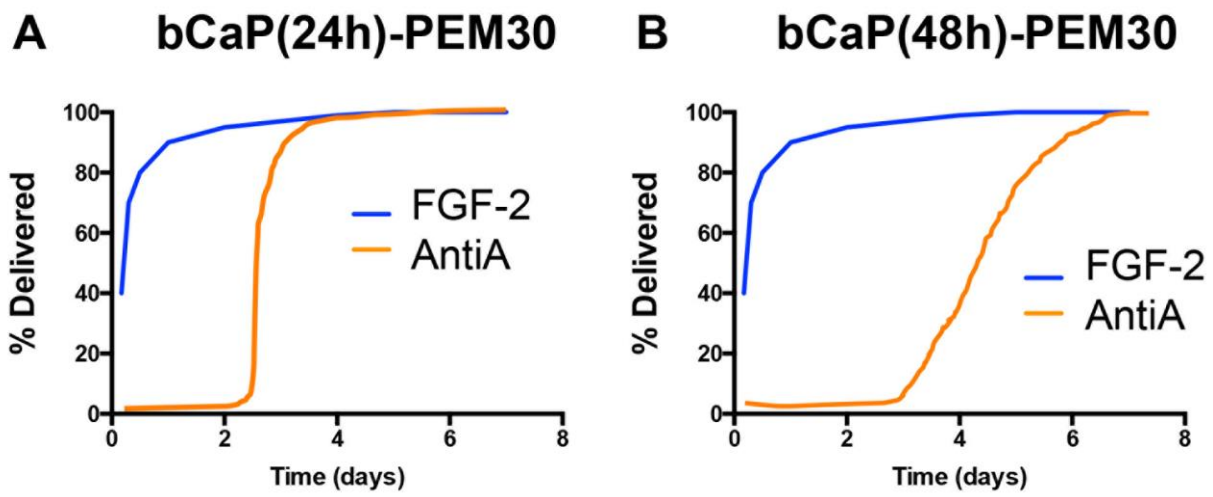

Figure 3.7 Theoretical delivery profiles of FGF-2 and AntiA from bCaP(24h)-PEM30 demonstrating burst delivery of AntiA **(A)** and bCaP(48h)-PEM30 demonstrating sustained delivery of AntiA **(B)**.

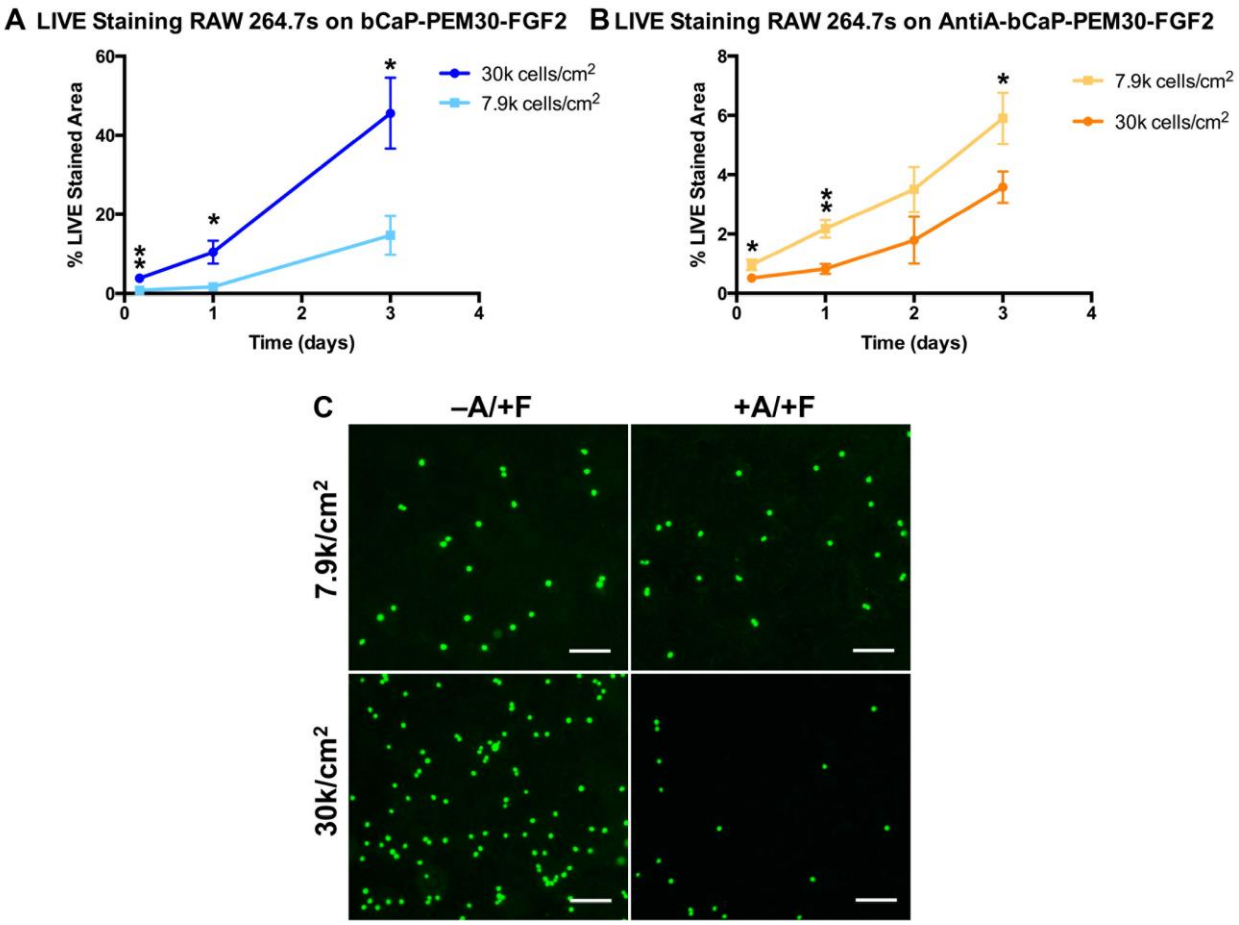

Figure 3.8 Percent LIVE® stained area of RAW 264.7 s cultured on bCaP-PEM30-FGF2 (-A/+F) **(A)**, and AntiA-bCaP-PEM30-FGF2 (+A/+F) **(B)** at seeding densities of 7.9k or 30k cells/cm^2 (* $p \leq 0.05$, ** $p \leq 0.01$). Fluorescent images of the cells at 4 h of culture **(C)**. Scale bar = 250 μm. AntiA = 213 μg/disk, FGF-2 = 150 ng/disk.

Figure 3.8A

Unpaired t test	
4 h P value	0.0084
Day 1 P value	0.0118
Day 3 P value	0.0141

Figure 3.8B

Unpaired t test	
4 h P value	0.0146
Day 1 P value	0.0023
Day 3 P value	0.0162

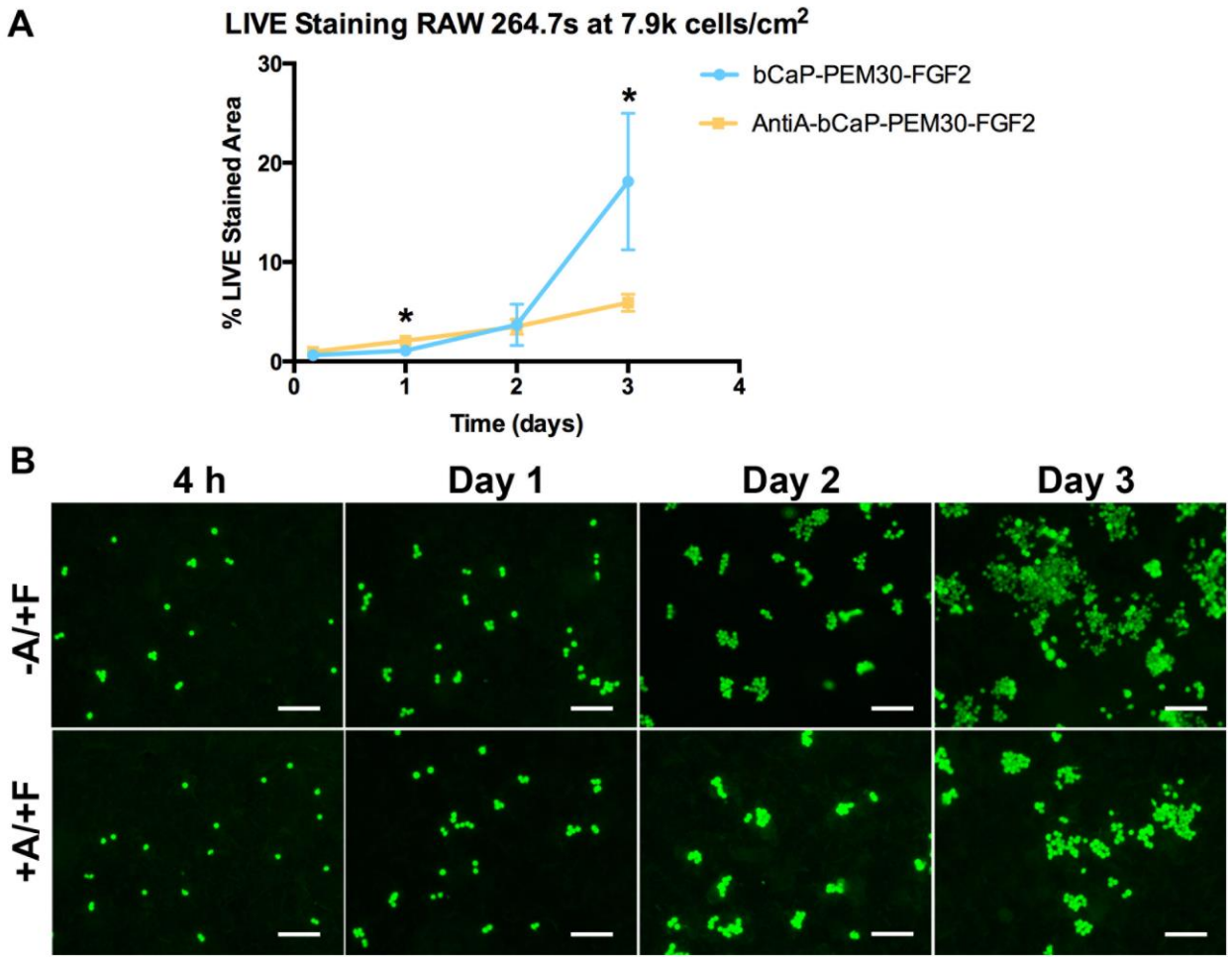

Figure 3.9 Percent LIVE® stained area of RAW 264.7 cells cultured on bCaP-PEM30-FGF2 (-A/+F) and AntiA-bCaP-PEM30-FGF2 (+A/+F) seeded at 7.9k cells/cm^2 **(A)**, (* $p \leq 0.05$). Fluorescent images of the cells at 4 h, 1 day, 2 days and 3 days of culture **(B)**. Scale bar = 250 μm. AntiA = 213 μg/disk, FGF-2 = 150 ng/disk.

Unpaired t test	
Day 1 P value	0.0211
Day 3 P value	0.0380

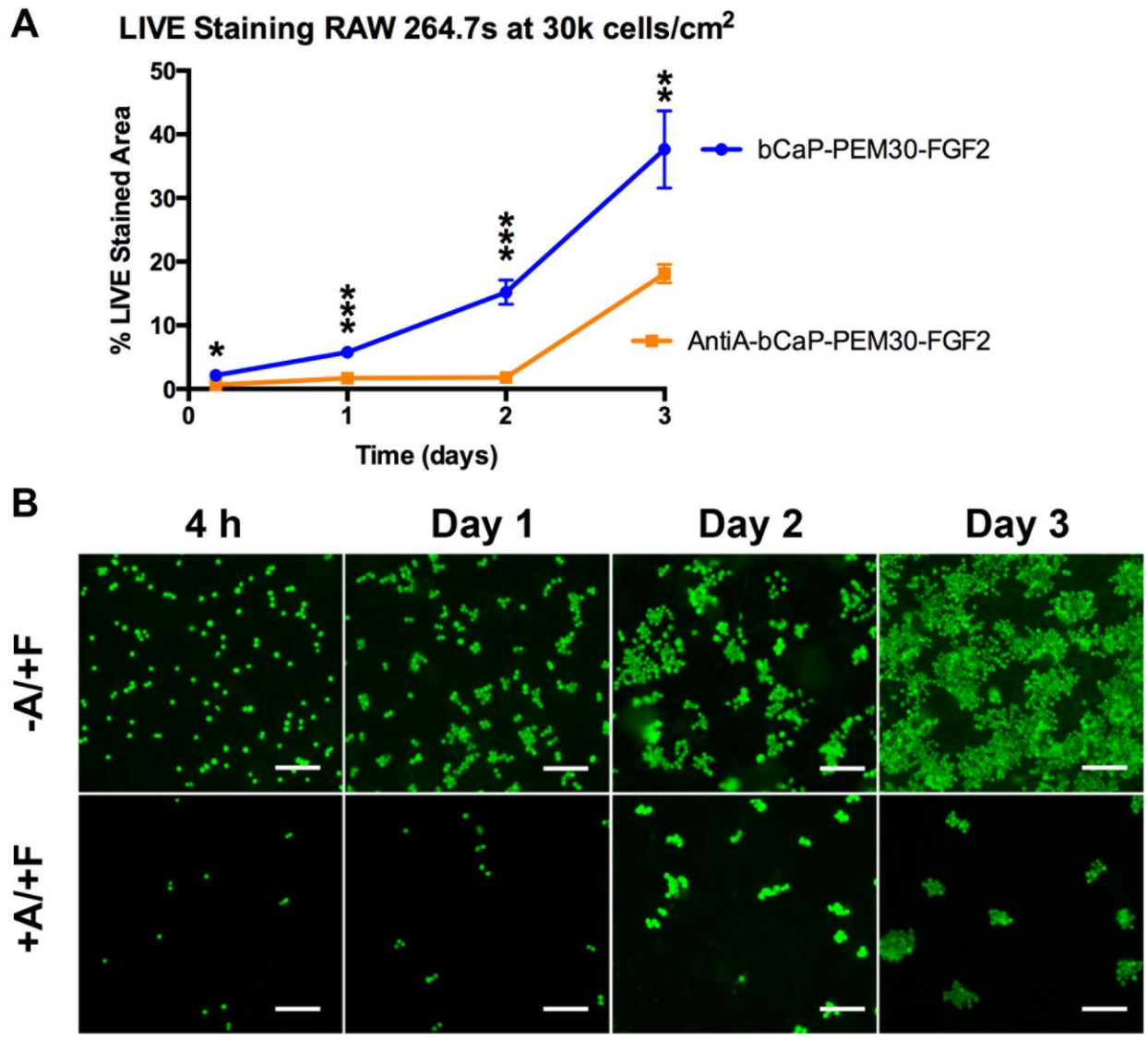

Figure 3.10 Percent LIVE® stained area of RAW 264.7 cells cultured on bCaP-PEM30-FGF2 (-A/+F) and AntiA-bCaP-PEM30-FGF2 (+A/+F) seeded at 30k cells/cm^2 **(A)**, (* $p \leq 0.05$, ** $p \leq 0.01$, *** $p \leq 0.001$). Fluorescent images of the cells at 4 h, 1, 2, and 3 days of culture **(B)**. Scale bar = 250 μm. AntiA = 213 μg/disk, FGF-2 = 150 ng/disk.

Unpaired t test	
4 h P value	0.0231
Day 1 P value	0.0002
Day 2 P value	0.0003
Day 3 P value	0.0056

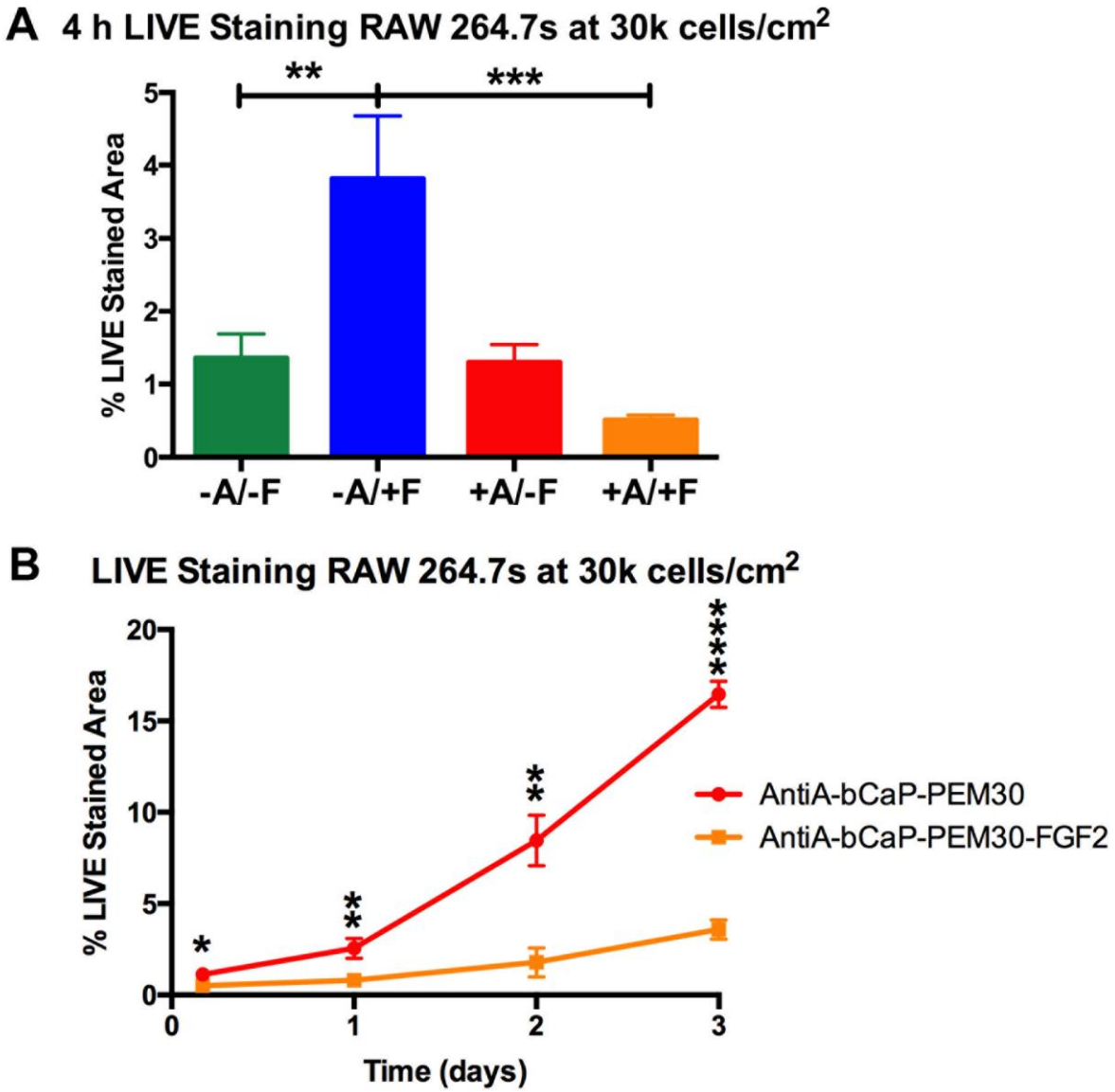

Figure 3.11 Percent LIVE® stained area of RAW 264.7 cells seeded at 30k cells/cm^2 on bCaP-PEM30 (green, -A/+F), bCaP-PEM30-FGF2 (blue, -A/+F), AntiA-bCaP-PEM30 (red, +A/-F), and AntiA-bCaP-PEM30-FGF2 (orange, +A/+F) at 4 h of culture, **(A)**. Percent LIVE® stained area of RAW 264.7s seeded at 30k cells/cm^2 on AntiA-bCaP-PEM30 (red), and AntiA-bCaP-PEM30-FGF2 (orange) at 4 h, and days 1-3, **(B)**. (* $p \leq 0.05$, ** $p \leq 0.01$, *** $p \leq 0.001$, **** $p \leq 0.0001$). AntiA = 213 μg/disk, FGF-2 = 150 ng/disk.

Figure 3.11A

ANOVA P value = 0.0002

Tukey's multiple comparisons test	Mean Diff.	95% CI of diff.	Significant?	Summary
-A/-F vs. -A/+F	-2.458	-3.651 to -1.265	Yes	**
-A/+F vs. +A/+F	3.307	2.113 to 4.500	Yes	***

Figure 3.11B

Unpaired t test	
4 h P value	0.0346
Day 1 P value	0.0060
Day 2 P value	0.0019
Day 3 P value	< 0.0001

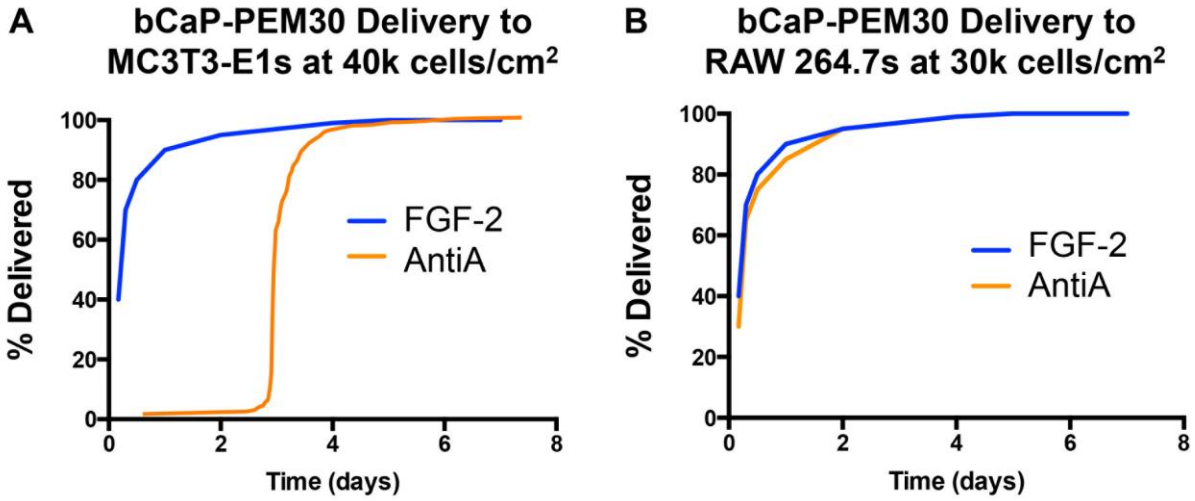

Figure 3.12 The theoretical sequential delivery profile of FGF-2 and AntiA from bCaP-PEM30 cultured with osteoprogenitor cells (MC3T3-E1s at 40k cell/cm^2) **(A)**, as compared to the co-delivery of factors from bCaP-PEM30 cultured with macrophages (RAW 264.7a at 30k cells/cm^2) **(B)**.

Chapter 4

Sequential Delivery of FGF-2 and BMP-2 from Biomimetic Calcium Phosphate/PEM Coatings for *In Vivo* Osteogenesis

4.1 Introduction

Roughly 6.8 million patients each year seek medical attention in the United States for bone fractures (American Academy of Orthopaedic Surgeons). With modern treatment methods, most bone fractures heal without any problems. However, a small, but significant proportion of broken bones do not heal even with the best surgical or non-surgical treatments and this can lead to a delayed- or non-union. Several factors can increase the risk of failed bone fracture healing including: complicated/severe breaks, older age, poor nutrition, smoking, infection, and diseases such as anemia, osteoporosis, vitamin D deficiencies, and diabetes, (American Academy of Orthopaedic Surgeons). Treatment methods for large nonunions include the use of bone grafts or bone graft substitutes. Autogenous and allogenic bone grafts have desirable osteoconductive and osteoinductive properties, with autografts being considered the gold standard for treating these types of defects [192, 193]. These methods provide scaffolding for patient's bone to heal across the nonunion/defect but lack the chemical signals and growth factors normally present to stimulate natural bone regeneration and can result in insufficient healing, especially when the autograft is taken from a patient with the increased risk factors that result in poor healing to begin with.

There are a number of growth factors involved in bone healing, however bone morphogenetic protein-2 (BMP-2) is the main one used clinically for bone repair. This is because BMP-2 is one of the main growth factors responsible for initiating the differentiation of

osteoprogenitors into osteoblasts leading to new bone formation [36]. BMP-2 delivered via a collagen sponge (INFUSE Bone Graft, Medtronic, FDA approved) significantly enhances bone formation and successful spinal fusion, [28]; however its use has been limited due to complications with the required high dose of BMP-2 necessary for adequate bone formation. These complications include severe inflammation, ectopic bone formation, osteolysis, seroma formation, and possible increase in the risk of malignancy, [19, 30]. These problems stem from the collagen sponge's inability to contain the supraphysiologic dose of BMP-2 in the local tissue environment and control its release. *There is a need to refine the delivery and improve the efficacy of BMP-2 so that it can be locally delivered in lower doses, with less risk of complications.*

Another growth factor necessary for bone healing, fibroblast growth factor 2 (FGF-2), has been shown to increase proliferation, migration, and bone morphogenetic protein 2 (BMP-2) sensitivity of osteoprogenitor cells when delivered at early time points [36, 78], and to inhibit osteoblast differentiation at later stages [88]. The synergistic combination of FGF-2 with BMP-2 has shown promise as a means to reduce the BMP-2 dose necessary for bone formation [93, 97]. Growth factors have different effects on natural bone regeneration depending on the developmental stage of the fracture healing process they are present during; therefore, sequence of delivery is important to optimize growth factor activity and healing. Too much and/or late stage exposure of FGF-2 at the same time as BMP-2 has been shown to reduce the amount of *in vitro* and *in vivo* bone formation [90, 93, 194]. BMP-2 delivered too early can also inhibit *in vitro* osteogenesis [104]. The benefit of sequential delivery of FGF-2 (early) and BMP-2 (late) has been further shown through growth factor spiking during *in vitro* osteogenesis studies [88,

90], providing additional motivation for the development of biomaterial systems for sequential delivery.

This chapter focuses on the use of a biomimetic calcium phosphate, poly-L-Lysine/poly-L-Glutamic acid (bCaP-PEM) coating applied to the commercially available bone graft substitute Healos® (DePuy Synthes Spine, Raynham, MA) to sequentially deliver FGF-2 and BMP-2 in a mouse calvarial defect model. It is hypothesized that early delivery of FGF-2 will stimulate the proliferation of osteoprogenitor cells, and delayed delivery of BMP-2 will stimulate the osteoprogenitor cells to differentiate into functioning osteoblasts, and this sequential delivery profile will enhance *in vivo* BMP-2 stimulated bone formation.

4.2 Materials and Methods

4.2.1 Design of Sequential Delivery System

For all *in vivo* testing a calcium phosphate layer was precipitated prior to a PLLys-PLGlut PEM application for delivery of BMP-2 only (Fig. 4.1A) or BMP-2and FGF-2 (Fig. 4.2B). The theoretical delivery profiles of the single- and sequential- delivery coatings are illustrated in Fig. 4.1C and D respectively. For the *in vivo* studies, two different coating architectures were used: amorphous calcium phosphate with 8 bilayers of PEM (CaP-PEM8), or nanocrystalline calcium phosphate with 30 bilayers of PEM (bCaP-PEM30).

4.2.2 Material Fabrication

4.2.2.a Preparation of CaP-PEM8 coated Healos®

Healos® (DePuy Synthes Spine, Raynham, MA) was trimmed to a thickness ~ 1mm, then scaffolds were cut out with a 3.5 mm biopsy punch (Integra Miltex, York, PA). Scaffolds were UV-sterilized for 10 min on each side prior to factor adsorption. A 0.5 μg dose of recombinant

human bone morphogenic protein 2 (BMP-2, R & D Systems, Minneapolis, MN) was applied to the Healos® scaffolds by adding 2 µl of 250 µg/ml stock made in PBS to each scaffold and allowing it to adsorbed for 1 h at room temperature.

After BMP-2 adsorption each scaffold was placed in a 1.5 ml micro-centrifuge tube and 1 ml of SBFx5 Solution A (prepared as described in Ch. 2) that is used to precipitate an amorphous CaP layer on the scaffold was added to each tube. Tubes were left open and covered in parafilm with 8-10 small holes poked through the parafilm. Tubes were placed in a 37°C oven. After ~24 h tubes were removed from the oven and sonicated (with scaffolds still in reacted SBFx5 Solution A) for ~ 10 sec to remove loosely bound CaP. Each scaffold was then placed in a 96-well plate and rinsed 3x with MilliQ water.

Each scaffold was then placed in a 1.5 ml centrifuge tube (EMD Millipore, Billerica, MA) with a 0.65 µm filter-membrane. The micro-centrifuge tubes are made up of two compartments separated by the membrane; this allows the sample to sit submerged in solution on top of the membrane until tubes are centrifuged, which then forces the solution through the scaffold and through the membrane, leaving the supernatant separated from the sample. 300 µl of 1 mg/ml poly-L-Glutamic acid (PLGlut, Sigma, St. Louis, MO) in saline was added to each tube and allowed to adsorb to the scaffold for 10 min. Note that the membrane is of sufficiently fine porosity that it does not allow the solution to go through it until the centrifugation step therefore the scaffold is completely immersed in the solution. After 10 min, tubes were centrifuged for ~10 sec at 1000 rpms and the supernatants contained below the membrane were discarded. Each scaffold was then rinsed 3x with saline with centrifugation after each rinse. Then 300 µl of 1 mg/ml poly-L-Lysine (PLLys, Sigma, St. Louis, MO) in saline was added to each tube and

allowed to adsorb for 10 min, then centrifuged and rinsed 3x with saline. This procedure was repeated until 8 bilayers of PEM were adsorbed (1 bilayer = PLGlut-PLLys).

After PEM8 application, recombinant human fibroblast growth factor 2 (FGF-2, R & D Systems, Minneapolis, MN) was adsorbed by adding 2 µl of various FGF-2 working stocks (prepared in saline) to each scaffold and allowed to bind for 1 h at room temperature. The following doses were tested: 0, 0.25, 5, 100, and 125 ng FGF-2. After FGF-2 adsorption, the scaffolds were rinsed 3x in saline then put in 300 µl DMEM high glucose, pyruvate medium, (No. 11995, Gibco BRL, Invitrogen) and stored in a 8-20°C refrigerator until ready for implantation. Prior to implantation the scaffolds were centrifuged for ~ 10 sec at 1000 rpms. This entire procedure is illustrated in Fig. 4.2.

4.2.2.b Preparation of bCaP-PEM30 coated Healos®

Healos® scaffolds were cut and sterilized as previously described. A 2 µg dose of recombinant human bone morphogenic protein 2 (BMP-2, R & D Systems, Minneapolis, MN) was applied to the Healos® scaffolds by adding 2 µl of 1 mg/ml stock made in PBS to each scaffold and allowing it to adsorbed for 1 h at room temperature.

For bCaP application, the two-step SBF method described in Ch. 2 was used to produce a nanocrystalline bCaP layer rather than just the amorphous layer previously described. During BMP-2 adsorption SBF Solution A was prepared as described in Ch. 2. Scaffolds were added to the beaker equipped with a stir bar. The beaker was covered with saran wrap with 20-30 holes punched into it and placed on a stir plate set to match the mixing during Solution A prep (~ 130 rpms) in a 37°C oven. After ~24 h the beaker was removed from the oven and sonicated (with scaffolds still in reacted Solution A) for ~ 10 sec. Prior to immersion in Solution B, the scaffolds

were gradually dehydrated by being passed through a graded series of increasing concentrations of ethyl alcohol.

Solution B was prepared as described in Ch. 2. Scaffolds were added to the beaker equipped with a stir bar. The beaker was covered with saran wrap with 20-30 holes punched into it and placed on a stir plate set to match the mixing during Solution B prep (~ 130 rpms) in a 50°C oven. After 7 or 24 h, the beaker was removed from the oven and sonicated (with scaffolds still in reacted Solution B) for ~ 10 sec. The scaffolds were gradually dehydrated by being passed through a graded series of increasing concentrations of ethyl alcohol.

After bCaP deposition, each scaffold was then placed in a 0.65 μm micro-centrifuge tube and 30 bilayers of PLGlut-PLLys were applied as previously described for PEM8. After PEM30 application, a 5 ng recombinant human fibroblast growth factor 2 (FGF-2, R & D Systems, Minneapolis, MN) dose was adsorbed and allowed to bind for 1 h at room temperature. After FGF-2 adsorption, the scaffolds were rinsed 3x in saline then put in 300 μl DMEM high glucose, pyruvate medium, (No. 11995, Gibco BRL, Invitrogen) and stored in a 8-20°C refrigerator until ready for implantation. Prior to implantation the scaffolds were centrifuged for ~ 10 sec at 1000 rpms. This entire procedure is illustrated in Fig. 4.3.

4.2.3 Characterization

4.2.3.a Scanning Electron Microscopy (SEM)

The microscopic morphology of the coated scaffolds was characterized using SEM (JSM - 5900LV, Jeol USA Inc. Peabody, MA). Coated scaffolds were also cut in half, allowing examination of the innermost fibers of the Healos® scaffold via SEM.

4.2.4 In Vivo Osteogenesis Assays with a Mouse Calvarial Defect Model

The CD1 female mice were purchased from Jackson Laboratory, (Bar Harbor, ME) and used for studies at 4-7 months of age. Col 3.6-cyan female reporter mice (with a CD1 background) were bred in house and used for studies at 4-7 months of age. Mice in this age range were used because they are considered skeletally mature. All animal experimental procedures were approved by the Animal Care and Use Committee of the University of Connecticut Health Center, (Farmington, CT).

Mice were anesthetized and placed in a prone position, and the cranium was shaved of fur, washed with betadine, and swabbed with alcohol. The periosteum was incised over the parietal bone in the frontal plane with a scalpel blade. A 3.5 mm diameter hole was created in the center and through one of the two parietal bones using a trephine and avoiding cranial sutures. A prepared scaffold was implanted in the calvarial defect, and then the periosteum and subcutaneous tissue was closed with sutures, followed by closing sutures of the skin incision. The animals were allowed to recover until ambulating and feeding normally. Mice were euthanized by asphyxiation with carbon dioxide, and calvaria were harvested after 1, 3, or 4 weeks post-surgery. Mice being sacrificed after 1 week were used to evaluate proliferating cells; therefore all mice in these groups received peritoneal cavity injections of 3 μg/g EdU (5-ethynyl-2-deoxyuridine, a nucleoside analog of thymidine) 1 day prior to euthanasia. New bone formation at 3 and 4 weeks was evaluated with x-ray and microCT analysis. 1-6 mice/group were used for the calvarial defect studies; specific “n” for each group/study will be indicated in results figures.

4.2.5 Statistical Analyses

Statistical significances were determined by unpaired t-tests and one-way ANOVA with Tukey post-tests, with a *p-value* ≤ 0.05 being considered statistically significant. Standard deviations are shown in all figures.

4.3 Results

4.3.1 Characterization of CaP, bCaP, and bCaP-PEM coated Healos®

Amorphous CaP could successfully be deposited on Healos® as evident by SEM (Fig. 4.4), and had similar morphology to when amorphous CaP was applied to the sand blasted disks for *in vitro* studies (Fig. 2.3B). bCaP prepared by either 7 h or 24 in Solution B could be deposited on Healos®, however, observed porosity decreased with increasing time in Solution B (Fig. 4.5). bCaP(7) prepared by 7 h in Solution B, on the outer/surface fibers of the Healos® scaffold had the same nanocrystalline morphology (Fig. 4.6C) to bCaP deposited on the sandblasted disks for *in vitro* studies (Fig. 2.3C). These nanocrystals were still evident on the innermost fibers of the Healos® scaffold however they were less densely packed (Fig. 4.6C top vs. bottom panel). Uniform deposition of bCaP(7) on outer and inner Healos® fibers was achieved. After PEM30 application to Healos-bCaP(7), the nanocrystals of bCaP(7) layer can no longer be observed (Fig. 4.7). Similar, uniform morphology was observed for the outer and inner fibers of the Healos® scaffold (Fig. 4.7 top vs. bottom panel).

4.3.2 In Vivo Osteogenesis Assays with a Mouse Calvarial Defect Model

4.3.2a Determining a Sub-optimal Dose of BMP-2 for CaP-PEM8 Delivery

0.5 μg BMP-2 delivered from Healos® scaffolds coated with amorphous CaP and 8 bilayers of PEM (BMP2-CaP-PEM8) resulted in minimal new bone formation as compared to the BMP-2-

free control scaffolds after 4-weeks post-surgery (Fig. 4.8). The new bone formation was only evident on the edges of the defect (Fig. 4.8 red circles). This was considered a desirable result because this dose of BMP-2 did not completely heal the defect after 4-weeks implantation; it was selected to be used as the control dose of BMP-2 that FGF-2 was used in combination with to enhance BMP-2-stimulated *in vivo* bone formation in future studies.

4.3.2b Proliferative Effects of the Dual Delivery of FGF-2 and BMP-2 from CaP-PEM8

The addition of 25 ng FGF-2 to scaffolds coated with BMP2-CaP-PEM8 increased the number of EdU positive host cells, therefore proliferating cells, present at the center of the calvarial defect 1-week after implantation as compared to the BMP-2 only control (Fig. 4.9A, B). The addition of 125 ng FGF-2 to scaffolds coated with BMP2-CaP-PEM8 significantly increased the number of EdU positive host cells, therefore proliferating cells, present at the center of the calvarial defect 1-week after implantation as compared to the BMP-2 only control and BMP2-CaP-PEM8-FGF2 (25 ng) (Fig. 4.9C, * $p \leq 0.05$, ** $p \leq 0.01$).

4.3.2b Osteogenic Effects of the Dual Delivery of FGF-2 and BMP-2 from CaP-PEM8

Though it was observed that the 125 ng dose of FGF-2 delivered with 0.5 μg BMP-2 (Healos-BMP2-CaP-PEM8-FGF2) significantly increased the number of proliferating cells within the center of the defect after 1-week implantation, this dose of FGF-2 had an inhibitory effect on new bone formation (Fig. 4.10A-D). After 4-weeks implantation, the FGF-2 and BMP-2 scaffolds (Healos-BMP2-CaP-PEM8-FGF2) resulted in 0.73 $\pm$ 0.12 mm^3 bone volume, compared to the BMP-2 only scaffolds (Healos-BMP2-CaP-PEM8) that resulted in 1.83 $\pm$ 1.13 mm^3 bone volume (Fig. 4.10E).

These results prompted additional testing of Healos® coated with BMP2-CaP-PEM8-FGF2 using the 0.5 μg dose of BMP-2, plus 0.25, 5, and 100 ng FGF-2. After 4-weeks implantation the BMP-2 only group resulted in 1.83 $\pm$ 1.13 mm^3 bone volume, and the FGF-2 doses resulted in 0.17 $\pm$ 0.17 (0.25 ng), 0.23 $\pm$ 0.24 (5ng), and 0.35 $\pm$ 0.24 (100 ng) mm^3 bone volume. All doses of FGF-2 tested resulted in significant decrease in new bone formation/volume compared to the BMP-2 only control (Fig. 4.11, * $p \leq 0.05$, ** $p \leq 0.01$).

4.3.2b Osteogenic Effects of the Sequential Delivery of FGF-2 and BMP-2 from bCaP-PEM30

Healos® coated with nanocrystalline bCaP and 30 bilayers of PEM, and no growth factors, (bCaP-PEM30) resulted in minimal to no bone formation after 3-weeks post- calvarial defect surgery (0.38 mm^3, Fig. 4.12A). Healos® coated with BMP2-bCaP-PEM30 (BMP-2 = 2 μg) resulted in new bone formation only observed around the defect edges (0.89 $\pm$ 0.32 mm^3, Fig. 4.12B, red circles). Healos® coated with BMP2-bCaP-PEM30-FGF2 (BMP-2 = 2 μg, FGF-2 = 5 ng) resulted in new bone formation observed around the defect edges and some within the center of the defect (1.32 $\pm$ 0.33 mm^3, Fig. 4.12C, red circles). The addition of BMP-2 and FGF-2 delivered from bCaP-PEM30 resulted in a trend of increasing bone volume as compared to the control scaffold with no growth factor and the BMP-2 only scaffold, however these results were not statistically significant (Fig. 4.12D). It should be noted that the BMP-2 only, and BMP-2 and FGF-2 groups could not be statistically compared to the growth factor-free control group because this group had a n = 1.

4.4 Discussion

Growth factors have different effects on natural bone regeneration depending on the developmental stage of the healing process they are present during. Specifically, the sequential delivery of FGF-2, then BMP-2 has been shown to increase *in vitro* osteogenesis over co-

delivery of both factors [88, 90]; therefore, there is a need for new biomaterials to biomimetically deliver multiple growth factors in a sequential manner to maximize their stimulatory effects. This chapter focused on the use of the novel, sequential delivery bCaP-PEM coating applied to a commercially available bone graft substitute, to deliver FGF-2 and BMP-2 to enhance *in vivo* osteogenesis in a mouse calvarial defect model over BMP-2 only delivery.

Both BMP-2 and FGF-2 have been successfully delivered individually from calcium phosphate/hydroxyapatite materials [195-201], and PEM films and particles [156, 160, 163, 202-205]. The combination of CaP and PEM without growth factors has been shown to stimulate osteogenesis due to CaP's biomimetic, osteoconductive properties [120, 123, 157, 180]. Furthermore, the combination of CaP and PEM has also been demonstrated to successfully deliver BMP-2 [116, 117]. Due to the synergistic properties of FGF-2 and BMP-2 used in combination on osteogenesis, it seemed logical to deliver both growth factors from a calcium phosphate/polyelectrolyte biomaterial to stimulate *in vivo* osteogenesis.

Amorphous CaP could be uniformly applied to the fibers of the Healos® scaffold (Fig. 4.4). Using the amorphous CaP coating with 8 bilayers of PEM (CaP-PEM8), calvarial defect studies were conducted in 4-7 month old female mice to determine first, a suboptimal dose of BMP-2, and then to study the proliferative and osteogenic effects of the addition of FGF-2 delivered with the BMP-2. In all studies the BMP-2 was adsorbed directly to the Healos® scaffold, then embedded under CaP-PEM8. In the groups with FGF-2, FGF-2 was adsorbed as the outermost layer of the scaffold coating (Healos-BMP2-CaP-PEM8-FGF2).

In the first study, 0.5 μg BMP-2 delivered from CaP-PEM8 coated Healos® scaffold resulted in minimal bone formation only evident along the edges of the defect after 4-weeks implantation (Fig. 4.8, red circles). This was considered a desirable result at the time; the goal of

this study was to determine a suboptimal dose of BMP-2 that could not completely heal the defect in the 4-week time point because it was hypothesized that the addition of FGF-2 to low dose BMP-2 could enhance *in vivo* osteogenesis; it was first necessary to determine a dose of BMP-2 that could be enhanced (because it could not heal the defect alone), and this was achieved with the 0.5 μg dose. With continued testing of the BMP-2 only group as the control for the FGF-2 dosing experiments, it was determined that the 0.5 μg dose was too suboptimal; with or without FGF-2 delivered from the CaP-PEM8 coating, minimal if any bone formation was observed after 4-weeks implantation. The lack of observed defect healing is why the dose of BMP-2 was increased to 2 μg for continued testing with the bCaP-PEM30 coating, in addition to the fact that the bCaP layer is much thicker than the amorphous CaP layer; this dose had demonstrated better *in vivo* efficacy for stimulating bone formation in a similar mouse calvarial defect model, [84, 108].

The reason FGF-2 was selected to be used in combination with BMP-2 was because it was hypothesized that the FGF-2 would stimulate the migration and proliferation of osteoprogenitor cells into the calvarial defect, therefore providing more cells within the defect to be differentiated and result in better overall healing. The next animal study looked at the proliferative effects of adding FGF-2 to the BMP2-CaP-PEM8 coated scaffold after just 1-week implantation. The addition of FGF-2 resulted in an observed increase in DAPI+ cells and increased EdU+ cells at the center of the defect as compared to the BMP-2 only group (Fig. 4.9). This indicated that not only were there more cells present at the center of the defect with increasing FGF-2, but these cells were also actively proliferating. These results confirmed the first part of the hypothesis and are supported by the literature [36, 78].

The second part of the hypothesis was that the increase in number of cells present at the center of the defect after 1-week would lead to overall increased bone formation after 4-weeks implantation. When looking at total bone volume after 4-weeks implantation, the 0.5 μg BMP-2 only group again resulted in minimal bone formation, only along the edges of the defect (Fig.4.10C, red circles). The addition of FGF-2 (125 ng) to the BMP-2 resulted in less bone formation as evident by microCT (Fig. 4.10D, red circle), and a decrease in quantified bone volume, as compared to the BMP-2 only group (Fig. 4.10E). These results indicate that even though the 125 ng FGF-2 was stimulating the proliferation of osteoprogenitors within the defect after 1-week, the dose had an overall inhibitory effect on new bone formation after 4-weeks. It is known that too much and/or late stage exposure of FGF-2 can inhibit *in vitro* and *in vivo* bone formation when delivered with BMP-2 because it can maintain cells in an undifferentiated state [90, 93, 194]. This led to the assumption that 125 ng FGF-2 was too high of a dose, and prompted additional testing with FGF-2 doses of 0.25, 5, and 100 ng in combination with the 0.5 μg BMP-2 (Healos-BMP2-CaP-PEM8-FGF2). All doses of FGF-2 tested significantly inhibited bone formation as compared to the BMP-2 only group (Fig. 4.11).

This led to the hypothesis that delivery of FGF-2 and BMP-2 from the CaP-PEM8 coating was occurring as co-delivery and not as the intended sequential delivery. These animal studies were conducted concurrently with the *in vitro* studies reported in Ch. 2 and 3. To recall, the *in vitro* diffusion studies described in section 2.2.3.b determined that the CaP-PEM8 coating significantly improved interlayer diffusion of embedded antimycin A (AntiA) as compared to a PEM8 only coating, however, 42% of the cells still accessed at least some of the AntiA within the first 24 h resulting in their death (Fig 2.7A). The conclusion made from this section was "the CaP-PEM8 coating would be insufficient for sequential delivery because the embedded 'Factor

2' can still be accessed immediately". In the present animal studies, it is most likely that the FGF-2 and BMP-2 are being delivered together from the CaP-PEM8 coating as a co-delivery system. As previously mentioned, it was also decided that the suboptimal dose of BMP-2 needed to be increased to 2 μg for continued testing.

Co-delivery of FGF-2 and BMP-2 from PEG hydrogels [84] or colloidal gelatin gels [102] can have inhibitory effects on *in vivo* bone formation when compared to BMP-2 alone. Some co-delivery systems such as collagen sponges have even shown that the combination of FGF-2 and BMP-2 was not only inhibitory compared to the BMP-2 only group, but was also inhibitory compared to the growth factor-free control [100]. Similar results were observed when the FGF-2 and BMP-2 were administered as bolus injections in a rat mandible defect; the co-delivery of factors was significantly worse at inducing bone apposition compared to BMP-2 alone, and was comparable to the control that was not treated with any growth factors [95].

Publications reporting co-delivery of FGF-2 and BMP-2 appear to have conflicting results both *in vitro* and *in* vivo because dose or dose ratio is not always considered. There are publications where the co-delivery of FGF-2 and BMP-2 enhanced *in vitro* and *in vivo* osteogenesis over single factor delivery and/or spiking [87, 92, 94, 97, 98, 206]; in these studies ng quantities of FGF-2 were used and were relatively low compared to the dose of BMP-2 used (usually μgs). Both Kuhn et al. and Wang et al. investigated the combined delivery of FGF-2 and BMP-2 and provide summaries of the contradictory results [88, 102]. In general, they observed that low doses of FGF-2 in combinations with BMP-2 were stimulatory (ng quantities), whereas high doses of FGF-2 with BMP-2 were inhibitory (μg quantities). The ratio of FGF-2 to BMP-2 is also important to consider, where doses of FGF-2 greater than BMP-2 tend to be inhibitory. Nakamura et al. hypothesizes that this phenomenon may be the result of high dose fibroblast

growth factor stimulating inhibitors of BMP-2 signaling (Smad 6) or stimulating osteoclastogenesis that leads to decreased bone formation or bone density [93]. The release kinetics from the delivery system may also influence the stimulatory or inhibitory effects of co-delivery of FGF-2 and BMP-2. As previously mentioned, FGF-2 promotes the mitogenic activity of osteoprogenitors, therefore rapid release of FGF-2 early on in bone healing may reduce the osteogenic potential of these cells leading to reduced bone formation.

Contrary to published co-delivery results, sequential delivery of FGF-2 and BMP-2 has lead to more consistent stimulatory effects. This is most likely due to the fact that growth factors in general, are very stage-specific during the bone healing process. The sequential delivery of first FGF-2, then BMP-2 when spiked into cell cultures results in enhanced *in vitro* osteogenesis over co- or single factor delivery [85, 88, 90, 91]. The challenge arises from developing a truly sequential delivery system. Many materials claim to be "sequential" when in reality they only provide the prevention of burst release of the factor they want delivered second; if you check the release profiles one will observe that both factors are being released simultaneously, they are just releasing at different rates [102, 107, 131, 156, 207, 208]. When release of FGF-2 and BMP-2 from a material is truly sequential, a stimulatory effect on osteogenesis is usually observed. Lei et al. developed core-shell microspheres where FGF-2 and BMP-2 were encapsulated in either the core or the shell. They demonstrated that the *in vitro* sequential delivery of first FGF-2 from the shell, and then BMP-2 from the core induced osteogenic differentiation of human mesenchymal stem cells better than the growth factors delivered in parallel [89]. Sequential delivery of BMP-2 first, then FGF-2 was inhibitory, again demonstrating that not only is sequential delivery important, but sequential delivery that mimics the natural biological process is key to enhancing osteogenesis.

In the present study, a stimulatory effect from the delivery of FGF-2 and BMP-2 on *in vivo* osteogenesis was observed when the growth factors were delivered from the bCaP-PEM30 coating (Fig. 4.12), proven to provide sequential delivery *in vitro* (Fig. 3.3) and higher doses of FGF-2 (5ng) and BMP-2 (2 μg) were used. Though these results were not statistically significant, continued studies focused on optimizing the relative dosing of FGF-2 to BMP-2, as well as continued work on tuning the *in vivo* delivery kinetics of the growth factors from the coating could lead to the bCaP-PEM coating being ideally suited as a sequential, multifactor delivery system capable of being applied to various scaffolds and/or implants for enhanced bone regeneration.

4.5 Conclusions

Both the novel dual delivery CaP-PEM8 coating, and the novel sequential delivery bCaP-PEM30 coating could be uniformly applied to the three-dimensional bone graft substitute, Healos®. Co-delivery of FGF-2 and BMP-2 from CaP-PEM8 coatings resulted in inhibited *in vivo* bone formation in a calvarial defect model, compared to the BMP-2 only coating. However, sequential delivery of FGF-2 then BMP-2, from bCaP-PEM30 coatings resulted in an observed trend of increased *in vivo* bone formation in a calvarial defect model, compared to the BMP-2 only coating. These results suggest the potential for bCaP-PEM30 coating applied to a 3-D implant to be used for sequential delivery of multiple growth factors to enhance *in vivo* bone formation. Regardless of the delivery system, these results and others previously published, stress the importance of dosing, dose ratio of two different factors, timing, and order of growth factor delivery used to enhance *in vivo* bone regeneration. Increased doses of BMP-2 with low dose FGF-2 should be further investigated.

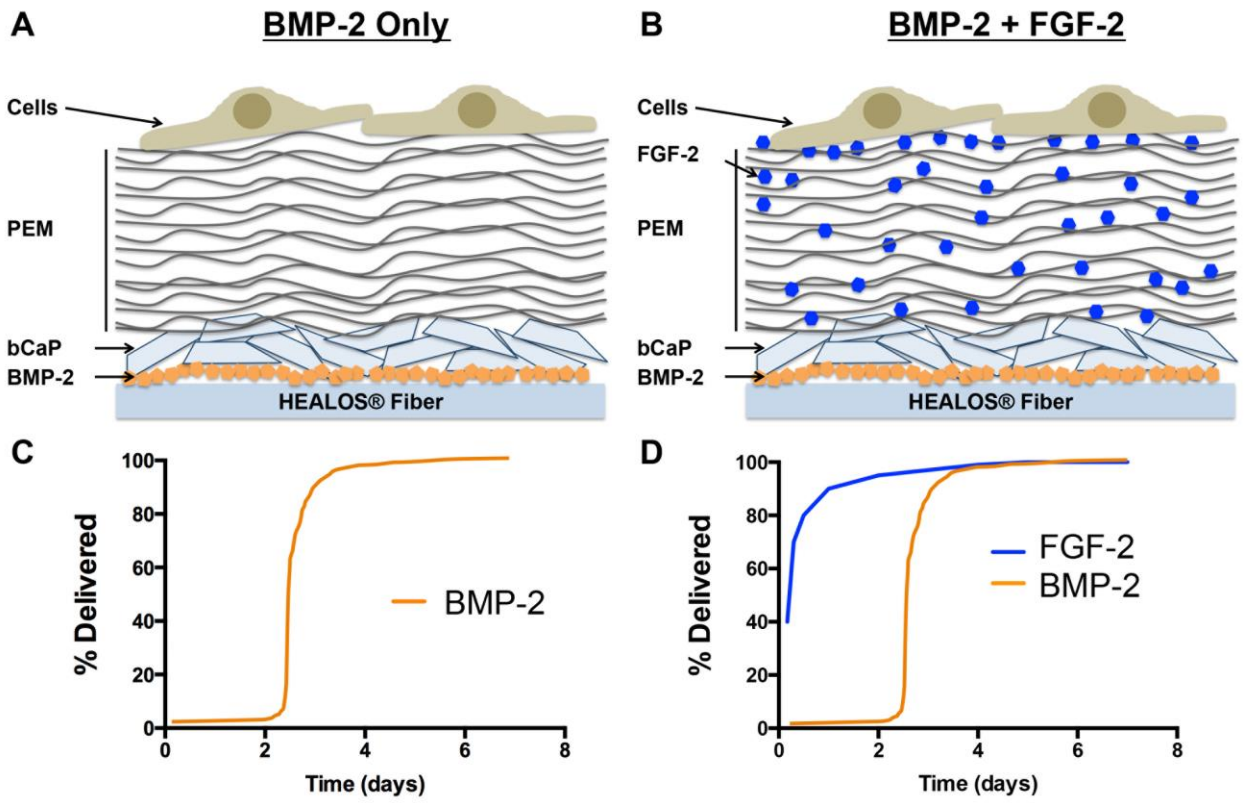

Figure 4.1 Schematic representation of BMP-2 only **(A)**, and BMP-2 and FGF-2 **(B)** delivery from Healos-bCaP-PEM. The theoretical single- **(C)**, and sequential- **(D)** delivery profiles from Healos-bCaP-PEM.

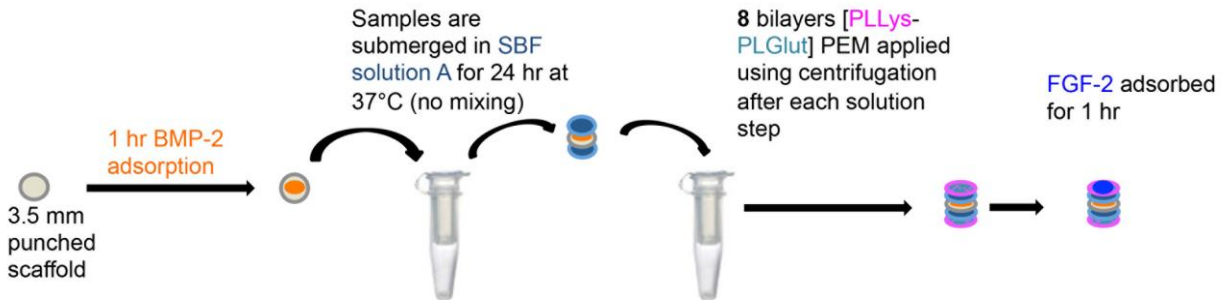

Figure 4.2 Schematic representation of the Healos-BMP2-CaP-PEM8-FGF2 procedure made with only amorphous calcium phosphate (CaP) with no mixing, and 8 bilayers of PEM.

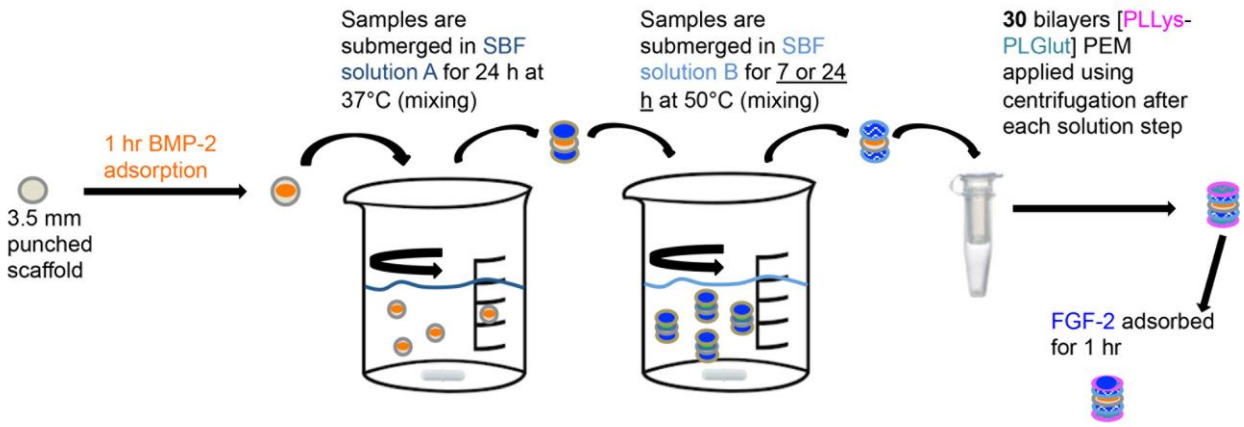

Figure 4.3 Schematic representation of the Healos-BMP2-bCaP-PEM30-FGF2 procedure made with biomimetic, nanocrystalline, calcium phosphate (bCaP) with mixing, and 30 bilayers of PEM.

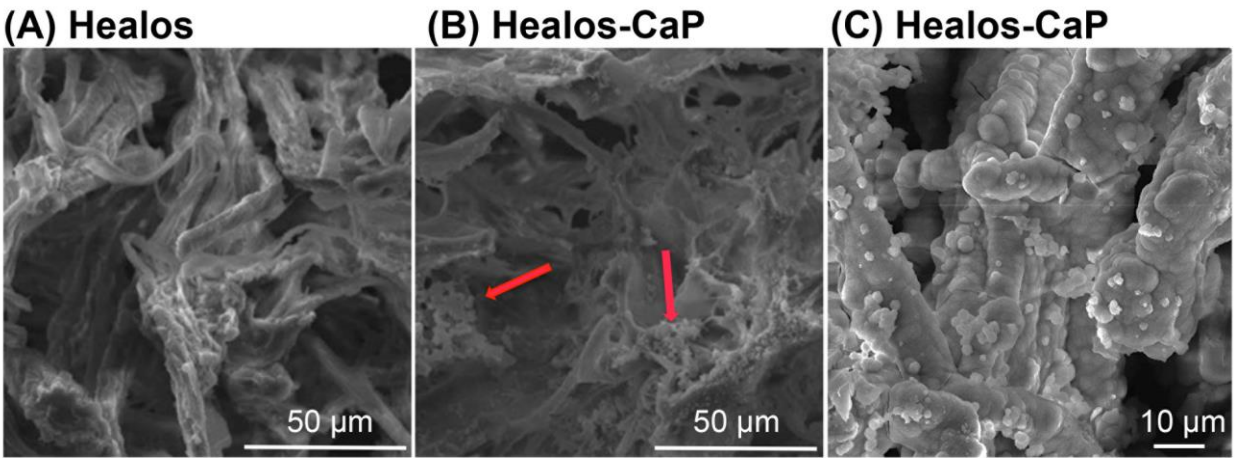

Figure 4.4 Low magnification SEM images of Healos® **(A)** and Healos® coated with amorphous CaP **(B)**, (scale bar = 50 µm). High magnification SEM image of Healos® coated with amorphous CaP **(C)**, (scale bar = 10 µm).

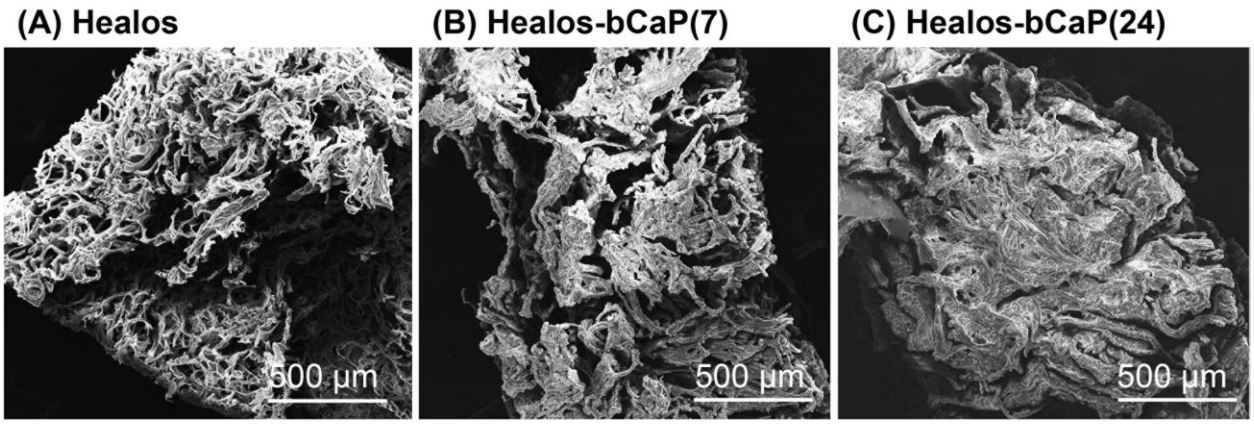

Figure 4.5 SEM images of Healos® **(A)**, Healos® coated with nanocrystallline bCaP(7) made by 7 h in Solution B **(B)**, and nanocrystalline bCaP(24) made by 24 h in Solution B **(C)**, (scale bar = 500 µm).

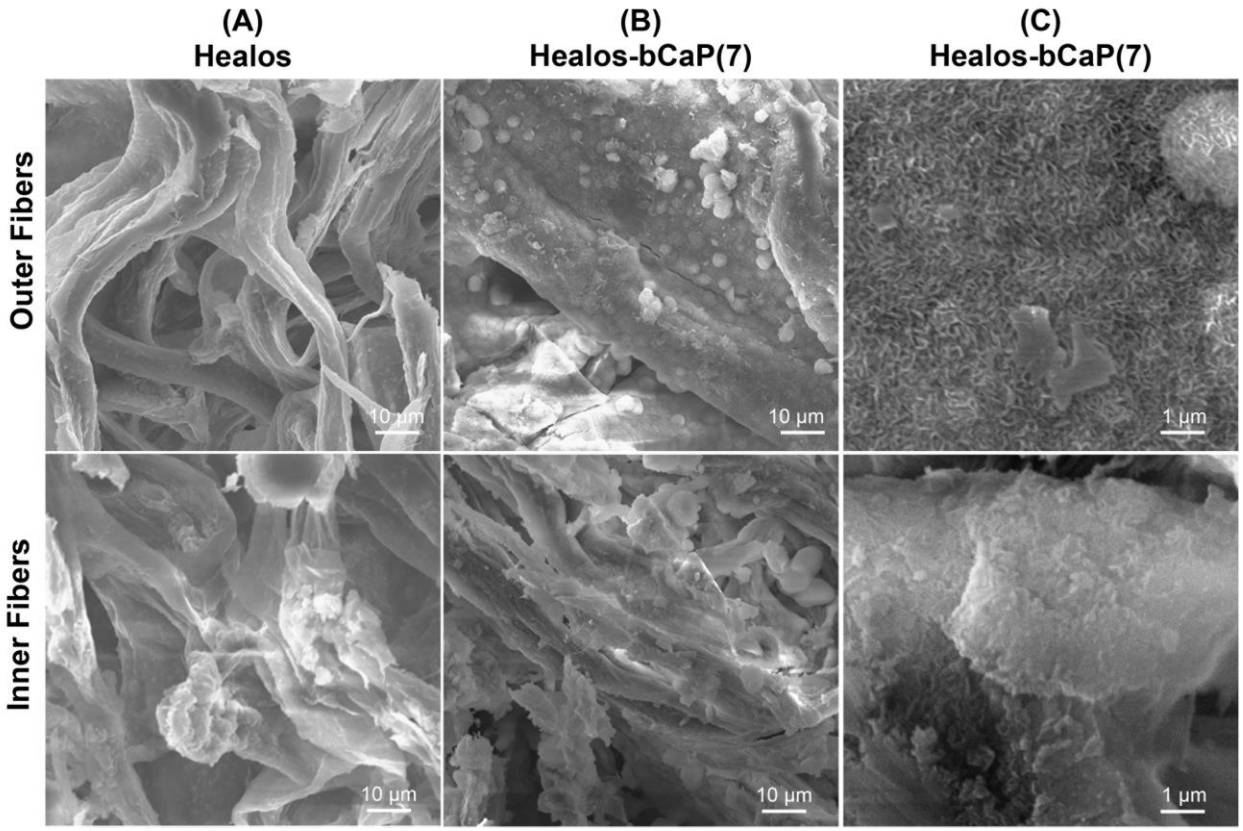

Figure 4.6 Low magnification SEM images of the outer and inner fibers of Healos® **(A)** and Healos® coated with nanocrystalline bCaP(7) **(B)**, (scale bar = 10 µm). High magnification SEM image of the outer and inner fibers of Healos® coated with nanocrystalline bCaP(7) **(C)**, (scale bar = 1 µm).

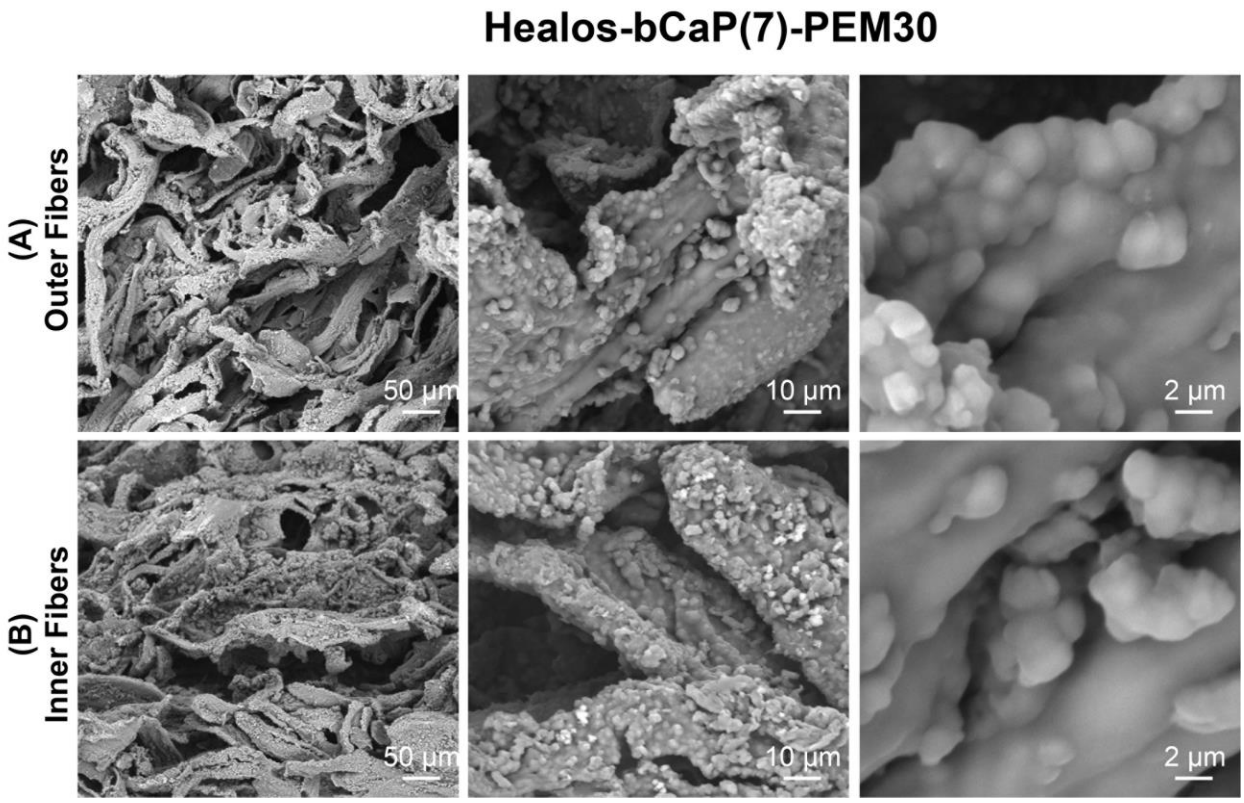

Figure 4.7 SEM images of the outer **(A)** and inner fibers **(B)** of Healos® coated with nanocrystalline bCaP(7) and 30 bilayers of PEM.

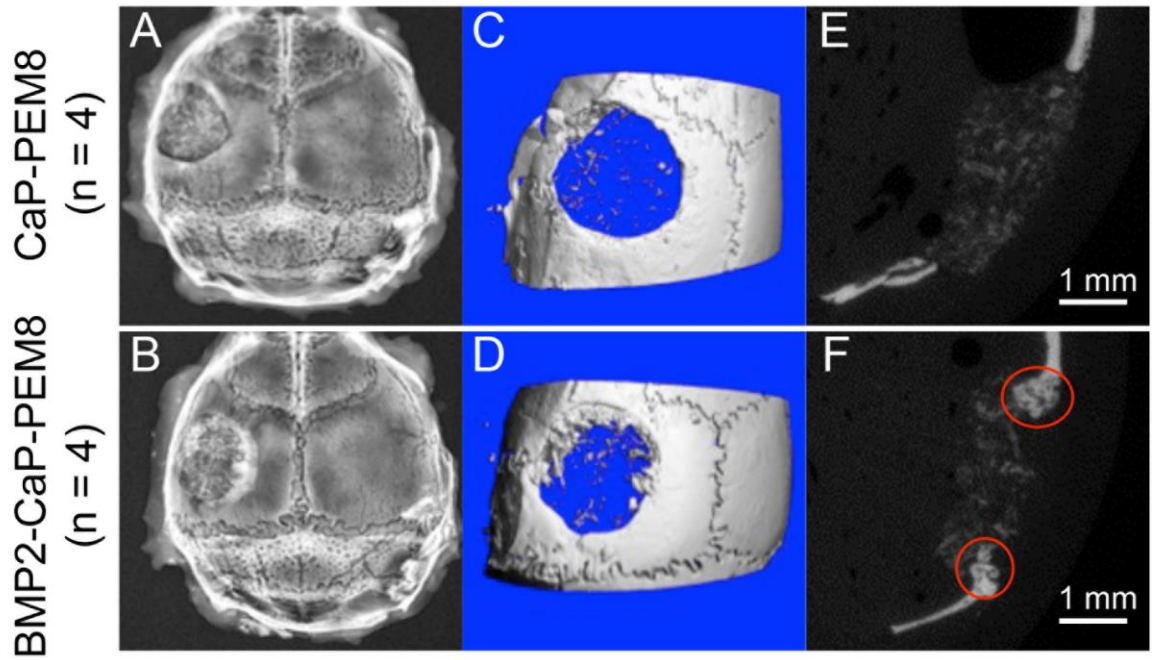

Figure 4.8 4-week post-surgery x-rays **(A, B)**, microCT 3-D reconstructions **(C, D)**, and microCT cross-sections **(E, F)** of calvaria implanted with Healos® coated with CaP-PEM8 (top panel) and BMP2-CaP-PEM8 (bottom panel). BMP-2 dose = 0.5 μg. New bone formation is circled in red.

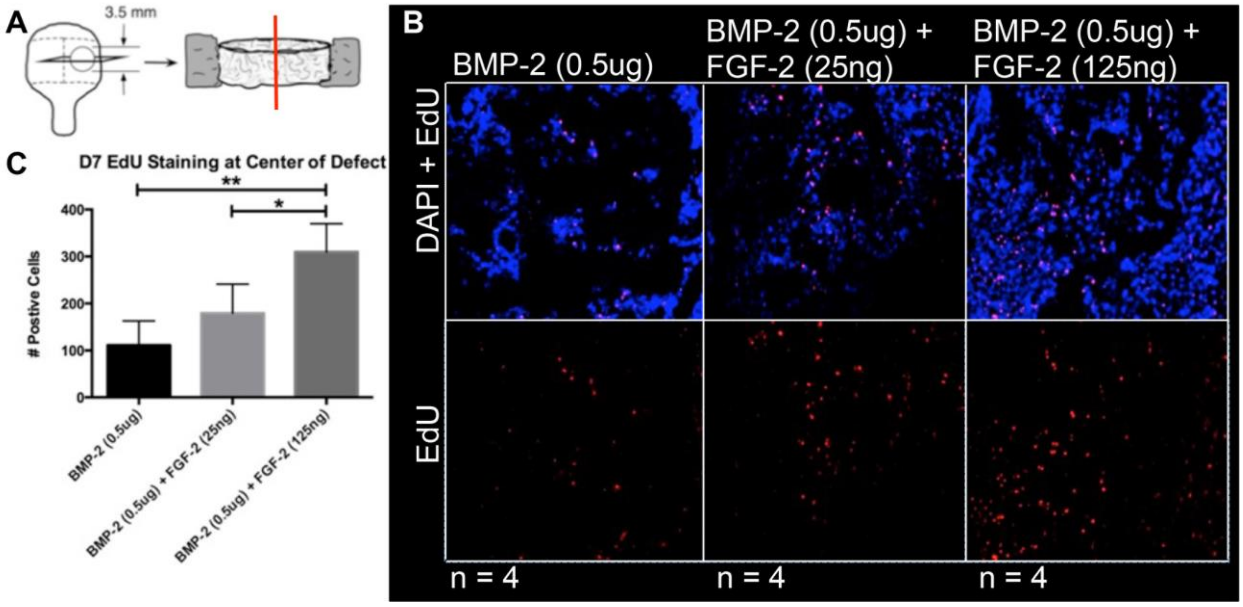

Figure 4.9 Schematic representation of where within the defect FGF-2 effects are being observed and quantified 1-week post-surgery **(A)**. Fluorescent images of DAPI and EdU stained cells showing increase in staining with the addition of 25 and 125 ng FGF-2 as compared to BMP-2 alone **(B)**. Quantified results showing 125 ng FGF-2 dose significantly increases number of EdU+ cells on day 7 as compared to BMP-2 alone and 25 ng FGF-2 dose **(C)**. (* $p \leq 0.05$, ** $p \leq 0.01$). (Healos® was coated with BMP2-CaP-PEM8 $\pm$ FGF2).

ANOVA P value = 0.0029

Tukey's multiple comparisons test	Mean Diff.	95% CI of diff.	Significant?	Summary
BMP-2 (0.5ug) vs. BMP-2 (0.5ug) + FGF-2 (125ng)	-198.1	-313.1 to -83.17	Yes	**
BMP-2 (0.5ug) + FGF-2 (25ng) vs. BMP-2 (0.5ug) + FGF-2 (125ng)	-130.3	-245.2 to -15.30	Yes	*

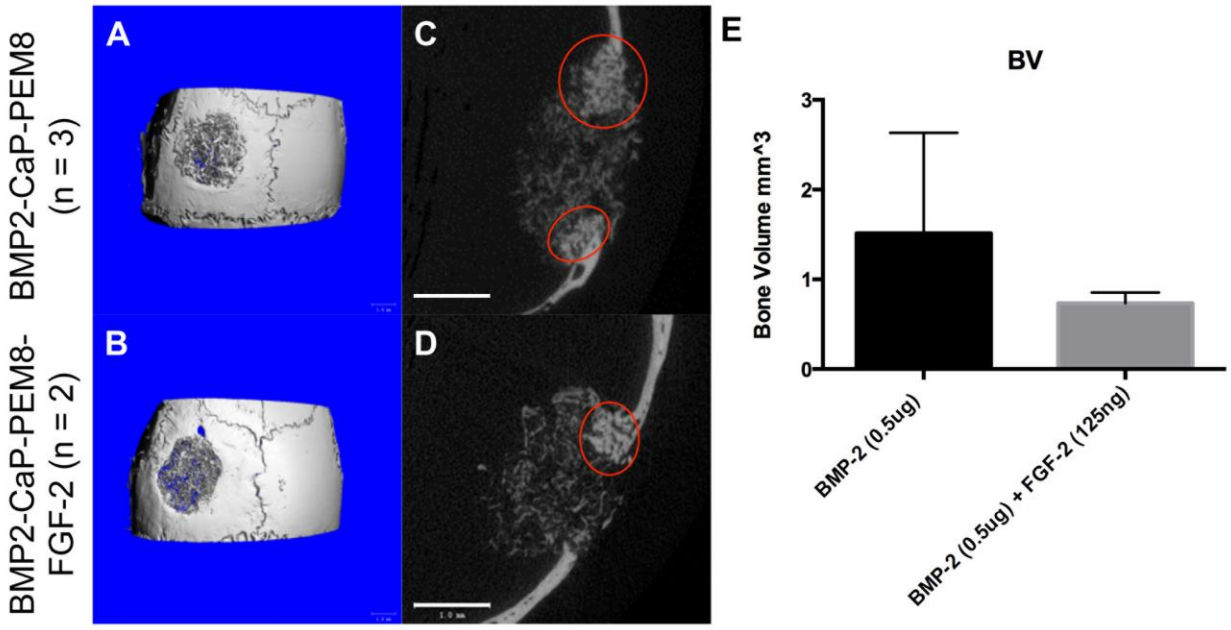

Figure 4.10 4-week post-surgery microCT 3-D reconstructions **(A, B)**, and microCT cross-sections **(C, D)**, of calvaria implanted with Healos® coated with BMP2-CaP-PEM8 (top panel) and BMP2-CaP-PEM8-FGF2 (bottom panel). BMP-2 dose = 0.5 µg, FGF-2 dose = 125 ng. New bone formation is circled in red and quantified in **(E)**.

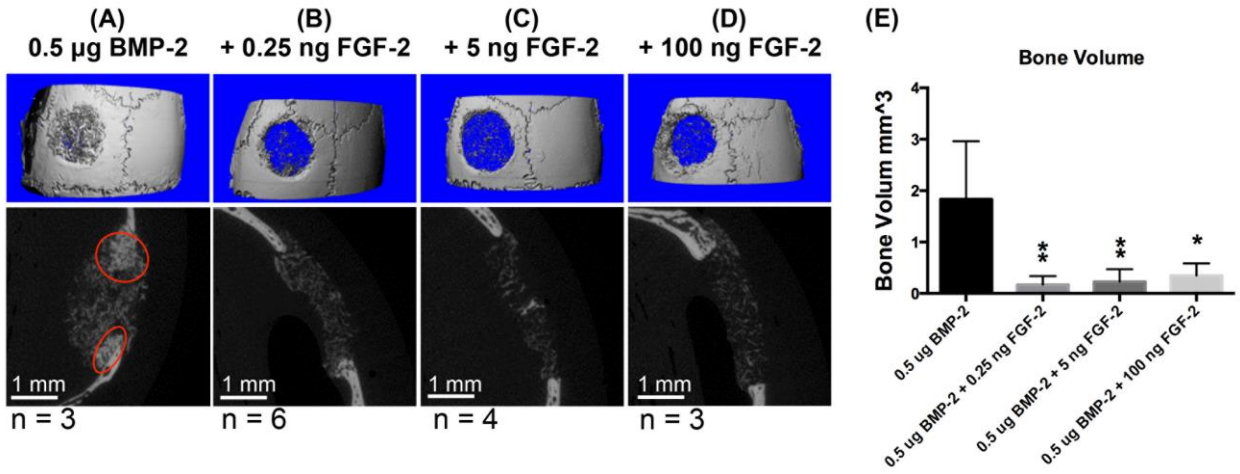

Figure 4.11 4-week post-surgery microCT 3-D reconstructions (top panel) and microCT cross-sections (bottom panel) of calvaria implanted with Healos® coated with BMP2-CaP-PEM8 **(A)**, and BMP2-CaP-PEM8-FGF2 with an FGF-2 dose = 0.25 ng **(B)**, 5 ng **(C)**, and 100 ng **(D)**. BMP-2 dose = 0.5 µg. New bone formation is circled in red and quantified in **(E)**. (* $p \leq 0.05$, ** $p \leq 0.01$).

ANOVA P value = 0.0027

Tukey's multiple comparisons test	Mean Diff.	95% CI of diff.	Significant?	Summary
0.5 ug BMP-2 vs. 0.5 ug BMP-2 + 0.25 ng FGF-2	1.662	0.6170 to 2.707	Yes	**
0.5 ug BMP-2 vs. 0.5 ug BMP-2 + 5 ng FGF-2	1.602	0.4733 to 2.731	Yes	**
0.5 ug BMP-2 vs. 0.5 ug BMP-2 + 100 ng FGF-2	1.482	0.2753 to 2.689	Yes	*

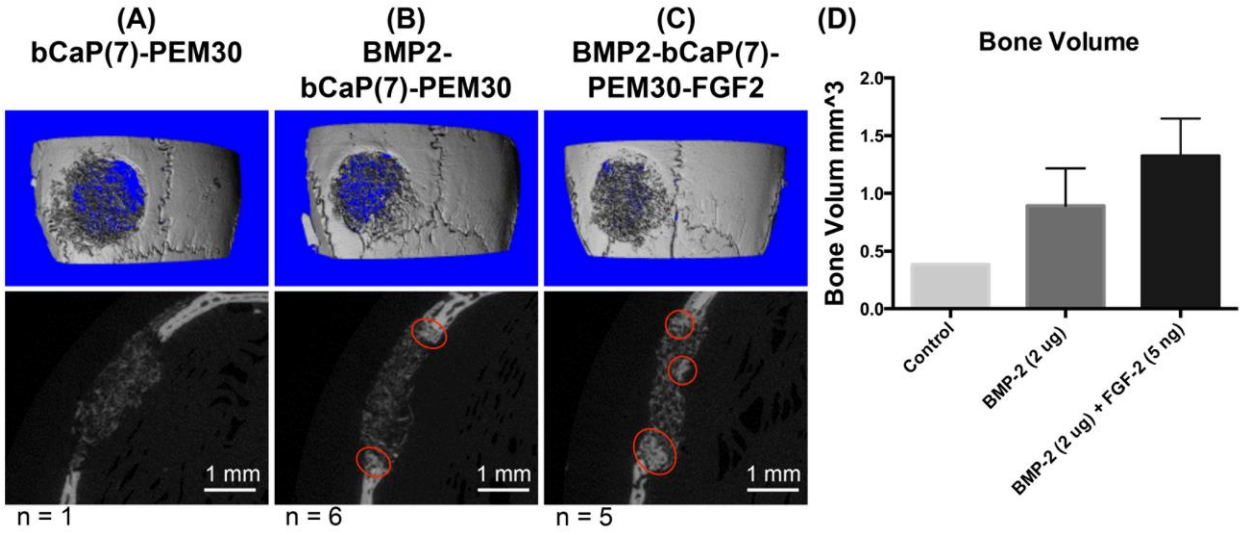

Figure 4.12 3-week post-surgery microCT 3-D reconstructions (top panel) and microCT cross-sections (bottom panel) of calvaria implanted with Healos® coated with bCaP(7)-PEM30 **(A)**, BMP2-bCaP(7)-PEM8 **(B)**, and BMP2-bCaP(7)-PEM8-FGF2 **(C)**. BMP-2 dose = 2 μg, FGF-2 dose = 5 ng. New bone formation is circled in red and quantified in **(D)**.

Chapter 5

Suggested Future Directions and Conclusions

The goal of these studies was to develop a biomaterial capable of sequential delivery of multiple, biologically active factors to better stimulate tissue repair that involves a complicated cascade of factors in order to regenerate tissue. More specifically, the hope was to develop a coating process that could sequentially deliver low dose FGF-2 and BMP-2 with a staggered release of at least several days that could be applied to a commercially available bone graft substitute to enhance *in* vivo osteogenesis, with the long-term goal being to overcome clinical complications with high dose BMP-2. This work focused on the incorporation of a biomimetic calcium phosphate (bCaP) layer into a poly-L-lysine/poly-L-glutamic acid PEM design to prevent interlayer diffusion of growth factors resulting in a sequential, multifactor delivery system that could be applied to two-dimensional (2-D) and three-dimensional (3-D) substrates. The work presented in this dissertation proved the hypothesis: *If the bCaP barrier layer could prevent diffusion of multiple factors within a PEM coating, then sequential delivery of factors could be achieved from a bCaP-PEM coated biomaterial.*

During this thesis research a variety of methods were used to modify the MC3T3-E1-mediated delivery kinetics from PEM coatings and are summarized in Table 5.1. It was shown that the unmodified poly-L-Lysine/poly-L-Glutamic acid PEM only coating resulted in interlayer diffusion and immediate access to an embedded factor (Fig. 2.7A, 2.9B), proving that a PEM only system could not provide sequential delivery of multiple factors. The addition of amorphous CaP to PEM prevented some interlayer diffusion of embedded antimycin A (AntiA), however significant access to the AntiA had occurred by 24 h (Fig. 2.7-2.8), suggesting it would also be

incapable of sequential delivery over the 3+ day time frame that was the goal of this research. The addition of nanocrystalline bCaP to PEM (bCaP-PEM30) successfully prevented interlayer diffusion of embedded AntiA and provided delayed access to the embedded factor beyond 24 h (Fig. 2.9).

An alternative approach to preventing interlayer diffusion within a PEM coating would be to use hydrophobic polyelectrolytes that result in linear growth with the layer-by-layer (LBL) application. Hydrophilic poly-L-Lysine (PLLys) and poly-L-Glutamic acid (PLGlut) were selected for use because it was known that these polyelectrolytes degraded via cell-mediated enzymatic action on the film itself [150], providing localized delivery and a system that does not rely on diffusion. Diffusion based systems were avoided because not only are they more difficult to control release from, but those system require excessive dosing of growth factor to provide the therapeutic concentration to the local tissue. A cell-mediated delivery system would allow us to use low concentrations of growth factor making the biomaterial safer and avoiding the off-target, unwanted side effects that are associated with clinical, supraphysiologic dosing [19, 27, 30]. The problem with PLLys and PLGlut is that they are hydrophilic, which means that during the LBL build up of the film, the polyelectrolytes are constantly rearranging causing an incorporated growth factor within the film to also constantly rearrange and resulting is a blended structure lacking any ability for sequential delivery. In the present studies, it was decided to incorporate a biomimetic calcium phosphate layer into the PEM system to prevent the interlayer diffusion of one of the growth factors and effectively provide sequential delivery. An alternative that is worth further investigation would be to use hydrophobic polyelectrolytes such as hyluronan (HA) and/or dextran sulfate (DS) that result in non-diffusing systems [146, 154]. Both of these polyelectrolytes result in linear growth. Interlayer diffusion does not occur in these systems,

which, as a result, form spatially organized structures wherein factors incorporated at a given step are able to interact only with neighboring factors that are in close proximity (two to three layers) [209]. The disadvantage to using HA and/or DS is that rather than being cell-mediated, their degradation is hydrolytic, meaning release of growth factors depends on the water content in the area; this could lead to diffusion of factors away from the target tissue. However, these polyelectrolytes can form compartmentalized films to potentially provide sequential delivery without the need for covalent cross-linking (which would inactivate the growth factor) or a barrier layer. Their use, with low doses of growth factor (minimizing the potential for diffusion), is a viable option for future work.

A combination of a cytotoxic compound (AntiA) and a proliferation compound (FGF-2) was found to be the ideal combination to study the multifactor, cell-mediated delivery kinetics of the bCaP-PEM coating. With the cytotoxic AntiA embedded beneath the coating it was easy to judge when the cells had significantly attained access to the second factor. Using this method we were able to show that bCaP-PEM coating was capable of local, cell-mediated delivery and did not release adsorbed factors through diffusion at the concentrations used in the present study. The bCaP-PEM30 coating was able to provide sequential delivery of first FGF-2 and then an embedded AntiA, delaying access to the AntiA for up to 3 days when cultured with osteoprogenitor cells (Fig. 3.3). Increasing the number of PEM bilayers (30 to 102) within the coating (Fig. 3.4), or changing the chemical composition of the polyelectrolytes (*L*- to *D*-enantiomers, Fig. 3.5) could not further delay osteoprogenitor access to the embedded AntiA but could potentially inhibit/delay delivery of the FGF-2. . Increasing (~24 μm) the thickness of the bCaP coating from the normal ~6 μm did not change the initial timing of access to the embedded AntiA, but did change the delivery of AntiA from burst to sustained delivery over the course of 4

days to the osteoprogenitor cells (Fig. 3.8-3.10). Changing the cell type used to evaluate delivery kinetics from the coating from osteoprogenitors to macrophages significantly increased access time to the embedded factor (Fig. 3.11-3.14). When the macrophages were seeded at a low density (7.9k cells/cm^2) the bCaP-PEM30 coating provided 3 days delayed access to the embedded factor (Fig. 3.12), similar to the osteoprogenitor cells. When the macrophages were seeded at a high density (30k cells/cm^2) the bCaP-PEM30 coating failed to provide any delayed access to the embedded factor (Fig. 3.13). These results highlight the importance of cell type and number when evaluating delivery kinetics from a cell-mediated delivery system.

Considering the variable delivery kinetics of the embedded AntiA from the bCaP-PEM coating *in* vitro, via changing the cell type used in the study, it is critical to better understand the mechanism of action various cell types that will interact with the bCaP-PEM coating *in vivo*, use to degrade the coating and access the embedded factor. Considering the increased *in* vitro delivery kinetics of the embedded AntiA from the bCaP-PEM coating that occurred when changing the cell type from pre-osteoblasts to monocyte/macrophages, it is difficult to predict the *in vivo* response from the *in vitro* studies. To better predict the *in vivo* response it is critical to better understand the mechanism of degradation of the various cell types that will interact with the bCaP-PEM coating *in vivo*. Continued *in vitro* cell assays should be performed using different cell types (macrophages, osteoprogenitors, osteoclasts, osteoblasts, etc.) as well as different seeding densities or mixtures of the cell types. Evaluation of the bCaP-PEM coating via scanning electron microscopy (SEM), after cell culture, should be performed to observe extent of coating degradation.

Both the novel dual delivery CaP-PEM8 coating, and the novel sequential delivery bCaP-PEM30 coating could be uniformly applied to the three-dimensional bone graft substitute,

Healos® (Fig. 4.4-4.7). Co-delivery of FGF-2 (0.25, 5, 100, 125 ng) and BMP-2 (0.5 μg) from CaP-PEM8 coatings resulted in inhibited *in vivo* bone formation in a calvarial defect model, compared to the BMP-2 only coating (Fig. 4.10-4.11). Considering these results, it was determined that the 0.5 μg BMP-2 dose was too low. However, sequential delivery of FGF-2 (5 ng) then BMP-2 (2 μg), from bCaP-PEM30 coatings resulted in an observed trend of increased *in vivo* bone formation in a calvarial defect model, compared to the BMP-2 only coating (Fig. 4.12). Further studies with a larger number of animals may increase this effect. Increasing the dose of BMP-2 is also necessary in order to see a benefit from combined FGF-2 delivery. These results and others previously published, stress the importance of dosing, ratio of doses, timing, and order of growth factor delivery used to enhance *in vivo* bone regeneration. Further studies need to be conducted to optimize the dosing of FGF-2 and BMP-2 to lead to robust, new bone formation *in vivo* that cannot be achieved by BMP-2 alone.

In summary, the work presented in this dissertation resulted in the development of novel biomimetic calcium phosphate/polyelectrolyte coating capable of cell-mediated, sequential, multifactor delivery, providing three-day delayed access of an embedded factor to osteoprogenitor and macrophage cells. This technology has the versatility to be applied to 2-D or 3-D substrates and can be utilized in multiple research applications where a sequential delivery profile activated by cell degradation of matrix is desired. The results suggest the biomimetic calcium phosphate/polyelectrolyte coating applied to a 3-D implant could be an ideal system for sequential delivery of multiple growth factors to enhance *in vivo* bone formation.

Table 5.1 Summary of cellular access timing to embedded AntiA (213 μg/disk) when cultured on the various coatings reported in this thesis. (FGF-2 Dose = 150 ng).

AntiA Embedded Beneath	Cell Type	Seeding Density (cells/cm^2)	Access Time
PEM8	MC3T3-E1	10k	< 24 h
CaP-PEM8	MC3T3-E1	10k	< 24 h
CaP-PEM30	MC3T3-E1	10k	< 24 h
PEM30	MC3T3-E1	40k	< 24 h
bCaP-PEM30	MC3T3-E1	40k	3 days
bCaP-PEM30-FGF2	MC3T3-E1	40k	3 days, burst delivery
bCaP-PEM102-FGF2	MC3T3-E1	40k	3 days
bCaP-PEM^{D}30-FGF2	MC3T3-E1	40k	3 days
bCaP(7)-PEM30-FGF2	MC3T3-E1	40k	3 days
bCaP(48)-PEM30-FGF2	MC3T3-E1	40k	3 days/sustained delivery
bCaP-PEM30-FGF2	RAW 264.7	7.9k	3 days
bCaP-PEM30-FGF2	RAW 264.7	30k	< 4 h

References

[1] Jiang B, Zhang G, Brey EM. Dual delivery of chlorhexidine and platelet-derived growth factor-BB for enhanced wound healing and infection control. Acta biomaterialia. 2013;9:4976-84.

[2] La WG, Jin M, Park S, Yoon HH, Jeong GJ, Bhang SH, et al. Delivery of bone morphogenetic protein-2 and substance P using graphene oxide for bone regeneration. International journal of nanomedicine. 2014;9 Suppl 1:107-16.

[3] Su J, Xu H, Sun J, Gong X, Zhao H. Dual delivery of BMP-2 and bFGF from a new nano-composite scaffold, loaded with vascular stents for large-size mandibular defect regeneration. International journal of molecular sciences. 2013;14:12714-28.

[4] Mehta M, Schmidt-Bleek K, Duda GN, Mooney DJ. Biomaterial delivery of morphogens to mimic the natural healing cascade in bone. Advanced drug delivery reviews. 2012;64:1257-76.

[5] Vo TN, Kasper FK, Mikos AG. Strategies for controlled delivery of growth factors and cells for bone regeneration. Advanced drug delivery reviews. 2012;64:1292-309.

[6] Chen FM, Zhang M, Wu ZF. Toward delivery of multiple growth factors in tissue engineering. Biomaterials. 2010;31:6279-308.

[7] Bauters C, Asahara T, Zheng LP, Takeshita S, Bunting S, Ferrara N, et al. Physiological assessment of augmented vascularity induced by VEGF in ischemic rabbit hindlimb. The American journal of physiology. 1994;267:H1263-71.

[8] Freedman SB, Isner JM. Therapeutic angiogenesis for coronary artery disease. Annals of internal medicine. 2002;136:54-71.

[9] Takeshita S, Pu LQ, Stein LA, Sniderman AD, Bunting S, Ferrara N, et al. Intramuscular administration of vascular endothelial growth factor induces dose-dependent collateral artery augmentation in a rabbit model of chronic limb ischemia. Circulation. 1994;90:II228-34.

[10] Takeshita S, Zheng LP, Brogi E, Kearney M, Pu LQ, Bunting S, et al. Therapeutic angiogenesis. A single intraarterial bolus of vascular endothelial growth factor augments revascularization in a rabbit ischemic hind limb model. The Journal of clinical investigation. 1994;93:662-70.

[11] Rosengart TK, Lee LY, Patel SR, Kligfield PD, Okin PM, Hackett NR, et al. Six-month assessment of a phase I trial of angiogenic gene therapy for the treatment of coronary artery disease using direct intramyocardial administration of an adenovirus vector expressing the VEGF121 cDNA. Annals of surgery. 1999;230:466-70; discussion 70-2.

[12] Schumacher B, Pecher P, von Specht BU, Stegmann T. Induction of neoangiogenesis in ischemic myocardium by human growth factors: first clinical results of a new treatment of coronary heart disease. Circulation. 1998;97:645-50.

[13] Eppler SM, Combs DL, Henry TD, Lopez JJ, Ellis SG, Yi JH, et al. A target-mediated model to describe the pharmacokinetics and hemodynamic effects of recombinant human vascular endothelial growth factor in humans. Clinical pharmacology and therapeutics. 2002;72:20-32.

[14] Henry TD, Annex BH, McKendall GR, Azrin MA, Lopez JJ, Giordano FJ, et al. The VIVA trial: Vascular endothelial growth factor in Ischemia for Vascular Angiogenesis. Circulation. 2003;107:1359-65.

[15] Simons M, Ware JA. Therapeutic angiogenesis in cardiovascular disease. Nature reviews Drug discovery. 2003;2:863-71.

[16] Simons M, Annex BH, Laham RJ, Kleiman N, Henry T, Dauerman H, et al. Pharmacological treatment of coronary artery disease with recombinant fibroblast growth factor-2: double-blind, randomized, controlled clinical trial. Circulation. 2002;105:788-93.

[17] Laham RJ, Sellke FW, Edelman ER, Pearlman JD, Ware JA, Brown DL, et al. Local perivascular delivery of basic fibroblast growth factor in patients undergoing coronary bypass surgery: results of a phase I randomized, double-blind, placebo-controlled trial. Circulation. 1999;100:1865-71.

[18] Ruel M, Laham RJ, Parker JA, Post MJ, Ware JA, Simons M, et al. Long-term effects of surgical angiogenic therapy with fibroblast growth factor 2 protein. The Journal of thoracic and cardiovascular surgery. 2002;124:28-34.

[19] Govender S, Csimma C, Genant HK, Valentin-Opran A, Amit Y, Arbel R, et al. Recombinant human bone morphogenetic protein-2 for treatment of open tibial fractures: a prospective, controlled, randomized study of four hundred and fifty patients. The Journal of bone and joint surgery American volume. 2002;84-A:2123-34.

[20] Jones AL, Bucholz RW, Bosse MJ, Mirza SK, Lyon TR, Webb LX, et al. Recombinant human BMP-2 and allograft compared with autogenous bone graft for reconstruction of diaphyseal tibial fractures with cortical defects. A randomized, controlled trial. The Journal of bone and joint surgery American volume. 2006;88:1431-41.

[21] Vaccaro AR, Lawrence JP, Patel T, Katz LD, Anderson DG, Fischgrund JS, et al. The safety and efficacy of OP-1 (rhBMP-7) as a replacement for iliac crest autograft in posterolateral lumbar arthrodesis: a long-term (>4 years) pivotal study. Spine. 2008;33:2850-62.

[22] Vaccaro AR, Whang PG, Patel T, Phillips FM, Anderson DG, Albert TJ, et al. The safety and efficacy of OP-1 (rhBMP-7) as a replacement for iliac crest autograft for posterolateral

lumbar arthrodesis: minimum 4-year follow-up of a pilot study. The spine journal : official journal of the North American Spine Society. 2008;8:457-65.

[23] Singh P, Suresh DK. Clinical evaluation of GEM 21S((R)) and a collagen membrane with a coronally advanced flap as a root coverage procedure in the treatment of gingival recession defects: A comparative study. Journal of Indian Society of Periodontology. 2012;16:577-83.

[24] Dandu SR, Murthy KR. Multiple Gingival Recession Defects Treated with Coronally Advanced Flap and Either the VISTA Technique Enhanced with GEM 21S or Periosteal Pedicle Graft: A 9-Month Clinical Study. The International journal of periodontics & restorative dentistry. 2016;36:231-7.

[25] Kawaguchi H, Oka H, Jingushi S, Izumi T, Fukunaga M, Sato K, et al. A local application of recombinant human fibroblast growth factor 2 for tibial shaft fractures: A randomized, placebo-controlled trial. Journal of bone and mineral research : the official journal of the American Society for Bone and Mineral Research. 2010;25:2735-43.

[26] Kitamura M, Akamatsu M, Machigashira M, Hara Y, Sakagami R, Hirofuji T, et al. FGF-2 stimulates periodontal regeneration: results of a multi-center randomized clinical trial. Journal of dental research. 2011;90:35-40.

[27] Lee K, Silva EA, Mooney DJ. Growth factor delivery-based tissue engineering: general approaches and a review of recent developments. Journal of the Royal Society, Interface / the Royal Society. 2011;8:153-70.

[28] Burkus JK, Transfeldt EE, Kitchel SH, Watkins RG, Balderston RA. Clinical and radiographic outcomes of anterior lumbar interbody fusion using recombinant human bone morphogenetic protein-2. Spine. 2002;27:2396-408.

[29] Service RF. Tissue engineers build new bone. Science. 2000;289:1498-500.

[30] Swiontkowski MF, Aro HT, Donell S, Esterhai JL, Goulet J, Jones A, et al. Recombinant human bone morphogenetic protein-2 in open tibial fractures. A subgroup analysis of data combined from two prospective randomized studies. The Journal of bone and joint surgery American volume. 2006;88:1258-65.

[31] Jahng TA, Fu TS, Cunningham BW, Dmitriev AE, Kim DH. Endoscopic instrumented posterolateral lumbar fusion with Healos and recombinant human growth/differentiation factor-5. Neurosurgery. 2004;54:171-80; discussion 80-1.

[32] Magit DP, Maak T, Trioano N, Raphael B, Hamouria Q, Polzhofer G, et al. Healos/recombinant human growth and differentiation factor-5 induces posterolateral lumbar fusion in a New Zealand white rabbit model. Spine. 2006;31:2180-8.

[33] Gohil SV, Adams DJ, Maye P, Rowe DW, Nair LS. Evaluation of rhBMP-2 and bone marrow derived stromal cell mediated bone regeneration using transgenic fluorescent protein reporter mice. Journal of biomedical materials research Part A. 2014;102:4568-80.

[34] Krishnamurthy R, Manning MC. The stability factor: importance in formulation development. Current pharmaceutical biotechnology. 2002;3:361-71.

[35] Manning MC, Patel K, Borchardt RT. Stability of protein pharmaceuticals. Pharmaceutical research. 1989;6:903-18.

[36] Barnes GL, Kostenuik PJ, Gerstenfeld LC, Einhorn TA. Growth factor regulation of fracture repair. Journal of bone and mineral research : the official journal of the American Society for Bone and Mineral Research. 1999;14:1805-15.

[37] Schindeler A, McDonald MM, Bokko P, Little DG. Bone remodeling during fracture repair: The cellular picture. Seminars in cell & developmental biology. 2008;19:459-66.

[38] Marsell R, Einhorn TA. The biology of fracture healing. Injury. 2011;42:551-5.

[39] Kolar P, Schmidt-Bleek K, Schell H, Gaber T, Toben D, Schmidmaier G, et al. The early fracture hematoma and its potential role in fracture healing. Tissue engineering Part B, Reviews. 2010;16:427-34.

[40] Bolander ME. Regulation of fracture repair by growth factors. Proceedings of the Society for Experimental Biology and Medicine Society for Experimental Biology and Medicine. 1992;200:165-70.

[41] Raheja LF, Genetos DC, Wong A, Yellowley CE. Hypoxic regulation of mesenchymal stem cell migration: the role of RhoA and HIF-1alpha. Cell biology international. 2011;35:981-9.

[42] Everts V, Delaisse JM, Korper W, Jansen DC, Tigchelaar-Gutter W, Saftig P, et al. The bone lining cell: its role in cleaning Howship's lacunae and initiating bone formation. Journal of bone and mineral research : the official journal of the American Society for Bone and Mineral Research. 2002;17:77-90.

[43] Dimitriou R, Tsiridis E, Giannoudis PV. Current concepts of molecular aspects of bone healing. Injury. 2005;36:1392-404.

[44] Jingushi S, Joyce ME, Bolander ME. Genetic expression of extracellular matrix proteins correlates with histologic changes during fracture repair. Journal of bone and mineral research : the official journal of the American Society for Bone and Mineral Research. 1992;7:1045-55.

[45] Cho TJ, Gerstenfeld LC, Einhorn TA. Differential temporal expression of members of the transforming growth factor beta superfamily during murine fracture healing. Journal of bone and mineral research : the official journal of the American Society for Bone and Mineral Research. 2002;17:513-20.

[46] Keramaris NC, Calori GM, Nikolaou VS, Schemitsch EH, Giannoudis PV. Fracture vascularity and bone healing: a systematic review of the role of VEGF. Injury. 2008;39 Suppl 2:S45-57.

[47] Einhorn TA. The cell and molecular biology of fracture healing. Clinical orthopaedics and related research. 1998:S7-21.

[48] Kearns AE, Khosla S, Kostenuik PJ. Receptor activator of nuclear factor kappaB ligand and osteoprotegerin regulation of bone remodeling in health and disease. Endocrine reviews. 2008;29:155-92.

[49] Boyce BF, Xing L. Functions of RANKL/RANK/OPG in bone modeling and remodeling. Archives of biochemistry and biophysics. 2008;473:139-46.

[50] Gilbert S. Osteogenesis: The Development of Bones. 6 ed. Sunderland, MA: Sinauer Associates; 2000.

[51] Ornitz DM, Marie PJ. FGF signaling pathways in endochondral and intramembranous bone development and human genetic disease. Genes & development. 2002;16:1446-65.

[52] Martini F. Osseos Tissue and Bone Structure. 7 ed. San Franciso, CA: Pearson Education Inc.; 2006.

[53] Nishimura R, Hata K, Harris SE, Ikeda F, Yoneda T. Core-binding factor alpha 1 (Cbfa1) induces osteoblastic differentiation of C2C12 cells without interactions with Smad1 and Smad5. Bone. 2002;31:303-12.

[54] Marie PJ, Debiais F, Hay E. Regulation of human cranial osteoblast phenotype by FGF-2, FGFR-2 and BMP-2 signaling. Histology and histopathology. 2002;17:877-85.

[55] Tu MG, Chen YW, Shie MY. Macrophage-mediated osteogenesis activation in co-culture with osteoblast on calcium silicate cement. Journal of materials science Materials in medicine. 2015;26:276.

[56] Itoh K, Udagawa N, Katagiri T, Iemura S, Ueno N, Yasuda H, et al. Bone morphogenetic protein 2 stimulates osteoclast differentiation and survival supported by receptor activator of nuclear factor-kappaB ligand. Endocrinology. 2001;142:3656-62.

[57] Hurley MM, Lee SK, Raisz LG, Bernecker P, Lorenzo J. Basic fibroblast growth factor induces osteoclast formation in murine bone marrow cultures. Bone. 1998;22:309-16.

[58] Kawaguchi H, Chikazu D, Nakamura K, Kumegawa M, Hakeda Y. Direct and indirect actions of fibroblast growth factor 2 on osteoclastic bone resorption in cultures. Journal of bone and mineral research : the official journal of the American Society for Bone and Mineral Research. 2000;15:466-73.

[59] Bruder SP, Fink DJ, Caplan AI. Mesenchymal stem cells in bone development, bone repair, and skeletal regeneration therapy. Journal of cellular biochemistry. 1994;56:283-94.

[60] Wozney JM. The bone morphogenetic protein family and osteogenesis. Molecular reproduction and development. 1992;32:160-7.

[61] Yasko AW, Lane JM, Fellinger EJ, Rosen V, Wozney JM, Wang EA. The healing of segmental bone defects, induced by recombinant human bone morphogenetic protein (rhBMP-2). A radiographic, histological, and biomechanical study in rats. The Journal of bone and joint surgery American volume. 1992;74:659-70.

[62] Lee SC, Shea M, Battle MA, Kozitza K, Ron E, Turek T, et al. Healing of large segmental defects in rat femurs is aided by RhBMP-2 in PLGA matrix. Journal of biomedical materials research. 1994;28:1149-56.

[63] Kenley R, Marden L, Turek T, Jin L, Ron E, Hollinger JO. Osseous regeneration in the rat calvarium using novel delivery systems for recombinant human bone morphogenetic protein-2 (rhBMP-2). Journal of biomedical materials research. 1994;28:1139-47.

[64] Boden SD, Schimandle JH, Hutton WC. Lumbar intertransverse-process spinal arthrodesis with use of a bovine bone-derived osteoinductive protein. A preliminary report. The Journal of bone and joint surgery American volume. 1995;77:1404-17.

[65] Boden SD, Schimandle JH, Hutton WC. 1995 Volvo Award in basic sciences. The use of an osteoinductive growth factor for lumbar spinal fusion. Part II: Study of dose, carrier, and species. Spine. 1995;20:2633-44.

[66] Toriumi DM, Kotler HS, Luxenberg DP, Holtrop ME, Wang EA. Mandibular reconstruction with a recombinant bone-inducing factor. Functional, histologic, and biomechanical evaluation. Archives of otolaryngology--head & neck surgery. 1991;117:1101-12.

[67] Toriumi DM, O'Grady K, Horlbeck DM, Desai D, Turek TJ, Wozney J. Mandibular reconstruction using bone morphogenetic protein 2: long-term follow-up in a canine model. The Laryngoscope. 1999;109:1481-9.

[68] Kirker-Head CA, Gerhart TN, Armstrong R, Schelling SH, Carmel LA. Healing bone using recombinant human bone morphogenetic protein 2 and copolymer. Clinical orthopaedics and related research. 1998:205-17.

[69] Gerhart TN, Kirker-Head CA, Kriz MJ, Holtrop ME, Hennig GE, Hipp J, et al. Healing segmental femoral defects in sheep using recombinant human bone morphogenetic protein. Clinical orthopaedics and related research. 1993:317-26.

[70] Fei Y, Gronowicz G, Hurley MM. Fibroblast growth factor-2, bone homeostasis and fracture repair. Current pharmaceutical design. 2013;19:3354-63.

[71] Montero A, Okada Y, Tomita M, Ito M, Tsurukami H, Nakamura T, et al. Disruption of the fibroblast growth factor-2 gene results in decreased bone mass and bone formation. The Journal of clinical investigation. 2000;105:1085-93.

[72] Kawaguchi H, Kurokawa T, Hanada K, Hiyama Y, Tamura M, Ogata E, et al. Stimulation of fracture repair by recombinant human basic fibroblast growth factor in normal and streptozotocin-diabetic rats. Endocrinology. 1994;135:774-81.

[73] Nakamura T, Hara Y, Tagawa M, Tamura M, Yuge T, Fukuda H, et al. Recombinant human basic fibroblast growth factor accelerates fracture healing by enhancing callus remodeling in experimental dog tibial fracture. Journal of bone and mineral research : the official journal of the American Society for Bone and Mineral Research. 1998;13:942-9.

[74] Radomsky ML, Thompson AY, Spiro RC, Poser JW. Potential role of fibroblast growth factor in enhancement of fracture healing. Clinical orthopaedics and related research. 1998:S283-93.

[75] Radomsky ML, Aufdemorte TB, Swain LD, Fox WC, Spiro RC, Poser JW. Novel formulation of fibroblast growth factor-2 in a hyaluronan gel accelerates fracture healing in nonhuman primates. Journal of orthopaedic research : official publication of the Orthopaedic Research Society. 1999;17:607-14.

[76] Schmid GJ, Kobayashi C, Sandell LJ, Ornitz DM. Fibroblast growth factor expression during skeletal fracture healing in mice. Developmental dynamics : an official publication of the American Association of Anatomists. 2009;238:766-74.

[77] Hughes SE. Differential expression of the fibroblast growth factor receptor (FGFR) multigene family in normal human adult tissues. The journal of histochemistry and cytochemistry : official journal of the Histochemistry Society. 1997;45:1005-19.

[78] Hurley MM AC, Marcello K, Gronowicz G, Raisz LGJ. Translational regulation of the FGF2 gene by 17β-Estradiol. Bone. 1996;17:Abs.31a.

[79] ten Harkel B, Schoenmaker T, Picavet DI, Davison NL, de Vries TJ, Everts V. The Foreign Body Giant Cell Cannot Resorb Bone, But Dissolves Hydroxyapatite Like Osteoclasts. PloS one. 2015;10:e0139564.

[80] Farhadi J, Jaquiery C, Barbero A, Jakob M, Schaeren S, Pierer G, et al. Differentiation-dependent up-regulation of BMP-2, TGF-beta1, and VEGF expression by FGF-2 in human bone marrow stromal cells. Plastic and reconstructive surgery. 2005;116:1379-86.

[81] Singhatanadgit W, Salih V, Olsen I. Up-regulation of bone morphogenetic protein receptor IB by growth factors enhances BMP-2-induced human bone cell functions. Journal of cellular physiology. 2006;209:912-22.

[82] Xiao L, Ueno D, Catros S, Homer-Bouthiette C, Charles L, Kuhn L, et al. Fibroblast growth factor-2 isoform (low molecular weight/18 kDa) overexpression in preosteoblast cells promotes bone regeneration in critical size calvarial defects in male mice. Endocrinology. 2014;155:965-74.

[83] Gronowicz G, Hurley MM, Kuhn LT. Optimizing BMP-2-induced bone repair with FGF-2. The Journal of the American Academy of Orthopaedic Surgeons. 2014;22:677-9.

[84] Charles LF, Woodman JL, Ueno D, Gronowicz G, Hurley MM, Kuhn LT. Effects of low dose FGF-2 and BMP-2 on healing of calvarial defects in old mice. Experimental gerontology. 2015;64:62-9.

[85] Fakhry A, Ratisoontorn C, Vedhachalam C, Salhab I, Koyama E, Leboy P, et al. Effects of FGF-2/-9 in calvarial bone cell cultures: differentiation stage-dependent mitogenic effect, inverse

regulation of BMP-2 and noggin, and enhancement of osteogenic potential. Bone. 2005;36:254-66.

[86] Fujimura K, Bessho K, Okubo Y, Kusumoto K, Segami N, Iizuka T. The effect of fibroblast growth factor-2 on the osteoinductive activity of recombinant human bone morphogenetic protein-2 in rat muscle. Archives of oral biology. 2002;47:577-84.

[87] Hanada K, Dennis JE, Caplan AI. Stimulatory effects of basic fibroblast growth factor and bone morphogenetic protein-2 on osteogenic differentiation of rat bone marrow-derived mesenchymal stem cells. Journal of bone and mineral research : the official journal of the American Society for Bone and Mineral Research. 1997;12:1606-14.

[88] Kuhn LT, Ou G, Charles L, Hurley MM, Rodner CM, Gronowicz G. Fibroblast growth factor-2 and bone morphogenetic protein-2 have a synergistic stimulatory effect on bone formation in cell cultures from elderly mouse and human bone. The journals of gerontology Series A, Biological sciences and medical sciences. 2013;68:1170-80.

[89] Lei L, Wang S, Wu H, Ju W, Peng J, Qahtan AS, et al. Optimization of release pattern of FGF-2 and BMP-2 for osteogenic differentiation of low-population density hMSCs. Journal of biomedical materials research Part A. 2015;103:252-61.

[90] Luong LN, Ramaswamy J, Kohn DH. Effects of osteogenic growth factors on bone marrow stromal cell differentiation in a mineral-based delivery system. Biomaterials. 2012;33:283-94.

[91] Maegawa N, Kawamura K, Hirose M, Yajima H, Takakura Y, Ohgushi H. Enhancement of osteoblastic differentiation of mesenchymal stromal cells cultured by selective combination of bone morphogenetic protein-2 (BMP-2) and fibroblast growth factor-2 (FGF-2). Journal of tissue engineering and regenerative medicine. 2007;1:306-13.

[92] Minamide A, Yoshida M, Kawakami M, Okada M, Enyo Y, Hashizume H, et al. The effects of bone morphogenetic protein and basic fibroblast growth factor on cultured mesenchymal stem cells for spine fusion. Spine. 2007;32:1067-71.

[93] Nakamura Y, Tensho K, Nakaya H, Nawata M, Okabe T, Wakitani S. Low dose fibroblast growth factor-2 (FGF-2) enhances bone morphogenetic protein-2 (BMP-2)-induced ectopic bone formation in mice. Bone. 2005;36:399-407.

[94] Ono I, Tateshita T, Takita H, Kuboki Y. Promotion of the osteogenetic activity of recombinant human bone morphogenetic protein by basic fibroblast growth factor. The Journal of craniofacial surgery. 1996;7:418-25.

[95] Springer IN, Niehoff P, Acil Y, Marget M, Lange A, Warnke PH, et al. BMP-2 and bFGF in an irradiated bone model. Journal of cranio-maxillo-facial surgery : official publication of the European Association for Cranio-Maxillo-Facial Surgery. 2008;36:210-7.

[96] Takita H, Tsuruga E, Ono I, Kuboki Y. Enhancement by bFGF of osteogenesis induced by rhBMP-2 in rats. European journal of oral sciences. 1997;105:588-92.

[97] Tanaka E, Ishino Y, Sasaki A, Hasegawa T, Watanabe M, Dalla-Bona DA, et al. Fibroblast growth factor-2 augments recombinant human bone morphogenetic protein-2-induced osteoinductive activity. Annals of biomedical engineering. 2006;34:717-25.

[98] van der Stok J, Wang H, Amin Yavari S, Siebelt M, Sandker M, Waarsing JH, et al. Enhanced bone regeneration of cortical segmental bone defects using porous titanium scaffolds incorporated with colloidal gelatin gels for time- and dose-controlled delivery of dual growth factors. Tissue engineering Part A. 2013;19:2605-14.

[99] Varkey M, Kucharski C, Haque T, Sebald W, Uludag H. In vitro osteogenic response of rat bone marrow cells to bFGF and BMP-2 treatments. Clinical orthopaedics and related research. 2006;443:113-23.

[100] Vonau RL, Bostrom MP, Aspenberg P, Sams AE. Combination of growth factors inhibits bone ingrowth in the bone harvest chamber. Clinical orthopaedics and related research. 2001:243-51.

[101] Wang L, Cao L, Shansky J, Wang Z, Mooney D, Vandenburgh H. Minimally invasive approach to the repair of injured skeletal muscle with a shape-memory scaffold. Molecular therapy : the journal of the American Society of Gene Therapy. 2014;22:1441-9.

[102] Wang H, Zou Q, Boerman OC, Nijhuis AW, Jansen JA, Li Y, et al. Combined delivery of BMP-2 and bFGF from nanostructured colloidal gelatin gels and its effect on bone regeneration in vivo. Journal of controlled release : official journal of the Controlled Release Society. 2013;166:172-81.

[103] Wang L, Huang Y, Pan K, Jiang X, Liu C. Osteogenic responses to different concentrations/ratios of BMP-2 and bFGF in bone formation. Annals of biomedical engineering. 2010;38:77-87.

[104] Raiche AT, Puleo DA. Cell responses to BMP-2 and IGF-I released with different time-dependent profiles. Journal of biomedical materials research Part A. 2004;69:342-50.

[105] Schliephake H. Application of bone growth factors--the potential of different carrier systems. Oral and maxillofacial surgery. 2010;14:17-22.

[106] Doty HA, Leedy MR, Courtney HS, Haggard WO, Bumgardner JD. Composite chitosan and calcium sulfate scaffold for dual delivery of vancomycin and recombinant human bone morphogenetic protein-2. Journal of materials science Materials in medicine. 2014;25:1449-59.

[107] Suarez-Gonzalez D, Lee JS, Diggs A, Lu Y, Nemke B, Markel M, et al. Controlled multiple growth factor delivery from bone tissue engineering scaffolds via designed affinity. Tissue engineering Part A. 2014;20:2077-87.

[108] Wen B, Karl M, Pendrys D, Shafer D, Freilich M, Kuhn L. An evaluation of BMP-2 delivery from scaffolds with miniaturized dental implants in a novel rat mandible model. Journal of biomedical materials research Part B, Applied biomaterials. 2011;97:315-26.

[109] Dawson E, Mapili G, Erickson K, Taqvi S, Roy K. Biomaterials for stem cell differentiation. Advanced drug delivery reviews. 2008;60:215-28.

[110] Lutolf MP, Hubbell JA. Synthetic biomaterials as instructive extracellular microenvironments for morphogenesis in tissue engineering. Nature biotechnology. 2005;23:47-55.

[111] Schwinte P, et al. Stabilizing effects of various polyelectrolyte multilayer films on the structure of adsorbed/embedded fibrinogen molecules: An ATR-FTIR study. Journal of Physical Chemistry B. 2001;105:11906-16.

[112] Langer RS, Peppas NA. Present and future applications of biomaterials in controlled drug delivery systems. Biomaterials. 1981;2:201-14.

[113] Sands RW, Mooney DJ. Polymers to direct cell fate by controlling the microenvironment. Current opinion in biotechnology. 2007;18:448-53.

[114] Wong SY, Moskowitz JS, Veselinovic J, Rosario RA, Timachova K, Blaisse MR, et al. Dual functional polyelectrolyte multilayer coatings for implants: permanent microbicidal base with controlled release of therapeutic agents. Journal of the American Chemical Society. 2010;132:17840-8.

[115] Gibbs DM, Black CR, Dawson JI, Oreffo RO. A review of hydrogel use in fracture healing and bone regeneration. Journal of tissue engineering and regenerative medicine. 2016;10:187-98.

[116] Fischer D, Li Y, Ahlemeyer B, Krieglstein J, Kissel T. In vitro cytotoxicity testing of polycations: influence of polymer structure on cell viability and hemolysis. Biomaterials. 2003;24:1121-31.

[117] Arnold LJ, Jr., Dagan A, Gutheil J, Kaplan NO. Antineoplastic activity of poly(L-lysine) with some ascites tumor cells. Proceedings of the National Academy of Sciences of the United States of America. 1979;76:3246-50.

[118] Barrere F, Layrolle P, Van Blitterswijk CA, De Groot K. Biomimetic coatings on titanium: a crystal growth study of octacalcium phosphate. Journal of materials science Materials in medicine. 2001;12:529-34.

[119] Leuschner F, Dutta P, Gorbatov R, Novobrantseva TI, Donahoe JS, Courties G, et al. Therapeutic siRNA silencing in inflammatory monocytes in mice. Nature biotechnology. 2011;29:1005-10.

[120] Zuo J, Jiang J, Dolce C, Holliday LS. Effects of basic fibroblast growth factor on osteoclasts and osteoclast-like cells. Biochemical and biophysical research communications. 2004;318:162-7.

[121] Lukasiewicz S, Szczepanowicz K, Blasiak E, Dziedzicka-Wasylewska M. Biocompatible Polymeric Nanoparticles as Promising Candidates for Drug Delivery. Langmuir. 2015;31:6415-25.

[122] Richert L, Schneider A, Vautier D, Vodouhe C, Jessel N, Payan E, et al. Imaging cell interactions with native and crosslinked polyelectrolyte multilayers. Cell biochemistry and biophysics. 2006;44:273-85.

[123] Schade R, Sikiric MD, Lamolle S, Ronold HJ, Lyngstadass SP, Liefeith K, et al. Biomimetic organic-inorganic nanocomposite coatings for titanium implants. In vitro and in vivo biological testing. Journal of biomedical materials research Part A. 2010;95:691-700.

[124] Crouzier T, Sailhan F, Becquart P, Guillot R, Logeart-Avramoglou D, Picart C. The performance of BMP-2 loaded TCP/HAP porous ceramics with a polyelectrolyte multilayer film coating. Biomaterials. 2011;32:7543-54.

[125] Ennett AB, Kaigler D, Mooney DJ. Temporally regulated delivery of VEGF in vitro and in vivo. Journal of biomedical materials research Part A. 2006;79:176-84.

[126] Santo VE, Frias AM, Carida M, Cancedda R, Gomes ME, Mano JF, et al. Carrageenan-based hydrogels for the controlled delivery of PDGF-BB in bone tissue engineering applications. Biomacromolecules. 2009;10:1392-401.

[127] Chen FM, Chen R, Wang XJ, Sun HH, Wu ZF. In vitro cellular responses to scaffolds containing two microencapulated growth factors. Biomaterials. 2009;30:5215-24.

[128] Patel ZS, Ueda H, Yamamoto M, Tabata Y, Mikos AG. In vitro and in vivo release of vascular endothelial growth factor from gelatin microparticles and biodegradable composite scaffolds. Pharmaceutical research. 2008;25:2370-8.

[129] Oldham JB, Lu L, Zhu X, Porter BD, Hefferan TE, Larson DR, et al. Biological activity of rhBMP-2 released from PLGA microspheres. Journal of biomechanical engineering. 2000;122:289-92.

[130] Xiang Q, Xiao J, Zhang H, Zhang X, Lu M, Zhang H, et al. Preparation and characterisation of bFGF-encapsulated liposomes and evaluation of wound-healing activities in the rat. Burns : journal of the International Society for Burn Injuries. 2011;37:886-95.

[131] Lim SM, Oh SH, Lee HH, Yuk SH, Im GI, Lee JH. Dual growth factor-releasing nanoparticle/hydrogel system for cartilage tissue engineering. Journal of materials science Materials in medicine. 2010;21:2593-600.

[132] Smith EL, Kanczler JM, Gothard D, Roberts CA, Wells JA, White LJ, et al. Evaluation of skeletal tissue repair, part 2: enhancement of skeletal tissue repair through dual-growth-factor-releasing hydrogels within an ex vivo chick femur defect model. Acta biomaterialia. 2014;10:4197-205.

[133] Decher GH, J.D.; Schmitt, J. Buildup of ultrathin multilayer films by a self-assembly process: III. Consecutively alternating adsorption of anionic and cationic polyelectrolytes on charged surfaces

G Decher JD Hong J Schmitt. Thin Solid Films. 1992;210:831-5.

[134] Lvov YD, G.; Haas, H.; Mohwald, H.; Kalachev, A. X-ray analysis of ultrathin polymer films self-assembled onto substrates. Physica B. 1994;198:89-91.

[135] Ai H, Jones SA, Lvov YM. Biomedical applications of electrostatic layer-by-layer nano-assembly of polymers, enzymes, and nanoparticles. Cell biochemistry and biophysics. 2003;39:23-43.

[136] Chluba J, Voegel JC, Decher G, Erbacher P, Schaaf P, Ogier J. Peptide hormone covalently bound to polyelectrolytes and embedded into multilayer architectures conserving full biological activity. Biomacromolecules. 2001;2:800-5.

[137] Boudou T, Crouzier T, Ren K, Blin G, Picart C. Multiple functionalities of polyelectrolyte multilayer films: new biomedical applications. Advanced materials. 2010;22:441-67.

[138] Guyomard AM, G. Glinel, K. Buildup of Multilayers Based on Amphiphilic Polyelectrolytes. Macromolecules. 2005;38:5737-42.

[139] Sukhisvili SG, S. Layered, erasable polymer multilayers formed by hydrogen-bonded sequential self-assembly. Macromolecules. 2002;35:301-10.

[140] Wang F, Ma N, Chen Q, Wang W, Wang L. Halogen bonding as a new driving force for layer-by-layer assembly. Langmuir. 2007;23:9540-2.

[141] Kinnane CR, Wark K, Such GK, Johnston AP, Caruso F. Peptide-functionalized, low-biofouling click multilayers for promoting cell adhesion and growth. Small. 2009;5:444-8.

[142] Izquierdo A, Ono SS, Voegel JC, Schaaf P, Decher G. Dipping versus spraying: exploring the deposition conditions for speeding up layer-by-layer assembly. Langmuir. 2005;21:7558-67.

[143] Jiang C, Markutsya S, Tsukruk VV. Collective and individual plasmon resonances in nanoparticle films obtained by spin-assisted layer-by-layer assembly. Langmuir. 2004;20:882-90.

[144] Caruso FN, K.; Furlong, D.N.; Okahata, Y. Assembly of Alternating Polyelectrolyte and Protein Multilayer Films for Immunosensing. Langmuir. 1997;13:3427-33.

[145] Elbert DH, C.B.; Hubbell, J.A. Thin Polymer Layers Formed by Polyelectrolyte Multilayer Techniques on Biological Surfaces. Langmuir. 1999;15:5355-62.

[146] Picart C, Mutterer J, Richert L, Luo Y, Prestwich GD, Schaaf P, et al. Molecular basis for the explanation of the exponential growth of polyelectrolyte multilayers. Proceedings of the National Academy of Sciences of the United States of America. 2002;99:12531-5.

[147] Zacharia NSD, D.M.; Modestino, M.; Hammond, P.T. Controlling diffusion and exchange in layer-by-layer assemblies. Macromolecules. 2007;40:1598-603.

[148] Sun B, Jewell CM, Fredin NJ, Lynn DM. Assembly of multilayered films using well-defined, end-labeled poly(acrylic acid): influence of molecular weight on exponential growth in a synthetic weak polyelectrolyte system. Langmuir. 2007;23:8452-9.

[149] Porcel C, Lavalle P, Decher G, Senger B, Voegel JC, Schaaf P. Influence of the polyelectrolyte molecular weight on exponentially growing multilayer films in the linear regime. Langmuir. 2007;23:1898-904.

[150] Benkirane-Jessel NL, P.; Hubsch, E.; Holl, V.; Senger, B.; Haikel, Y.; Voegel, J.C.; Ogier, J.; Schaaf, P. Short-Time Tuning of the Biological Activity of Functionalized Polyelectrolyte Multilayers. Advanced Functional Materials. 2005;15:648-54.

[151] Kong W, et al., . Immobilized bilayer glucose isomerase in porous trimethylamine polystyrene based on molecular deposition. Journal of the Chemical Society, Chemical Communications. 1994;11:1297-8.

[152] Lvov Y, et al. Successive Deposition of Alternate Layers of Polyelectrolytes and a Charged Virus. Langmuir. 1994;10:4232-6.

[153] Vodouhe C, Le Guen E, Garza JM, Francius G, Dejugnat C, Ogier J, et al. Control of drug accessibility on functional polyelectrolyte multilayer films. Biomaterials. 2006;27:4149-56.

[154] Wood KC, Chuang HF, Batten RD, Lynn DM, Hammond PT. Controlling interlayer diffusion to achieve sustained, multiagent delivery from layer-by-layer thin films. Proceedings of the National Academy of Sciences of the United States of America. 2006;103:10207-12.

[155] Garza JM, Jessel N, Ladam G, Dupray V, Muller S, Stoltz JF, et al. Polyelectrolyte multilayers and degradable polymer layers as multicompartment films. Langmuir. 2005;21:12372-7.

[156] Min J, Braatz RD, Hammond PT. Tunable staged release of therapeutics from layer-by-layer coatings with clay interlayer barrier. Biomaterials. 2014;35:2507-17.

[157] Salama A, El-Sakhawy M. Preparation of polyelectrolyte/calcium phosphate hybrids for drug delivery application. Carbohydrate polymers. 2014;113:500-6.

[158] Cai K, Rechtenbach A, Hao J, Bossert J, Jandt KD. Polysaccharide-protein surface modification of titanium via a layer-by-layer technique: characterization and cell behaviour aspects. Biomaterials. 2005;26:5960-71.

[159] Chua PH, Neoh KG, Kang ET, Wang W. Surface functionalization of titanium with hyaluronic acid/chitosan polyelectrolyte multilayers and RGD for promoting osteoblast functions and inhibiting bacterial adhesion. Biomaterials. 2008;29:1412-21.

[160] Almodovar J, Bacon S, Gogolski J, Kisiday JD, Kipper MJ. Polysaccharide-based polyelectrolyte multilayer surface coatings can enhance mesenchymal stem cell response to adsorbed growth factors. Biomacromolecules. 2010;11:2629-39.

[161] Facca S, Cortez C, Mendoza-Palomares C, Messadeq N, Dierich A, Johnston AP, et al. Active multilayered capsules for in vivo bone formation. Proceedings of the National Academy of Sciences of the United States of America. 2010;107:3406-11.

[162] Facca S, Ferrand A, Mendoza-Palomares C, Perrin-Schmitt F, Netter P, Mainard D, et al. Bone formation induced by growth factors embedded into the nanostructured particles. Journal of biomedical nanotechnology. 2011;7:482-5.

[163] Macdonald ML, Rodriguez NM, Shah NJ, Hammond PT. Characterization of tunable FGF-2 releasing polyelectrolyte multilayers. Biomacromolecules. 2010;11:2053-9.

[164] Nadiri A, Kuchler-Bopp S, Mjahed H, Hu B, Haikel Y, Schaaf P, et al. Cell apoptosis control using BMP4 and noggin embedded in a polyelectrolyte multilayer film. Small. 2007;3:1577-83.

[165] Peterson AM, Pilz-Allen C, Kolesnikova T, Mohwald H, Shchukin D. Growth factor release from polyelectrolyte-coated titanium for implant applications. ACS applied materials & interfaces. 2014;6:1866-71.

[166] Shah NJ, Hyder MN, Quadir MA, Dorval Courchesne NM, Seeherman HJ, Nevins M, et al. Adaptive growth factor delivery from a polyelectrolyte coating promotes synergistic bone tissue repair and reconstruction. Proceedings of the National Academy of Sciences of the United States of America. 2014;111:12847-52.

[167] Shah NJ, Macdonald ML, Beben YM, Padera RF, Samuel RE, Hammond PT. Tunable dual growth factor delivery from polyelectrolyte multilayer films. Biomaterials. 2011;32:6183-93.

[168] Goldberg AJ, Liu Y, Advincula MC, Gronowicz G, Habibovic P, Kuhn LT. Fabrication and characterization of hydroxyapatite-coated polystyrene disks for use in osteoprogenitor cell culture. Journal of biomaterials science Polymer edition. 2010;21:1371-87.

[169] Lee AL, Wang Y, Cheng HY, Pervaiz S, Yang YY. The co-delivery of paclitaxel and Herceptin using cationic micellar nanoparticles. Biomaterials. 2009;30:919-27.

[170] Sundararaj SC, Thomas MV, Peyyala R, Dziubla TD, Puleo DA. Design of a multiple drug delivery system directed at periodontitis. Biomaterials. 2013;34:8835-42.

[171] Simmons CA, Alsberg E, Hsiong S, Kim WJ, Mooney DJ. Dual growth factor delivery and controlled scaffold degradation enhance in vivo bone formation by transplanted bone marrow stromal cells. Bone. 2004;35:562-9.

[172] Barrere F, van BC, de GK, Layrolle P. Nucleation of biomimetic Ca-P coatings on ti6A14V from a SBF x 5 solution: influence of magnesium. Biomaterials. 2002;23:2211-20.

[173] Barrere F, van Blitterswijk CA, de Groot K, Layrolle P. Influence of ionic strength and carbonate on the Ca-P coating formation from SBFx5 solution. Biomaterials. 2002;23:1921-30.

[174] Habibovic PB, F.; van Blitterswijk, C.A.; de Groot, K.; Layrolle, P. Biomimetic Hydroxyapatite Coating on Metal Implants. Journal of American Ceramic Society. 2002;85:517-22.

[175] Kim HM, Kim Y, Park SJ, Rey C, Lee HM, Glimcher MJ, et al. Thin film of low-crystalline calcium phosphate apatite formed at low temperature. Biomaterials. 2000;21:1129-34.

[176] Choi EM. Magnolol protects osteoblastic MC3T3-E1 cells against antimycin A-induced cytotoxicity through activation of mitochondrial function. Inflammation. 2012;35:1204-12.

[177] Suh KS, Lee YS, Seo SH, Kim YS, Choi EM. Gold nanoparticles attenuates antimycin A-induced mitochondrial dysfunction in MC3T3-E1 osteoblastic cells. Biological trace element research. 2013;153:428-36.

[178] Marie PJ. Fibroblast growth factor signaling controlling osteoblast differentiation. Gene. 2003;316:23-32.

[179] Ou G, Charles L, Matton S, Rodner C, Hurley M, Kuhn L, et al. Fibroblast growth factor-2 stimulates the proliferation of mesenchyme-derived progenitor cells from aging mouse and human bone. The journals of gerontology Series A, Biological sciences and medical sciences. 2010;65:1051-9.

[180] Schade RDS, M.; Liefeith, K.; F¨uredi-Milhofer, H. Interaction of Cells with Organic-Inorganic Nanocomposite Coatings for Titanium Implants. Bioceramics Development and Applications. 2011;1:1-4.

[181] Zan X, Sitasuwan P, Feng S, Wang Q. Effect of Roughness on in Situ Biomineralized CaP-Collagen Coating on the Osteogenesis of Mesenchymal Stem Cells. Langmuir. 2016.

[182] Richard C, Roghani M, Moscatelli D. Fibroblast growth factor (FGF)-2 mediates cell attachment through interactions with two FGF receptor-1 isoforms and extracellular matrix or

cell-associated heparan sulfate proteoglycans. Biochemical and biophysical research communications. 2000;276:399-405.

[183] Bian L, Zhai DY, Tous E, Rai R, Mauck RL, Burdick JA. Enhanced MSC chondrogenesis following delivery of TGF-beta3 from alginate microspheres within hyaluronic acid hydrogels in vitro and in vivo. Biomaterials. 2011;32:6425-34.

[184] Murshid SA, Kamioka H, Ishihara Y, Ando R, Sugawara Y, Takano-Yamamoto T. Actin and microtubule cytoskeletons of the processes of 3D-cultured MC3T3-E1 cells and osteocytes. Journal of bone and mineral metabolism. 2007;25:151-8.

[185] Gohel AR, Hand AR, Gronowicz GA. Immunogold localization of beta 1-integrin in bone: effect of glucocorticoids and insulin-like growth factor I on integrins and osteocyte formation. The journal of histochemistry and cytochemistry : official journal of the Histochemistry Society. 1995;43:1085-96.

[186] Gronowicz G, Egan JJ, Rodan GA. The effect of 1,25-dihydroxyvitamin D3 on the cytoskeleton of rat calvaria and rat osteosarcoma (ROS 17/2.8) osteoblastic cells. Journal of bone and mineral research : the official journal of the American Society for Bone and Mineral Research. 1986;1:441-55.

[187] Hsu BB, Jamieson KS, Hagerman SR, Holler E, Ljubimova JY, Hammond PT. Ordered and kinetically discrete sequential protein release from biodegradable thin films. Angewandte Chemie. 2014;53:8093-8.

[188] Anderson JM, Rodriguez A, Chang DT. Foreign body reaction to biomaterials. Seminars in immunology. 2008;20:86-100.

[189] Sheikh ZB, P.; Barzilay, O.; Fine, N.; Glogauer, M. Macrophages, Foreign Body Giant Cells and Their Response to Implantable Biomaterials. Materials. 2015;8:5671-701.

[190] Maria SM, Prukner C, Sheikh Z, Mueller F, Barralet JE, Komarova SV. Reproducible quantification of osteoclastic activity: characterization of a biomimetic calcium phosphate assay. Journal of biomedical materials research Part B, Applied biomaterials. 2014;102:903-12.

[191] Tigges U, Hyer EG, Scharf J, Stallcup WB. FGF2-dependent neovascularization of subcutaneous Matrigel plugs is initiated by bone marrow-derived pericytes and macrophages. Development. 2008;135:523-32.

[192] Samartzis D, Shen FH, Goldberg EJ, An HS. Is autograft the gold standard in achieving radiographic fusion in one-level anterior cervical discectomy and fusion with rigid anterior plate fixation? Spine. 2005;30:1756-61.

[193] Nandi SK, Roy S, Mukherjee P, Kundu B, De DK, Basu D. Orthopaedic applications of bone graft & graft substitutes: a review. The Indian journal of medical research. 2010;132:15-30.

[194] Kalajzic I, Kalajzic Z, Hurley MM, Lichtler AC, Rowe DW. Stage specific inhibition of osteoblast lineage differentiation by FGF2 and noggin. Journal of cellular biochemistry. 2003;88:1168-76.

[195] Chung SM, Jung IK, Yoon BH, Choi BR, Kim DM, Jang JS. Evaluation of Different Combinations of Biphasic Calcium Phosphate and Growth Factors for Bone Formation in Calvarial Defects in a Rabbit Model. The International journal of periodontics & restorative dentistry. 2016;36 Suppl:s49-59.

[196] Clarke SA, Brooks RA, Lee PT, Rushton N. The effect of osteogenic growth factors on bone growth into a ceramic filled defect around an implant. Journal of orthopaedic research : official publication of the Orthopaedic Research Society. 2004;22:1016-24.

[197] Edwards RB, 3rd, Seeherman HJ, Bogdanske JJ, Devitt J, Vanderby R, Jr., Markel MD. Percutaneous injection of recombinant human bone morphogenetic protein-2 in a calcium

phosphate paste accelerates healing of a canine tibial osteotomy. The Journal of bone and joint surgery American volume. 2004;86-A:1425-38.

[198] Ruhe PQ, Boerman OC, Russel FG, Mikos AG, Spauwen PH, Jansen JA. In vivo release of rhBMP-2 loaded porous calcium phosphate cement pretreated with albumin. Journal of materials science Materials in medicine. 2006;17:919-27.

[199] Seeherman HJ, Bouxsein M, Kim H, Li R, Li XJ, Aiolova M, et al. Recombinant human bone morphogenetic protein-2 delivered in an injectable calcium phosphate paste accelerates osteotomy-site healing in a nonhuman primate model. The Journal of bone and joint surgery American volume. 2004;86-A:1961-72.

[200] Shuang Y ZY, Fujioka-Kobayashi M, Sculean A, Miron RJ. In vitro characterization of an osteoinductive biphasic calcium phosphate in combination with recombinant BMP2. BMC Oral Health. 2015.

[201] Tsurushima H, Marushima A, Suzuki K, Oyane A, Sogo Y, Nakamura K, et al. Enhanced bone formation using hydroxyapatite ceramic coated with fibroblast growth factor-2. Acta biomaterialia. 2010;6:2751-9.

[202] Crouzier T, Ren K, Nicolas C, Roy C, Picart C. Layer-by-layer films as a biomimetic reservoir for rhBMP-2 delivery: controlled differentiation of myoblasts to osteoblasts. Small. 2009;5:598-608.

[203] Gand A, Hindie M, Chacon D, Van Tassel PR, Pauthe E. Nanotemplated polyelectrolyte films as porous biomolecular delivery systems. Application to the growth factor BMP-2. Biomatter. 2014;4:e28823.

[204] Guillot R, Gilde F, Becquart P, Sailhan F, Lapeyrere A, Logeart-Avramoglou D, et al. The stability of BMP loaded polyelectrolyte multilayer coatings on titanium. Biomaterials. 2013;34:5737-46.

[205] Macdonald ML, Samuel RE, Shah NJ, Padera RF, Beben YM, Hammond PT. Tissue integration of growth factor-eluting layer-by-layer polyelectrolyte multilayer coated implants. Biomaterials. 2011;32:1446-53.

[206] Hu T, Abbah SA, Toh SY, Wang M, Lam RW, Naidu M, et al. Bone marrow-derived mesenchymal stem cells assembled with low-dose BMP-2 in a three-dimensional hybrid construct enhances posterolateral spinal fusion in syngeneic rats. The spine journal : official journal of the North American Spine Society. 2015;15:2552-63.

[207] Basmanav FB, Kose GT, Hasirci V. Sequential growth factor delivery from complexed microspheres for bone tissue engineering. Biomaterials. 2008;29:4195-204.

[208] Kang MS, Kim JH, Singh RK, Jang JH, Kim HW. Therapeutic-designed electrospun bone scaffolds: mesoporous bioactive nanocarriers in hollow fiber composites to sequentially deliver dual growth factors. Acta biomaterialia. 2015;16:103-16.

[209] Porcel C, Lavalle P, Ball V, Decher G, Senger B, Voegel JC, et al. From exponential to linear growth in polyelectrolyte multilayers. Langmuir. 2006;22:4376-83.